Innovative In Situ Combustion Technique: Moving Air Injection from Toe to Heel in a Single Well for Enhanced Oil Recovery

by

Juan David Antolinez Jimenez

A thesis submitted in partial fulfillment of the requirements for the degree of

Master of Science

in

Petroleum Engineering

Department of Civil and Environmental Engineering
University of Alberta

Abstract

Enhanced oil recovery (EOR) methods play a pivotal role in the petroleum industry, enabling the extraction of hydrocarbons that would otherwise remain trapped in reservoirs. Among these methods, thermally induced approaches have garnered significant attention, with two prominent techniques being Steam Assisted Gravity Drainage (SAGD) and In-Situ Combustion (ISC). ISC, in particular, has gained popularity due to its potential environmental benefits and economic advantages.

In the ISC process, an oxidizing agent is injected into heavy bitumen formations. This injection initiates a controlled combustion process within the reservoir, leading to an increase in temperature. The temperature rise reduces the viscosity of the bitumen, making it easier to flow through the reservoir. The continuous air injection ensures the mobilization of less viscous hydrocarbons toward the production well.

Despite the promise of ISC, achieving optimal operational results in the field has proven to be a complex endeavour. Various challenges have led to suboptimal recovery rates, including incomplete combustion, uneven temperature distribution, and difficulties controlling the combustion front. In order to tackle these difficulties and maximize the benefits of ISC, it is crucial to modify and fine-tune the approach to suit the particular conditions of the reservoir.

Numerous analytical and numerical simulation models have been developed and published to understand and optimize ISC processes. However, with the advancement of technology and increasing knowledge, new methods within the ISC framework need to be explored. This thesis investigates different approaches to ISC, primarily concentrating on the "Toe-to-Heel Air Injection" (THAI) method.

The research begins by verifying a pre-existing THAI lab-scale model, followed by kinetic upscaling to ensure accuracy and applicability to real-world reservoir scenarios. It then explores adjustments, including boundary expansion for the field-scale model, to study its implications on oil recovery, fluid dynamics, and combustion front control. Additionally, the study examines the extension of injector wells, the modification of air injection rates, and introduces steam injection as a preheating method.

To achieve the main objective of this research, the study devises an innovative strategy that employs a moving air injection interval within a single well, which simultaneously functions as both producer and injector. This approach is implemented within an expanded boundary field-scale model, aiming to enhance the control and efficiency of ISC processes by selectively injecting air into areas that require oxygen to sustain process stability.

Results indicate that progressively moving the air injection interval every 18 months in a single horizontal well, improved oil recovery by 8% compared to the conventional THAI method. Additionally, the proposed configuration showed earlier economically viable oil production. Parameters such as oil saturation, flue gas composition, temperature, and coke availability were also observed to be more efficient and improved in this proposed method.

Findings indicate that the novel technique has the potential to surpass the current state of the art in both economic performance and environmental sustainability. However, further research and numerical simulations are necessary, as the developed model exhibited issues with coke combustion and the in-situ combustion front's progression along the horizontal well. Modifying reaction kinetics and incorporating a sensitivity analysis for different time intervals of air injection progression along the well, along with the potential co-injection of water, could enhance the model's predictability and overall performance.

Preface

This thesis is submitted in partial fulfillment of the requirements for the Master of Science in Petroleum Engineering at the University of Alberta. The research presented is entirely original, and no part of this dissertation, nor any work substantially similar, has been submitted or is being submitted for any other degree or academic qualification at any other institution.

A version of Chapter 2 from this thesis has been published as Antolinez JD, Miri R, Nouri A. "In Situ Combustion: A Comprehensive Review of the Current State of Knowledge," *Energies*. 2023; vol. 16, issue 17, 6306. My contributions to the paper included conceptualization, methodology, validation, investigation, and the preparation of the original draft. Dr. Rahman Miri contributed to methodology, validation, and formal analysis, while Dr. Alireza Nouri was responsible for validation, review and editing, funding acquisition, and supervision.

Dedication

I dedicate this work to my family, whose unwavering support and encouragement have fueled my pursuit of education and professional growth, even from afar. Their love has been a guiding light in my journey's brightest and darkest moments. My heartfelt dedication extends to my family members, whose advice and love have been a constant source of strength.

To my life partner, Edwin, your unwavering support and energy infuse purpose into my life and bring me joy. Your love, patience and fantastic sense of humour have been guiding lights throughout my academic journey in Edmonton.

I want to thank everyone who accompanied me on this journey in Edmonton. To my friends, your laughter, love, and shared moments have enriched my life. I am deeply grateful to have each one of you by my side.

Acknowledgments

I extend my sincere appreciation to the University of Alberta for being a beacon of knowledge and a home for students. My alma mater has provided an unforgettable and enriching experience. I am grateful for the unwavering support of the university community, dedicated professors, and faculty staff who lead with purpose.

A special note of gratitude goes to my supervisor, Dr. Alireza Nouri, whose invaluable guidance, knowledge, patience, and insights have played a pivotal role in allowing me to pursue my master's dreams and complete this work. I would also like to acknowledge Dr. Rahman Miri for his unwavering support and extend my heartfelt gratitude to Dr. Mahmood Salimi for his valuable input and motivation during this journey.

Heartfelt thanks to COLFUTURO for providing the essential support that enabled me to realize my dreams of studying in Canada. I am genuinely grateful for the opportunities this institution affords many Colombians to pursue post-secondary studies globally.

Additionally, I acknowledge the financial support received from NSERC Discovery Grant RGPIN-2017-06257 and the Canada First Research Excellence Fund through the Future Energy Systems (Thermal Well Design and Testing). Their support has been instrumental in successfully completing the research presented in this work.

Table of Contents

List of Tables

List of Figures

.

Nomenclature

1D	One Dimensional
3D	Three Dimensional
A	Frequency factor
API	American Petroleum Institute
ARC	Accelerated Rate Calorimeter
bbl	Barrel
BHP	Bottom-hole pressure
CAPRI	Catalytic upgrading process in situ
cm	centimetres
CMG	Computer Modelling Group Ltd.
COSH	Combustion Override Split-production Horizontal Well
cP	centipoise
CSS	Cyclic steam stimulation
C^a_{fuel}	Fuel concentration
CWE	Cold water equivalent
C_i	Concentration of component i
ρ	Density
DLD	Direct line drive
DSC	Differential Scanning Calorimeter
DTA	Differential Thermal Analyzer
EOR	Enhanced Oil Recovery
E_a	Activation energy
F_{ij}	Outlet molar flow rate of component i in phase j
F_{ijo}	Inlet molar flow rate of component i in phase j
ft	foot
ft³	Cubic foot
HI	Horizontal injector
HP	Horizontal producer
HPAI	High-Pressure Air Injection
HTO	High-temperature oxidation
H_{rk}	Enthalpy of the reaction r
IC	Immobile component
in	inches
ISC	In-situ combustion
J	Joules
Kh	Horizontal Permeability
kPa	Kilopascal
Krg	Gas relative permability
Krog	Oil relative permeability at So
Krow	Oil relative permeability at Sw
Krw	Water relative permeability
Kv	Vertical Permeability
$k\tau$	Damkhöler number
LC	Light component
LTO	Low-temperature oxidation
m	meter
m³	Cubic meter
MC	Mobile component
mD	millidarcy
mm	millimetres
M_i	Molecular mass
MOZ	Mobile Oil Zone
MTO	Medium-temperature oxidation
Nij	Accumulated amount of component i in phase j
NTGR	Negative Temperature Gradient Region
ºC	Degree Celsius
µo	Oil Viscosity
OOIP	Original Oil In Place
Pc	Critical Pressure
P^b_i	Partial pressure of component i
PDSC	Pressurized Differential Scanning Calorimeter
PIHC	Pre-ignition heating cycle
psi	Pounds per square inch
ϕ	Porosity
PVT	Pressure, volume, temperature
q_i	Molar flux for component i
$q^{h,adv}$	Advection term
$q^{h,cond}$	Conduction term
Rij	Rate of generation or consumption of the i-th component in the j-th phase
RTO	Ramped-Temperature Oxidation
r_k	Reaction Rate
R	Universal gas constant
SAGD	Steam-Assisted Gravity Drainage
SARA	Saturate, aromatic, resin and asphaltene
scf	standard cubic foot
SLD	Staggered Line Drive
$s^R_{r,i}$	Stoichiometric coefficient of the reactant
$s^P_{r,i}$	Stoichiometric coefficient of the product
S_p	Pressure scaling factor
S_t	Time scaling factor
So	Oil Saturation
Sw	Water saturation
T	Temperature
Tc	Critical Temperature
TGA	Thermogravimetric Analyzer
THAI	Toe-to-Heel Air Injection
U_i	Internal energy
VI	Vertical injector

Chapter 1: Introduction

1.1 Overview

As conventional oil reservoirs approach a point where production becomes uneconomical, and reserves continue to deplete, there is a significant shift in focus within the industry. The emphasis is now on the economic recovery of heavy and extra-heavy oil reserves, particularly those in Canada and Venezuela. This strategic pivot is essential for sustaining energy supplies to meet future demands, as outlined by Fazlyeva et al. (2023).

The province of Alberta, Canada, is a significant hub for global oil production, holding the world's fourth-largest oil reserves. According to the Alberta Energy Regulator (2023), these reserves comprise 158.9 billion barrels of proven oil, accounting for 10.3% of the world's total oil reserves. Beneath Alberta's varied landscapes, vast deposits of bitumen—a heavy and viscous form of crude oil—are found predominantly in the province's oil sands. Key regions such as Athabasca, Cold Lake, and Peace River, spanning an area of 142,200 km², are crucial for extracting these valuable resources (Figure 1.1).

Figure 1.1 Alberta Oil Sands Map (Patchett et al., 2012).

Over the years, developing effective recovery mechanisms for the Alberta oil sands has been crucial for maximizing the region's oil potential. The Government of Canada (2020) highlights that with advancements in extraction technologies, the potential recoverable oil could increase to

approximately 300 billion barrels. This underscores the importance of technological innovation in transforming Alberta's vast oil sands into an even more significant global energy resource.

1.1.1 Thermal oil recovery methods

Traditionally, primary and secondary recovery methods have been pivotal in extracting conventional crude oil before reservoir depletion. However, heavy oil extraction typically requires tertiary (enhanced) oil recovery techniques due to their more challenging extraction conditions. Currently, two main commercial methods are widely used for extracting bitumen from oil sands: (1) Surface mining, which is applicable for shallow deposits with depths of ≤ 75 meters and (2) In-situ (thermal) recovery methods, which are employed for deeper deposits with depths of 75 meters or more. According to Souraki et al. (2012), 80% of the resources must be extracted using in-situ methods.

Generally, these thermal recovery methods propose transferring external heat to the fluid by either injecting hot fluids (e.g., hot water, steam, or solvent) or by generating the heat in-situ (i.e. within the reservoir itself) (Speight, 2013). As a result, the heavy oil viscosity will be reduced, and the mobility of the oil will be increased to move it to a production well.

Thermal methods like Steam-Assisted Gravity Drainage (SAGD) have emerged as transformative thermal recovery methods, proving highly effective in recovering bitumen from deeper and less accessible zones. While methods like this have been prominent, the constantly evolving landscape of oil extraction compels the exploration of new, environmentally sustainable techniques. Consequently, researchers are actively investigating other thermal recovery methods, such as In-Situ Combustion (ISC), to enhance efficiency further and reduce environmental impact.

1.1.2 In-Situ Combustion (ISC)

ISC is an advanced oil recovery technique that employs physical or chemical methods to ignite a portion of the oil directly within the reservoir. This ignition creates a combustion front that travels through the oil-bearing formation, significantly heating the surrounding area. The heat generated by this combustion front reduces bitumen's viscosity, thereby enhancing hydrocarbons' fluidity and mobility. As a result, oil resources become more accessible and easier to extract. This method

not only increases the efficiency of oil recovery but also extends the productive life of the reservoir, making it a promising option for tapping into more challenging and less accessible oil deposits.

Authors like Moore et al. (1999a) describe ISC as "the propagation of a high-temperature front for which the fuel is a coke-like substance laid down by thermal cracking reactions." This technical definition highlights the complex chemical transformations involved in the process. However, a more straightforward explanation presents in-situ combustion as a thermal recovery mechanism that generates energy directly within the reservoir. This mechanism is achieved by injecting an oxidizing agent—either air or oxygen-enriched air—which ignites and burns a portion of the heavy oil, typically between 5 to 10% of the oil in place, according to Gutierrez et al. (2009).

ISC is one of the oldest thermal recovery methods of heavy oil and bitumen, dating back to the early 1920s (Howard, 1923; Wolcott, 1923; Kuhn et al., 1953; Grant et al., 1954; Chu, 1977; Cheih, 1982). Ever since its appearance, this technology has been carried out all over the world. In Canada, Lloydminster-type sands in Alberta and Saskatchewan have good features for implementing this technology, also called ‘fireflooding’. To date, the most successful project is located in Romania in the Suplacu de Barcău field (Panait-Patica et al., 2006).

This method is gaining prominence as researchers delve into its advantages and feasibility for widespread application. According to Brigham et al. (2007), some of this technology's advantages include 1) Improved Sweep Efficiency: The combustion front creates a natural drive that enhances oil displacement, improving the overall sweep efficiency and ensuring a more comprehensive recovery. 2) Energy Efficiency: In contrast to some thermal recovery methods, ISC exhibits favourable energy efficiency, utilizing the reservoir's inherent heat to mobilize oil. 3) Reduced Environmental Impact: The combustion process generates fewer greenhouse gas emissions than other recovery methods, aligning with contemporary environmental sustainability goals. 4) Adaptability to Heterogeneous Reservoirs: ISC techniques showcase adaptability to heterogeneous reservoirs, making them suitable for various geological conditions at low operating costs.

Figure 1.2.a illustrates the conventional ISC configuration, which utilizes a vertical injector and a vertical producer separated by hundreds of meters. Despite the significant advantages of ISC technology, its practical application has faced numerous challenges. Many ISC projects in the 1990s failed to deliver the expected results. As Sarathi (1999) points out, these failures stemmed from poor reservoir selection, unfavorable reservoir characteristics, inadequate project design, and

adverse economic conditions. Specifically, operational challenges in Canada were attributed to a limited understanding of the crucial kinetic parameters involved in the ISC process (Moore et al., 1999a). Researchers such as Xia et al. (2005) argue that the long-distance oil displacement configuration (Figure 1.2.b) commonly observed in conventional ISC projects often leads to operational challenges, including air channeling, which results in poor combustion performance and suboptimal oil recovery. The oil must travel considerable distances through regions of heavy, cold oil, which has discouraged operators from adopting this method for oil recovery.

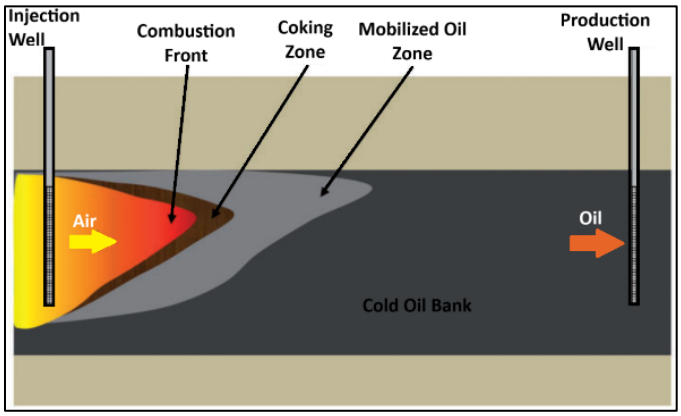

(a)

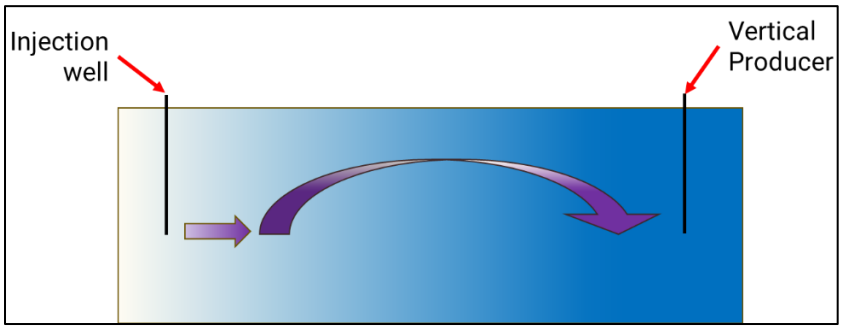

(b)

Figure 1.2. (a) Schematic illustration of conventional in-situ combustion. (Adapted from Perkins (2018) and (b) Long Distance Oil Displacement in conventional ISC projects (Adapted from Greaves et al. (2012)

1.1.3 Toe-to-Heel Air Injection (THAI)

Significant advancements have been made in ISC techniques, with one notable example being the development of the Toe to Heel Air Injection (THAI) method. This approach utilizes a more effective configuration, where gravity assists oil mobility through a short-distance oil displacement process. The method involves a vertical air injector perforated near the toe of a horizontal production well, as shown in Figure 1.2. In this process, a combustion front burns part of the oil,

generating heat that lowers its viscosity, allowing the oil to flow more easily by gravity to the production well. Unlike the conventional ISC configuration, where oil must travel long distances, in THAI, the oil only needs to move a few meters. Many experts have hailed this advancement as 'a new dawn' in combustion recovery (Xia et al., 2003), as it addresses the limitations of traditional ISC projects. In theory, THAI enhances efficiency and offers better control over fluid movement, marking a significant improvement in oil recovery techniques.

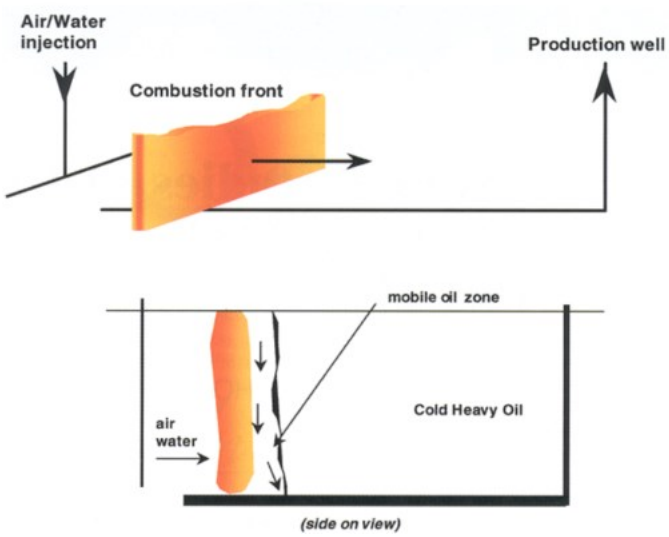

Figure 1.3 Toe-to-Heel Air Injection Schematic (Ayasse et al., 2005)

The THAI method, which employs two wells, theoretically offers superior oil recovery compared to conventional in situ combustion (ISC) techniques. However, its field implementation in Canada has encountered significant challenges. The method lacks the ability to control airflow in critical areas, resulting in combustion instabilities, gas channeling, and loss of control over the injected air. This misdirected airflow caused the premature extinguishment of the combustion front, leading to the cancellation of projects in Conklin, AB, and Kerrobert, SK. These failures also resulted in a loss of investment, interest, and credibility in the THAI method as a thermal oil recovery (Turta et al., 2018).

1.1.4 Proposed THAI Configuration

This research introduces a novel approach by introducing a single horizontal well that serves dual functions as an injector and a producer. This innovative design is expected to significantly boost oil recovery by directing airflow precisely to the areas where it is most needed. This targeted method can potentially enhance operational control, reduce environmental impacts, lower costs,

and promote more efficient oil recovery, effectively addressing the limitations observed in traditional THAI methods.

For the implementation of the proposed THAI configuration, which is the main focus of this study, several key surface and downhole components are required. As seen in Figure 1.4, the primary injection surface equipment includes air storage tanks for O_2 and N_2, along with high-capacity air compressors to deliver air at the required pressure, temperature, and flow rate for injection. These compressors are coupled with air filtration and dehydration units to ensure clean, dry air is injected into the well, preventing contamination or damage to the reservoir. A coiled tubing unit is essential for dynamically adjusting the injection and production intervals every 18 months along the wellbore, allowing for precise control of the combustion front as it advances. Additionally, surface control panels are used to monitor and regulate air injection flow rates, while temperature and pressure sensors, as well as observation wells, help manage the combustion process and ensure operational safety. On the production side, choke manifolds, fluid separation units, and flowlines are necessary to handle the oil and gas production effectively.

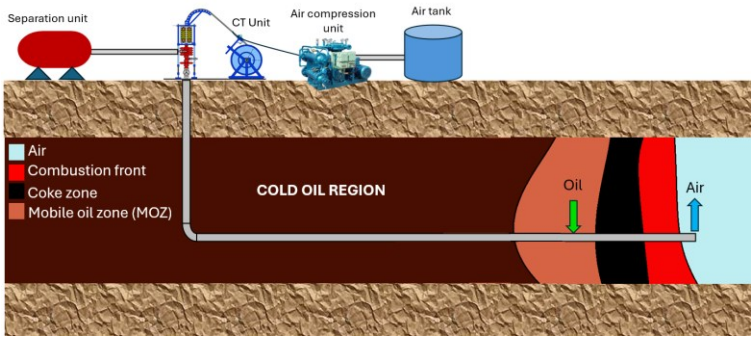

Figure 1.4 Proposed THAI configuration with surface equipment.

Downhole, as illustrated in Figure 1.5.a, the wellbore employs a Dual Parallel Simultaneous Injection and Production completion system within a single wellbore, utilizing dual tubing to separate the air injection flow from the production stream. Strategically placed packers and a Retrievable Bridge Plug (RBP) isolate different wellbore sections, ensuring that the injected air does not interfere with the oil production zone. In this configuration, one tubing is dedicated to dynamic air injection, introducing air through an adjustable set of perforations, while the second parallel tubing facilitates continuous production of mobilized oil and combustion gases. The proposed method starts by injecting air at the toe, igniting a portion of the surrounding oil and forming a mobile oil zone (MOZ). For the first time, a dynamic air injection system is introduced,

gradually shifting from toe to heel (Figure 1.5.b), supplying oxygen to sustain, control, and propagate the combustion front. The displaced, less viscous oil in the MOZ then flows by gravity toward the production zone, which is positioned further back along the well, closer to the heel, before the injection point.

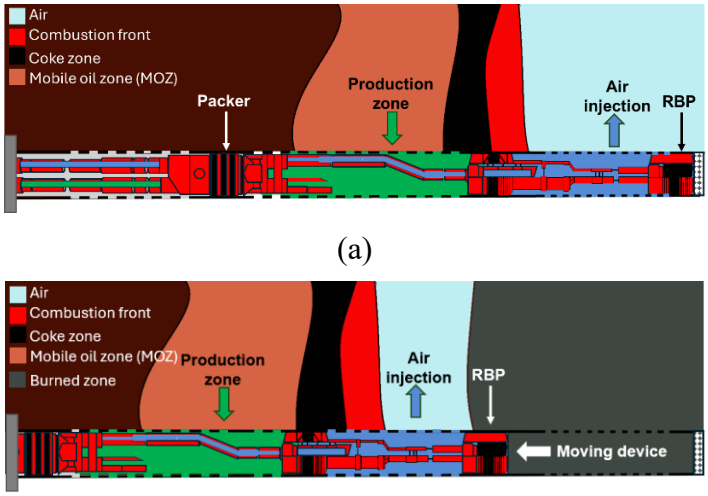

Figure 1.5. (a) Proposed THAI downhole configuration at the start of the operation and (b) during the shift of the air injection interval.

Authors like Turta (2013) highlight the critical need for accurate numerical modelling of in-situ combustion, prompting many researchers to develop models to predict how the THAI process behaves under field conditions. As interest in air recovery methods grows due to their potential to enhance oil recovery, it becomes essential to create robust numerical reservoir simulations to improve predictability. Unlike the SAGD process, in-situ combustion presents substantial challenges in accurately capturing the kinetics of the reactions that lead to the combustion of bitumen. Therefore, researchers like Gutierrez et al. (2012) address critical challenges in creating effective numerical models and provide recommendations for what these models should include.

Numerous researchers have attempted to numerically model the THAI process, exploring various methodologies for kinetic reactions and techniques for upscaling kinetic parameters to field scale (Turta et al., 2018; M. Yang et al., 2018; Ado, 2020a; Anbari et al., 2023; Lopeman et al., 2023). Despite the diversity of approaches, there remains no consensus on the best method to predict the

THAI process's behaviour accurately. This lack of consensus indicates a clear need for further improvements in this study area

As Alberta remains a crucial player in the global energy sector, the exploration and adoption of advanced recovery techniques such as THAI are set to transform oil extraction practices and help secure a sustainable energy future. The importance of accurate numerical modelling of in situ combustion cannot be overstated, and this research is dedicated to enhancing the understanding of in situ combustion and advancing its implementation.

This groundbreaking implementation technology seeks to advance our knowledge and verify the technology's effectiveness by introducing a field-scale model with innovative features to academia. By understanding its limitations, exploring the complexities of in-situ combustion, assessing the technology's feasibility, and considering its advantages and potential challenges, this research could lead to further innovations in in-situ combustion technologies, potentially setting new standards for the industry and driving it toward more sustainable practices.

1.2 Research Objectives

This research aims to develop a field-scale numerical model to evaluate the effectiveness of an innovative air injection technology. This technology utilizes a single well for both injection and production, featuring a movable air injection interval that progressively moves at fixed time intervals.

Another goal is to determine the parameters that have the most significant impact on the results of the in-situ combustion technology within a field-scale model through multiple ISC simulations.

1.3 Research Hypothesis

In situ combustion is a theoretically complex yet economically viable and environmentally friendly thermal recovery technology compared to conventional thermal methods. Despite some operational failures, it has gained increasing attention over the past few decades. When properly implemented and accurately simulated, this method can effectively predict the behaviour of heavy

oil extraction processes. Unlike traditional in-situ combustion that uses two vertical wells, its variant, THAI, takes advantage of the concept of short-distance displacement.

Current ISC technology faces challenges, particularly with achieving complete combustion and understanding how kinetics influence the accurate depiction of subsurface processes. Regarding THAI, only a few pilot projects have advanced to the commercialization stage, highlighting the need for further research to refine the methodology and fully understand its limitations.

The hypothesis of this research is that the variant of toe-to-heel air injection, which uses a single well serving as both injector and producer and is capable of injecting air in a progressively moving manner, results in superior performance compared to existing ISC methods. This innovative approach aims to inject air along the trailing back side of the combustion front, ensuring air is delivered precisely where needed to sustain and advance the combustion process. By feeding the combustion front and the area behind it, the hypothesis is that this method can enhance the efficiency and effectiveness of the in-situ combustion process. Supporting this hypothesis, it is anticipated that such a system will improve the uniformity of the combustion front propagation, reduce the likelihood of premature air breakthroughs, and maximize the recovery of hydrocarbons. Additionally, by using a single well for dual purposes, the overall cost and complexity of the operation could be significantly reduced while maintaining or even improving the performance of the thermal recovery process. The progressive movement of the air injection point could also allow for more precise control over the combustion dynamics, leading to better management of reservoir conditions and optimized production rates.

1.4 Significance of the work

Alberta is home to the world's fourth-largest bitumen deposits, boasting 158.9 billion barrels of proven oil reserves, as reported by the Alberta Energy Regulator (2023). In an effort to extract these reserves with more significant environmental consideration, operators are increasingly focusing on more environmentally friendly methods. These innovative technologies aim to minimize ecological impact while accessing hydrocarbons in challenging locations. Bitumen trapped in Alberta oil sands feature high viscosity values, which hinders the economic extraction

from the subsurface. Methodologies like in situ combustion help tackle this issue because no GHG gasses are expelled into the atmosphere, and the combustion occurs within the reservoir.

Operators consider the economic advantages of implementing an ISC project. Previous authors have not considered implementing a more stable toe-to-heel air injection variant using one single well from which air injection and oil production occur. In addition, mitigation of common air channelling issues, poor combustion front movement, and stalling of the combustion front can be reduced by using only one single well that selectively injects where air is most needed to sustain correct combustion and obtain expected results.

1.5 Thesis Outline

This thesis is formatted into five different chapters.

Chapter 1 (current chapter) aims to provide general background, scope, and organization.

Chapter 2 contains a literature review of the current state of knowledge of in situ combustion, in situ combustion kinetics, variants, combustion laboratory tests, ISC pilots and field experience, criteria for selecting in situ combustion and future work.

Chapter 3 details the numerical verification work of a previously conducted experimental-scale numerical model and the upscaling technique used, culminating in verifying its corresponding numerical field-scale model.

Chapter 4 presents the simulated results from various adjustments made to the field-scale model, including alterations to air injection rates, the number and positioning of injector wellbores, and the expansion of model boundaries. Additionally, it introduces and evaluates a novel approach involving a single wellbore toe-to-heel air injection. This chapter also includes a detailed analysis and discussion of the results, exploring the implications of these modifications on the efficiency and effectiveness of the extraction process.

Chapter 5 summarizes the significant findings of this research, highlighting key insights and outcomes. It offers suggestions for future research directions within this topic, aiming to build upon the work presented. Additionally, this chapter provides the conclusions, synthesizing the overall contributions of the study and reflecting on its implications for the field of hydrocarbon extraction.

Chapter 2: In-situ Combustion: A Comprehensive Review of the Current State of Knowledge

This chapter has been published as an article in the Energies Journal (MDPI).

Summary

In-situ combustion or fireflooding is a promising enhanced oil recovery (EOR) technique for producing heavy oils and bitumen. This method involves the in-place heating and combustion of hydrocarbons, resulting in reduced viscosity and increased mobility for improved flow toward the production wellbore. Despite its potential, widespread commercial implementation of in-situ combustion has been hindered due to technical and economic challenges like inadequate project design and improper reservoir selection. This literature review paper provides a comprehensive overview of the current knowledge of in-situ combustion by addressing its principles, historical development, combustion processes, underlying kinetics, and testing methods. Additionally, the review tackles existing gaps in the literature and the challenges associated with modelling and implementation in field applications. It also suggests solutions drawn from historical field experiences of the technology. Finally, the review paper proposes comprehensive screening guidelines derived from various literature sources for implementing in situ combustion. This framework underscores the technique's potential for efficient and sustainable hydrocarbon extraction, shaping its future as a transformative enhanced oil recovery technology.

2.1 Introduction

The energy and industrial sectors are increasingly focusing on hard-to-reach and significant oil reserves essential for future energy supply due to the depletion and nearing end of commercial viability of conventional oil reserves. However, commercial extraction of heavy oil poses significant challenges due to its high viscosity and density, particularly in countries such as Canada and Venezuela, where viscosity values can reach up to 10^6 cP. The primary challenge is to reduce the oil's viscosity to facilitate easier production of hydrocarbons. To tackle this challenge, operators employ thermal methods like steam injection and in-situ combustion as effective solutions (Moore et al., 1999a). While steam injection may seem feasible, it has significant environmental drawbacks, such as requiring vast amounts of water and energy and generating large amounts of greenhouse gases. In contrast, in-situ combustion is a promising and less

environmentally harmful solution that ignites a portion of the heavy oil in the reservoir while reducing its viscosity and enabling its easier extraction.

Moore et al. (1999a) define in-situ combustion as “the propagation of a high-temperature front for which the fuel is a coke-like substance laid down by thermal cracking reactions.” In other terms, it is a thermally-induced enhanced oil recovery method where the thermal energy is generated in situ, i.e. in place or in the reservoir, by injecting an oxidizing gas (air or oxygen-enriched air) that burns a portion of the heavy oil acting like a fuel, i.e. 5 to 10% of the oil-in-place (Gutierrez et al., 2009). Typically, this oil is predominantly composed of heavier components.

The in-situ combustion method is known to be the oldest thermal recovery method (Sarathi, 1999; Brigham et al., 2007) dating back from the early 1920s (Wolcott, 1923; Howard, 1923; Kuhn et al., 1953; Grant et al., 1954; Chu, 1977; Cheih, 1982). Since then, many projects have been carried out all over the world. The first successful ISC project in the U.S. occurred in 1920 in southern Ohio to melt paraffin and increase oil production (Mills, 1923). Similarly, the first field experiment of in-situ combustion outside the U.S. took place in the Soviet Union in 1935 (Sheinman et al., 1938). In Canada, Lloydminster-type sands in Alberta and Saskatchewan have good features for implementing fireflooding. To date, the most successful project is located in the Suplacu de Barcău field in northwestern Romania, and it has become the largest of this type in the world (Panait-Patica et al., 2006).

Throughout the implementation of in situ combustion, both successful operations and failures have occurred due to various factors. Despite demonstrating exceptional theoretical thermal recovery efficiency, multiple projects in the 1990s encountered failure. The causes behind these failures include an inadequate selection of reservoirs, unfavourable characteristics of both the reservoir and the fluid, deficient design and operational practices, and unfavourable economic factors (Sarathi, 1999). Specifically, in Canada, problems like the lack of control of the operation are attributed to a poor understanding of the main kinetic parameters (Moore et al., 1999a). This has led to many early failures in field tests (55% of the projects in the USA between 1960 and 1990 failed) (Sarathi, 1999). Consequently, the level of interest in ISC has dramatically decreased, which is why operation and production engineers consider it their last oil recovery option (Guo et al., 2016). Additional factors contribute to this issue, including the substantial investment required to acquire air compressors, the intricate nature of the combustion process, which demands a high

level of specialized expertise, and the scarcity of qualified personnel available to tackle this complex task (Turta, 2013).

Nevertheless, this recovery method offers several advantages, including eliminating steam-related costs, significantly reducing greenhouse gas emissions, avoiding water recycling processes, in situ upgrading of heavy oil, and avoiding energy-intensive methods further down the production chain. Such benefits make this approach more environmentally sound and economically viable (Castanier et al., 2003; Xia et al., 2003; Gates et al., 2008; Kapadia et al., 2011, 2013, 2015; Hart et al., 2017). According to Storey et al. (2022), ISC can be used to produce more environmentally friendly energy through the in-situ production of hydrogen (Hajdo et al., 1985; Kapadia et al., 2011) and from the naturally high heat flow of ISC via enhanced geothermal systems (Davis et al., 2009; Çınar, 2013; Cheng et al., 2014; Y. Zhu et al., 2019).

Overall, in situ combustion is considered a promising yet complex technique for extracting hard-to-reach oil reserves. While it offers significant potential, its implementation in field projects remains challenging. This literature review paper critically evaluates current knowledge on in situ combustion by focusing on experimental studies and identifying the critical challenges for modelling and implementation. Through synthesizing the latest research, this paper aims to provide insight into the most effective approaches for field implementation, outlining the key concepts and methodologies involved. Furthermore, this review identifies existing gaps in current knowledge and highlights areas where further research is needed to understand this technology's potential fully. In summary, this paper provides a comprehensive analysis of in situ combustion, from kinetic reactions to engineering challenges, and seeks to inform future research and development in the field.

2.2 Forward and reverse combustion

When it comes to enhancing oil recovery, in situ combustion techniques have received significant interest. Three notable methods in this domain are dry forward combustion, wet forward

combustion, and reverse combustion. These techniques involve the controlled ignition of oil within the reservoir to improve oil mobility and extraction.

Table 1 provides an overview of the different ISC processes. The remainder of this section briefly overviews these techniques, their advantages and limitations, and a practical understanding of how they contribute to ISC practices.

Table 2.1 Comparison of dry forward combustion, wet forward combustion and reverse combustion.

ISC Mechanism	Definition	Applied to	Advantages	Disadvantages
Dry Forward combustion	Most popular version of ISC. The combustion front is generated in situ, in the same propagation direction as the injected air and combustion front.	Heavy oil reservoirs.	The combustion provides the formation with a complete burning of formation, leaving the formation hydrocarbon-free.	Limit viscosity reduction to recover hydrocarbons. Low heat is transferred from the combustion front to the downstream zones.
Wet Forward Combustion	Combination of forward combustion and waterflooding. The addition of water or steam in the process	Thin reservoirs.	Increases process efficiency. Improved heat transfer. Improved sweep efficiency.	Simultaneous co-injection of both water and gas can be challenging.
Reverse	The combustion front is initiated at the production well and moves backward against the airflow.	Reservoirs with low effective permeability	A significant amount of cracking occurs.	Less upgraded oil is recovered. Spontaneous ignition near the injection well.

2.2.1 Dry forward combustion

This technique involves the injection of air into a designated injector well, followed by the ignition of oil either through natural means (autoignition) or external heat sources (such as electrical or gas heaters). It is worth noting that the accidental ignition of an oil reservoir was initially observed in the 1920s during an air injection operation for pressure maintenance, leading to the discovery of the conventional in-situ combustion EOR method (Ramey, 1971).

Once the oil ignition occurs, different heat zones are created within the reservoir due to heat and mass transport. These zones give rise to distinct temperature profiles, as illustrated in Figure 2.1. A combustion front is established among the zones where a portion of the oil (coke) undergoes combustion, generating heat. This heat is then transferred via convection through the water, facilitating oil mobilization. Continuous air injection is employed to sustain the advancement of

the combustion front towards the production well, with the combustion front and the injected air moving in the same direction.

In conventional dry forward combustion, the injection of oxygen (air) into the reservoir serves the purpose of igniting the coke, sustaining the combustion front, and displacing the oil towards the production well. This process can be likened to cigarette burning or the glowing hot zone observed in barbecue coals (Brigham et al., 2007).

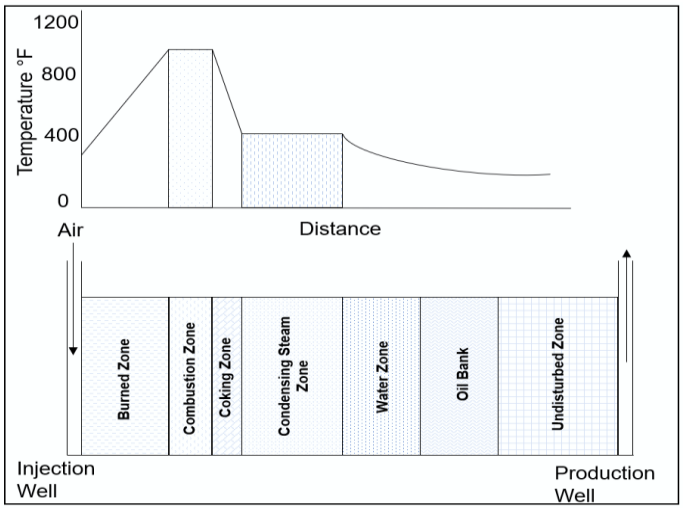

Figure 2.1 In-situ combustion temperature profile and zones (Adapted from Sarathi (1999)).

Figure 2.1 is an idealized representation of a Dry Forward Combustion process based on a combustion tube experiment. The zones depicted above move alongside the airflow direction; the exact definition of each of these zones is described elsewhere (Sarathi, 1999).

2.2.2 Wet forward combustion

In the dry forward combustion mechanism, only oxygen is injected; however, during this process, much of the heat remains in the zone behind the combustion front since the heat capacity of the gas is very low. On the other hand, water can be injected with air to improve the heat transfer forward. To address this issue, wet combustion was designed to get some heat to the zone ahead of the combustion front (Turta, 2022).

2.2.3 Reverse combustion

Reverse combustion, also called countercurrent ISC, works like a cigarette (Turta, 2022). The combustion front is initiated near the production well, and the more it is blown into the cigarette

(into the reservoir), the more it moves toward the injector well. At the same time, the oil is displaced towards the production well. This results in the air and combustion front moving in opposite directions.

Although not a very promising technique beyond laboratory tests (Stosur, 1977; Sarathi, 1999; Turta, 2013), this method was proposed for high-viscosity oil and tar reservoirs where the hydrocarbons have to flow from hot to cold regions, resulting in reduced mobility and increased flow restrictions. To address this challenge, the method keeps the major portion of the heat between the production well and the mobilized oil. This method enables hydrocarbons to flow more efficiently during production with minimal heat losses. Nevertheless, according to Brigham et al. (Brigham et al., 2007), there are two main reasons why it has not been successful:

1 Need for high-cost tubulars that can withstand the high temperatures of the produced fluids. Also, reverse combustion generally requires more oxygen than forward combustion; therefore, the costs will be higher.

2 Some deposits of unburned heavy hydrocarbons will remain in the reservoir. Eventually, these materials will tend to react, and the process will shift to forward combustion.

2.3 Other ISC approaches

2.3.1 THAI

THAI is a method of enhanced oil recovery (EOR) that involves injecting oxygen-enriched air into the subsurface at the toe of a horizontal well to create a combustion front that can sweep the heated oil along the horizontal production well. The process is designed to mobilize heavy oil and bitumen that would otherwise be difficult to produce using traditional methods. The technology of THAI was first proposed in the early 90s by the Improved Oil Recovery group at the University of Bath (Greaves et al., 2001). However, it was not until the late 90s that it was first patented by Greaves et al. (1997), and in the early 2000s, the first pilot projects were undertaken to test the technology (Ayasse et al., 2005). THAI is considered a promising enhanced oil recovery technique and is still being studied and developed. See Figure 2.2 for a schematic of the technique.

As a pre-screening criterion, the applicability of the THAI technology is suitable for heavy oil reservoirs with a minimum thickness of around 12-14 meters and located at depths exceeding 800-1000 m, where Steam Assisted Gravity Drainage (SAGD) cannot be applied(Xia et al., 2003b).

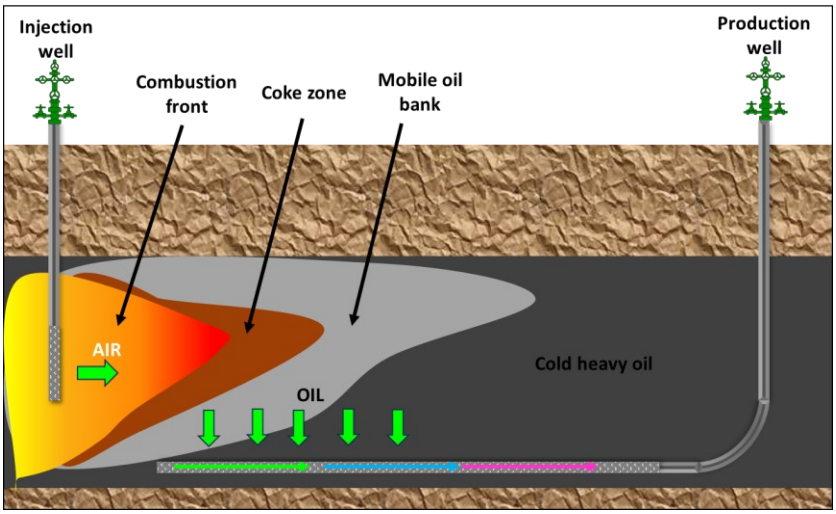

Figure 2.2 THAI process schematic (Adapted from Perkins, 2018).

2.3.2 THAI-CAPRI

THAI has a catalytic variant known as CAPRI, which stands for Catalytic upgrading process in situ. THAI–CAPRI™ was first proposed by Weissman et al. (1996) as a means to further upgrade the oil in situ through catalytic agents placed along the outer surface of the horizontal production well. By doing so, and due to the high pressures and temperatures in the reservoir, hydroconversion and thermal cracking reactions can occur, producing upgraded light oil at the surface (Speight, 2013). In simpler terms, it is like having an "in-situ" refinery. It is an additional upgrade that can achieve better results than solely implementing a THAI operation. According to Turta (2013), lab tests have proven that CAPRI technology can upgrade heavy oil by 3° API degrees over straight THAI.

2.3.3 High-Pressure Air Injection (HPAI)

Among the array of methods explored for the recovery of light oils, High-Pressure Air Injection (HPAI) stands out as a promising variant of in situ combustion (Yannimaras et al., 1995). This approach has been generally implemented in deep, thin, and low-permeability reservoirs (Yannimaras et al., 1995; Fassihi et al., 1997; Moore et al., 1999b; Turta et al., 2007; Montes et al., 2010). It has also been implemented in naturally fractured reservoirs (Gutierrez et al., 2012).

The process involves injecting oxygen-enriched air into the reservoir at high pressure and temperature to improve sweep efficiency. Then, a spontaneous ignition occurs, generated and favoured by bond scission reactions (in the 200-300° C range) between oil and oxygen. This combustion produces flue gases like CO_2 and N_2, which help reduce the oil viscosity and improve mobility toward the production well.

This technique has proven efficient in many scenarios where the conditions and properties of the reservoir are deemed suitable for this type of recovery. The benefits of implementing this method include improved oil mobility and excellent displacement efficiency, among others. Additionally, it presents other advantages, such as the self-correcting nature of the combustion zone facilitated by an enhanced oxygen utilization efficiency.

2.3.4 Combustion Override Split-production Horizontal Well (COSH)

Kisman et al. (1994) proposed a row of injector wells injecting an oxidizing gas that causes several combustion fronts that are propagated downwards, thus displacing the oil to the horizontal production well placed below the injection wells. This complex method requires using adjacent gas-producing wells that act as vent wells (for flue gas production) to keep the combustion process more stable (Turta, 2013; Wei, 2020). This method has been extensively simulated and has shown reduced energy costs and a similar performance to SAGD's. Nevertheless, more experimental work is needed to prove the concept.

2.3.5 Comparison

In conclusion, THAI, THAI-CAPRI, HPAI, and COSH are all in situ combustion methods to improve oil recovery. Each method has its unique approach and objectives. THAI focuses on controlled air injection to enhance heavy oil recovery, while COSH utilizes gravity drainage and oxygen injection. HPAI combines thermal and chemical processes while sweeping flue gasses, and CAPRI involves catalytic agents for in situ upgrading. Despite their characteristics, these methods share the goal of maximizing oil recovery through in situ combustion. For a comprehensive overview of each method's essential features, advantages, and limitations, see Table 2.2.

Table 2.2 Comparison of different combustion methods

ISC Mechanism	Definition	Applied to	Advantages	Disadvantages
THAI	Combines a vertical air injector + horizontal production well.	Lower pressure, quality, thinner and deeper than SAGD-fit reservoirs.	Up to 80% of the OOIP recovery. Oil upgrading up to 10° API. Fewer surface facilities. More controllable process than ISC. Negligible water use and less greenhouse gas emissions (Greaves et al., 2001).	Challenging to control the combustion front movement and complexities associated with heterogeneities.
HPAI	Air is injected into the reservoir at high temperature and pressure. Oxygen reacts with the hydrocarbons to improve mobility.	Light oils in deep, thin, high-pressure reservoirs with low permeability.	More reactions and more oxygen utilization, High mobility ratios. Possible high recovery factor, low air and energy requirement (Storey et al., 2022).	Possible air breakthrough at the production well.
CAPRI	A variant of the THAI process. In-situ refinery-type catalyst on the surface of the production well.	Economic viability needs to be assessed for in situ upgrading of fluids.	Further upgrading of the hydrocarbons in-situ.	Possible production of heavy metals and Sulphur
COSH	Utilizing gravity drainage as a driving mechanism. Incorporating multiple vertical injector wells in the upper region of the reservoir. The combustion front by oxygen injection propagates towards the production well beneath the injection wells.	Thick reservoirs.	Performance expected to be similar to that of SAGD	The effectiveness has not been definitively proven. Uncertainties persist, highlighting the need for additional studies.

2.4 Kinetics

Reaction kinetics can be defined as the study of the rate and extent of chemical reactions involved in ISC processes. According to Sarathi (1999), this study is essential due to the following reasons:

1. To evaluate the reactivity of the oil.
2. To determine the conditions required to achieve ignition and whether self-ignition will occur in the reservoir upon air injection.

3. To gain insight into the nature of fuel formed and its impact on combustion.
4. To establish parameter values for the kinetic (reaction rate) models used in the numerical simulation of ISC processes.

Unlike other EOR methods, ISC depends on the occurrence of chemical reactions between the crude oil and the injected air (Sarathi, 1999). It is crucial to understand how these reactions occur, how they switch from one to another (from Low-Temperature Oxidation to High-Temperature Oxidation) and what they depend upon to understand in situ combustion kinetics properly (Moore et al., 1999b).

During in-situ combustion processes, hydrocarbons/heavy oil/bitumen and the oxygen-enriched injected air are expected to react and interact, resulting in inevitable chemical changes due to the chemical reactions involved. As shown in Figure 2.3, the reactions zones across the reservoir can be categorized into three different temperature ranges: (1) low-temperature reactions (reservoir temperature up to 300 °C; LTO), (2) medium-temperature reactions (300-350 °C; MTO) and (3) high-temperature reactions (350-525 °C; HTO) (Dabbous et al., 1974; Ranjbar, 1995; Adagülü et al., 2007; Gargar et al., 2014; Yuan et al., 2020; Storey et al., 2022). The three ISC kinetic regimes are briefly summarized in Table 2.3, and further details are provided in the following subsections.

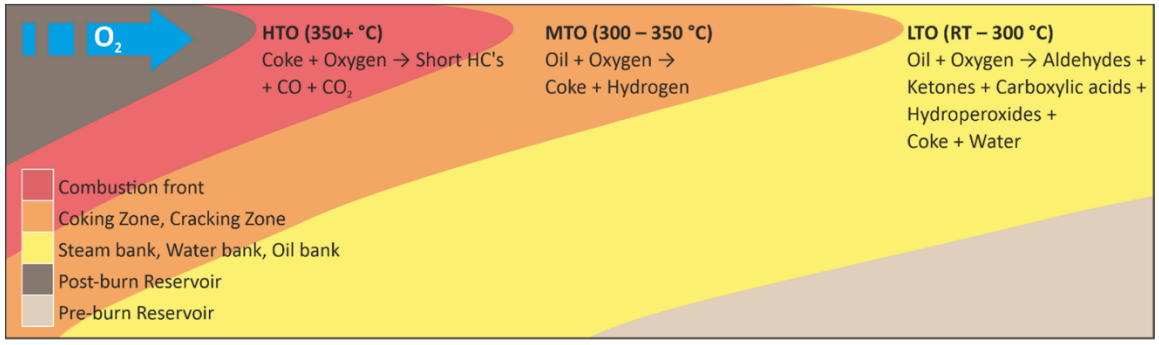

Figure 2.3 Reaction zones across the reservoir. LTO reactions occur furthest from the combustion front, MTO reactions promote fuel deposition, and the combustion front burns when HTO reactions occur (Storey et al., 2022)

Table 2.3 Summary of Kinetic Reactions in In-Situ Combustion

Temperature region	Low-temperature reactions	Medium temperature reactions (Negative Temperature Gradient Region)	High-Temperature reactions
Dominant oxidation mode	Oxygen-addition reactions	No oxidation. Thermal cracking and pyrolysis take place.	Bond-scission reactions (combustion reactions)
Reaction	hydrocarbons + oxygen →Oxygenated species + coke + water	hydrocarbons → HC (liquid/solid) + HC (gas) + Hydrogen	coke + oxygen → short-chain HCs + CO + CO2 + water + energy
Temperature	< 300° C	280-350° C	380-800° C
Description	Oxygen dissolves in the oil, producing partially oxygenated hydrocarbons, further polymerizing and promoting the formation of emulsions and asphaltenes. LTO reactions also promote the formation of some of the fuel (oxygenated hydrocarbon) needed further in the process.	Endothermic and homogeneous (gas-gas) reactions. Most of the coke (fuel) is produced here.	These heterogeneous (gas-solid/gas-liquid) reactions occur at the combustion front. Oxygen reacts with unoxidized oil, coke, and oxygenated compounds to produce CO_x, water, and energy.

2.4.1 Low-temperature oxidation (LTO) reactions

First observed by Belgrave et al. (1993), LTO reactions in heavy oils take place at temperatures below 300 °C, where the oxygen dissolves in the oil, causing it to polymerize by oxidative dehydrogenation-type reactions. These reaction modes are known as oxygen addition reactions (Butler, 1991).

Previous studies have collectively indicated that these reactions do not contribute to the mobilization of the oil (Alexander et al., 1962; Moore et al., 1995; Sarathi, 1999; Gutierrez et al., 2009, 2012; Turta, 2013; Turta et al., 2018). These reactions take place mainly during the ignition period. Still, it is critical that this low-temperature region switches to a high-temperature combustion region with an adequate air flux to avoid poor operating performance. According to Moore (1993), gross heterogeneities will undoubtedly promote the development of regions of low flux, making the process fall back into LTO reactions. These reactions usually produce a combination of partially oxygenated hydrocarbons (such as aldehydes, alcohols, ketones, and hydroperoxides) and minimal to no carbon oxides (Sarathi, 1999). However, these compounds are

undesired as they promote the formation of stable emulsions with water (Gutierrez et al., 2009), and compositionally speaking, LTO reactions contribute primarily to the formation of asphaltenes (pentane-insoluble fraction) (Moschopedis et al., 1973, 1975; Adegbesan, 1982;) and eventually coke. These compounds are highly undesired as they increase the original oil viscosity, boiling range, and density (Alexander et al., 1962; Brigham et al., 2007; Storey et al., 2022).

It has been proved that LTO reactions significantly contribute to the formation of fuel available for combustion (Alexander et al., 1962; Belgrave et al., 1993) as the coke generated during LTO reactions becomes the fuel for HTO reactions (Al-Saadoon, 1970).

According to Moore (1993), the temperature range for LTO reactions depends on the oil composition. Figure 2.4 shows that LTO reactions observe a rapid oxygen uptake period for heavy oils. Still, after this, it has been evidenced that there is a decline in the oxygen consumption rate at a temperature range of 250 to 300°C. Dechaux et al. (1979) refer to this zone as the "negative temperature gradient region" (NTGR). The pyrolysis reactions take place within this region (Alizadeh, 2020).

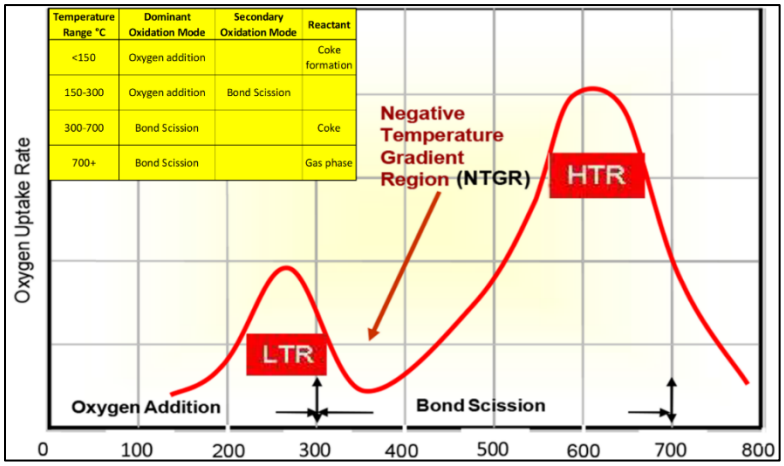

Figure 2.4 Oxygen uptake rate with respect to temperature (Adapted from Sur (2022))

2.4.2 Medium-temperature oxidation reactions

Based on the previous figure, the Negative Temperature Gradient Region (NTGR) represents a specific temperature range where the rate of chemical reactions declines. Consequently, the oxygen uptake rate reaches its minimum value. It is within this region that significant reactions such as pyrolysis, thermal cracking, or intermediate-temperature oxidation take place. These reactions yield abundant fuel or coke, a low volatile heavy hydrocarbon insoluble in toluene. The

resulting coke is deposited within the mineral matrix, contributing to the maintenance of the combustion front (Sarathi, 1999; Alamatsaz, 2014). It has also been noticed that when operations cannot overcome the NTGR, the oxidation kinetics cannot switch to the high-temperature region, and therefore, much of the oil is left behind as residue (Moore et al., 1992). For heavy oils, this NTGR occurs in the range of 250 to 350 °C (Alamatsaz, 2014; Alizadeh, 2020). According to Gutierrez et al. (2022), the general reaction formula for this thermal cracking is:

$$\text{Hydrocarbon}_{(\text{liquid})} \rightarrow \text{Hydrocarbon}_{(\text{liquid and/or solid})} + \text{Hydrocarbon vapour} \quad (1)$$

The reactions involved in this region are considered endothermic and homogeneous, i.e. they occur in a single phase, in this case, gas-gas. According to Abu-Khamsin et al. (1988), thermal cracking reactions undergo three different overlapping stages: distillation, visbreaking (mild cracking), and coking (severe cracking). During distillation, the oil loses most of its light to medium fractions. Visbreaking and coking are considered pyrolysis reactions, where most thermal cracking occurs, and coke is formed. According to Abu-Khamsin et al. (1988), the reaction kinetics of pyrolysis takes place in chain reactions as follows:

$$\text{Crude oil} \xrightarrow{\text{heat}} \text{Visbroken oil} + \text{Gas}, \quad (2)$$

$$\text{Visbroken oil} \xrightarrow{\text{heat}} \text{Coke} + \text{Gas}\ , \quad (3)$$

More recent studies have shown that this NTGR does have some traces of trapped oxygen that reacts with some of the hydrocarbons in oxygen-induced cracking reactions (oxidative cracking reactions). Remarkably, these reactions play a pivotal role in enhancing the hydrocarbon composition, generating lighter hydrocarbons as thermal cracking reactions increase. Furthermore, these reactions are also considered present during 2D and 3D conical combustion experiments Gutierrez et al. (2022).

Many authors, e.g. Belgrave (1987), suggest that the studies performed by Hayashitani et al. (1978) were of great importance in the kinetic characterization and determination of pseudo components of thermally cracked Athabasca Bitumen. Under an inert condition and temperatures of 360°C, 397°C and 422 °C, they cracked the bitumen and the liquid products were separated into maltenes and asphaltenes-coke residue using n-pentane as solvent. Asphaltenes were further recovered using

benzene as a solvent. They also sub-fractioned maltenes into light, middle, and heavy oils by distillation.

Adegbesan (1982) and Belgrave (1987) described a pseudo-component LTO reaction scheme for Athabasca bitumen using a semi-flow batch reactor in the 60°C to 150°C temperature range and at oxygen partial pressures of 50 kPa to 2,233 kPa. Such kinetic characterization led to the duplication of the findings of Hayashitani et al. (1978) as far as the separation of the maltenes and asphaltenes-coke fractions in n-pentane. According to Hayashitani et al. (1978), coke was characterized as the toluene-insoluble bitumen fraction. Solvent extraction and chromatographic techniques were combined to separate the maltenes into saturates, aromatics, oils, and resins (Figure 2.5).

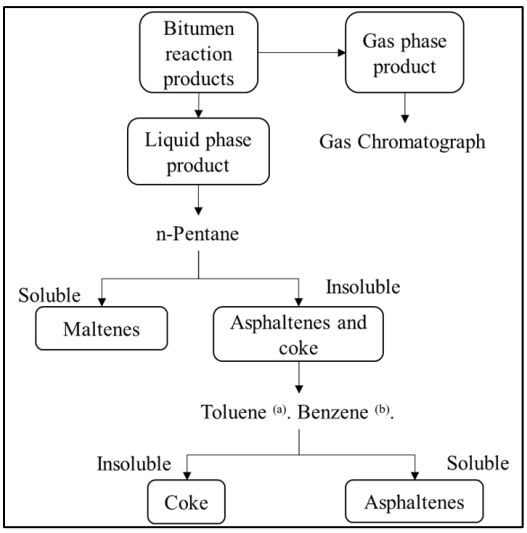

Figure 2.5 Separation Scheme for the Original Athabasca bitumen and Reaction Products. (a) Adegbesan's (1982) solvent, (b) Hayashitani et al.'s (1978) solvent (Adapted from Belgrave (1987))

2.4.3 High-temperature oxidation reactions (HTO)

According to Belgrave et al. (1993), these reactions mainly occur on the ISC front. In this region, the oxidation reactions burn the deposited coke in the presence of oxygen. These fast bond-scission reactions produce carbon oxides, carbon monoxide, water, and energy (Moore et al., 1999; Turta et al., 2018). According to the literature, the HTO reactions occur between the oxygen and the coke laid down at temperatures between 380 to 800°C (Moore et al., 1999b). It has been

demonstrated that the effective mobilization of the oil is only achieved when temperatures reach so high that the oxidation kinetics permit the occurrence of bond-scission reactions.

As stated earlier, oxygen addition reactions are not desired when mobilizing heavy hydrocarbons as they promote the formation of stable emulsions with water. On the other hand, bond-scission reactions are highly effective at mobilizing oil and are the desired state when implementing air injection and heavy oil combustion (Gutierrez et al., 2009). Therefore, it is critical for a field project to keep the combustion in the HTO region, also known as the bond scission mode, by a continuous supply of oxygen.

The reaction scheme for HTO, according to Storey et al. (2022), is as follows:

$$\mathrm{HTO}_{(>350°\mathrm{C})}: \mathrm{coke} + \mathrm{oxygen} \rightarrow \mathrm{short} - \mathrm{chain\ HCs} + \mathrm{CO} + \mathrm{CO_2}, \quad (4)$$

2.5 Experiments

Laboratory tests can accurately determine critical factors needed to implement an in-situ combustion project in a reservoir system. According to Gutierrez et al. (2009), oxidation and combustion tests are performed mainly for three reasons:

1. To better understand the oxidation patterns and heat release characteristics of the oil and the oil/rock systems.
2. To determine the kinetic parameters associated with the relevant chemical reactions and,
3. To gain an insight into the anticipated recovery performance of the combustion process when implemented in a specific reservoir.

However, there is still no unique test that can cover all these aspects and provide a thorough understanding of the overall performance of ISC. The laboratory tests are classified into quantitative, qualitative, and combustion performance tests, which are summarized in Table 2.4.

Table 2.4 Summary of In-Situ Combustion Testing Methods: Description, Advantages, and Limitations

Type of Test	Description	Test name	Advantages	Limitations
Qualitative tests	Used for screening purposes. Qualitatively estimate kinetic parameters of oxidation reactions.	TGA, DTA, DSC, PDSC, ARC	They are simple, quick and inexpensive to perform.	They do not provide any insight into the recovery performance. It is not very realistic as only one reaction model is assumed.
Quantitative tests	These studies replicate the flow conditions in the reservoir and determine the oxidation kinetics parameters. A reactor cell containing oil and sand is heated, the air is flown, and the residual oil and effluent gases are analyzed to determine the parameters which could be used in thermal reservoir simulators to predict field performance.	RTO	Useful in understanding and determining oxidation regimes (oxygen addition vs bond scission).	Does not reflect the same kinetic behavior observed during combustion tube tests due to peroxidation
Combustion performance studies	Physical setup aimed at simulating and observing the advancement of a real combustion front within a reactor cell. Provides an understanding of the parameters affecting the combustion.	Combustion tube tests	Useful at understanding combustion parameters (air and fuel requirements, air-fuel ratio)	Scaled experiments: upscaling is not a straightforward process.

Further details on these three tests follow.

2.5.1 Qualitative tests

According to Gutierrez et al. (2009), these are fingerprinting or screening tests capable of estimating the main kinetic parameters involved in the oxidation reactions, including the activation energy, reaction order and frequency factor. Qualitative tests observe physical changes during combustion, helping identify key associated parameters. However, they are not recommended when trying to replicate the flow conditions in the reservoir as they do not provide insight into the recovery performance.

In the literature (Sarathi, 1999), these tests are found to be the Thermogravimetric Analyzer (TGA), Differential Thermal Analyzer (DTA), High-Pressure TGA, Differential Scanning Calorimeter (DSC), Pressurized Differential Scanning Calorimeter (PDSC) and Accelerated Rate

Calorimeter (ARC). Overall, it can be said that these techniques are qualitative, rapid tests that calculate the kinetic parameters assuming one single kinetic reaction model, which is not necessarily what happens in the reservoir. For more details about each test, the reader is encouraged to read the extensive insight provided in Chapter 3-Kinetics and Combustion Tube Studies by Sarathi (1999).

2.5.2 Quantitative Tests – Ramped-Temperature Oxidation Test (RTO)

According to Moore et al. (1999), a good oil for in situ combustion recovery must be screened in terms of two different parameters: the kinetics of the ignition and how the transition from the low- to high-temperature oxidation regimes occurs. Therefore, the RTO involves heating oil-saturated cores in a plug flow reactor under a continuous stream of air or oxygen-enriched gas. This has proven to be extremely useful in defining the different reaction kinetics and oxidation regimes (i.e., oxygen addition reactions vs. bond-scission reactions) and understanding their impact on oil recovery (Moore et al., 1999, 1999b; Sarathi, 1999).

It is important to note that the RTO is not meant to replicate the procedures and results of a combustion tube test or field operation. This is because 1D combustion tube tests cannot predict the minimum air flux as these apparatuses implement high heat capacities, thus making it extremely difficult for kinetics to achieve the high-temperature combustion mode (Alamatsaz, 2014).

According to Moore et al. (1999), the objective of an RTO test is to highlight the importance of the negative temperature gradient region and to understand that the effectiveness of the in-situ combustion process depends on the oxidation mode and temperature. It is crucial that numerical simulators also incorporate this negative temperature gradient region to have a valid in situ combustion model (Moore et al., 1992).

2.5.3 Combustion performance tests (Combustion Tube tests)

The combustion tube in Figure 2.6 is a traditional device utilized to maximize oil recovery and make informed decisions by evaluating the in-situ combustion performance, air requirements, behaviour, and failure criteria in a laboratory setting. These tests usually comprise tubes with a thin stainless-steel wall packed with reservoir material like sand and rocks. After the packing has been carried out, the sample is saturated with crude oil, and then the tube is enclosed in a pressure

jacket. The reservoir material saturated with oil is then ignited to replicate the behaviour of oil in a reservoir during in situ combustion. It is also important to note that the tests must be conducted in an adiabatic condition so no heat transfer is present. Therefore, it is suggested that heaters and a piece of insulation equipment be used. However, there is some discrepancy as some studies suggest that some of the heaters used can cause the unwanted displacement of the combustion front, thus skewing the experiment's results (Belgrave et al., 1990).

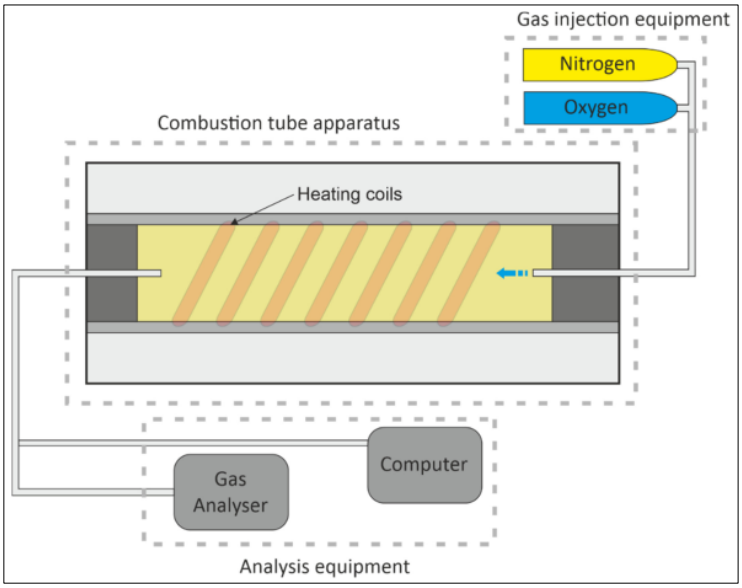

Figure 2.6 General diagram of a combustion test apparatus (Storey et al., 2022).

Much literature has found innovative ways to investigate different aspects of combustion experiments. Some assess the factors influencing the fuel deposition and air requirements of ISC (Alexander et al., 1962; Sharma et al., 2021). These authors agree that fuel (in the form of coke) availability is governed by the hydrogen-to-carbon ratio (H/C ratio), oil density, and oil saturation (availability of fuel decreased as the H/C ratio and API gravity increased, but it increased for higher oil saturation). On the contrary, there are some authors like Gutiérrez et al. (2022, 2022a) who differ from the conventional belief that coke is the primary fuel for ISC. According to their work, laboratory tests and field data have shown that light oils, with limited coke deposition, can still achieve successful ISC projects. Aleksandrov et al. (2017) investigated the influence of fracture orientation on the air injection direction in the success of an ISC project. Their study showed that parallel fractures led to poorer ISC performance than perpendicular fractures. Other studies (Ismail et al., 2020) have focused on the role of some clay minerals that act as catalytic agents during the reactions of the ISC. The study found that ISC consumed saturates as an ignitor, increased the

aromatics fraction, reduced viscosity, and decreased the amount of asphaltenes in produced oil. It also found that the presence of clays aided the combustion process by forming cribriform structures on the asphaltenes' surface.

Despite all these findings, it has been well studied that the main application of the combustion tube tests is the assessment of the “compatibility” of the crude oil found in the reservoir and how it impacts the coke deposition, air requirements, pressure, temperature and ultimately how the combustion front can propagate (Tzanco et al., 1991; Fassihi et al., 1997; Çınar et al., 2011; Hascakir et al., 2013). When properly designed and conducted, a combustion tube test can yield valuable information about the rock/oil system's combustion characteristics. Additionally, this data can aid in creating accurate engineering and economic projections of a field test's performance. Therefore, laboratory combustion tube studies serve as a crucial initial phase in the design of an ISC project.

2.6 Simulation coupling

Several numerical simulators have tried to model the reaction kinetics involved in ISC. For instance, Belgrave et al. (1993) proposed a comprehensive reaction kinetics model including LTO, thermal cracking, and HTO. This model has been widely used to simulate lab and field scale ISC processes (Coates et al., 1995; Coates et al., 2001; Rahnema et al., 2012; Alamatsaz, 2014). In his study, coke was the only fuel for HTO, and bitumen comprised only maltenes and asphaltenes. Like Jia et al. (2006), other authors proposed a four-reaction kinetic model that divided the maltenes into a slow reactive and more reactive fraction. However, their study did not provide any detailed information on these fractions. Additionally, a study conducted by Ado (2020) delves into comparing the predictive capabilities of different kinetic schemes employed to replicate the THAI process.

Comparable efforts, such as the pioneering work of Rojas et al. (2021), have introduced a concise three-step reaction scheme that effectively replicates the ignition process, temperature profiles, combustion velocity, and fluid production. This scheme holds promise for its applicability in the scaled-up simulation of in situ combustion scenarios. Yang et al. (2017) have contributed by developing a reaction kinetics framework to emulate the post-SAGD in situ combustion process. This comprehensive scheme encompasses Low-Temperature Oxidation (LTO), thermal cracking, and High Temperature Oxidation (HTO) reactions. Their study substantially enhances the

understanding of fuel nature, with their kinetic model predicting the oxidation and combustion dynamics of Athabasca oil sands. Additionally, Turta et al. (2023) conducted an exhaustive analysis focusing on determining ignition delay and the incidence of high-temperature oxidation and LTO reactions. These determinations were meticulously deduced via gas composition analysis.

Some pyrolysis reaction kinetic models based on saturates, aromatics, resins and asphaltenes (SARA) fractions were developed, including the work of Freitag et al. (2006). Sequera et al. (2010) interpreted Jia et al.'s (2006) model in a novel manner in terms of SARA fractions. They incorporated a SARA-based LTO (oxygen-addition) model based on an RTO experiment's simulation and history matching. They found that aromatics and resins can oxidize at low temperatures in the presence of an intermediate product (hydroperoxide), thus forming heavier compounds like asphaltenes. This model is the one that has been incorporated into numerical simulators like the thermal simulator STARS™ from CMG. To find a comprehensive list of reaction kinetics schemes used for modelling in-situ combustion in existing literature, the reader is referred to the work carried out by Ahmadi (2023) and Storey et al. (2022).

Within simulators, combustion processes almost exclusively use chemical reactions (Computer Modelling Group Ltd., 2021). These reactions are incorporated as source/sink terms in the mass and energy conservation equations solved in numerical simulators. Below is a systematic approach detailing the integration of chemical reactions into a numerical simulator like STARS by CMG. It is crucial to emphasize that all moles and energy associated with each component participating in a reaction are considered. Hence, the stoichiometry of reactions involving a component "i" within reaction "r" must ensure mass conservation; this adherence to mass conservation follows the stipulated principle:

$$\sum_{i=1}^{n} s_{r,i}^{R} M_i = \sum_{i=1}^{n} s_{r,i}^{P} M_i, \quad (5)$$

where $s_{r,i}^{R}$ and $s_{r,i}^{P}$ are the reactions' stoichiometric coefficients of the reactant and product, respectively, and M_i is the molecular mass.

Considering this, to build the kinetic model, most simulators often assume multiple LTO reactions, at least one thermal cracking reaction, and two or more HTO reactions. These reactions are modelled using the Arrhenius equation (Phillips et al., 1985a; Gutierrez et al., 2009; Nissen et al.,

2015; Storey et al., 2022; Fazlyeva et al., 2023). With this equation, the objective is to determine the speed of reaction or reaction rate of either the oxygen uptake or the hydrocarbon (fuel) consumption as follows:

$$\text{Reaction Rate } (r_k) = A e^{\left(-\frac{E_a}{RT}\right)} C_{fuel}^{a} P_i^{b}, \tag{6}$$

where A is the frequency factor, Ea is the activation energy, C_{fuel}^{a} is the fuel concentration, P_i^b is the partial pressure of component i, typically oxygen, and a and b are the reaction orders with respect to the fuel concentration and partial pressure of oxygen, respectively.

According to CMG (Computer Modelling Group Ltd., 2021), the general, heterogeneous mass transfer of the reaction taking place is commonly represented by:

$$\sum_{i=1}^{n} s_{r,i}^{R} \rightarrow \sum_{i=1}^{n} s_{r,i}^{P} + H_{rk}, \tag{7}$$

where H_{rk} is the enthalpy of the reaction r.

As such, if one decides to conduct a rearrangement and incorporate the reaction rate r_k, yields:

$$Q_i^{reac} = \sum_{k=1}^{n} (s_{r,i}^{P} - s_{r,i}^{R}) \times r_k, \tag{8}$$

$$Q^{h,reac} = \sum_{k=1}^{n} H_{rk} \times r_k \tag{9}$$

where Q_i^{reac} and $Q^{h,reac}$ are the chemical reactions terms.

Commercial reservoir simulators incorporate these chemical reaction terms into the mass balance and energy balance conservation equations as source/sink terms. As detailed in the work carried out by Zhu et al. (2011) and Nissen et al. (2015), these governing equations follow:

Mass balance equation:

$$\frac{\partial C_i}{\partial t} + \nabla \cdot q_i = Q_i^{well} + Q_i^{reac}, \tag{10}$$

Energy conservation equation:

$$\frac{\partial U_i}{\partial t} + \nabla \cdot \left(q^{h,adv} + q^{h,cond}\right) = Q^{h,well} + Q^{h,reac}, \tag{11}$$

where C_i is the concentration of component i, U_i is the internal energy, q_i is the molar flux for component i; $q^{h,adv}$ and $q^{h,cond}$ are advection and conduction terms, respectively, and Q_i^{well} and

$Q^{h,well}$ are well sink/source terms. Incorporating equation 6 into equations 8 and 9 yields the coupled terms:

$$Q_i^{reac} = \sum_{k=1}^{n} (s_{r,i}^{P} - s_{r,i}^{R}) \times Ae^{\left(-\frac{E_a}{RT}\right)} C_{fuel}^{a} P_i^{b}, \quad (12)$$

$$Q^{h,reac} = \sum_{k=1}^{n} H_{rk} \times Ae^{\left(-\frac{E_a}{RT}\right)} C_{fuel}^{a} P_i^{b} \quad (13)$$

Now, incorporating equations 12 and 13 into the governing equations 10 and 11 gives:

$$\frac{\partial C_i}{\partial t} + \nabla \cdot q_i = Q_i^{well} + \sum_{k=1}^{n} (s_{r,i}^{P} - s_{r,i}^{R}) \times Ae^{\left(-\frac{E_a}{RT}\right)} C_{fuel}^{a} P_i^{b}, \quad (14)$$

$$\frac{\partial U_i}{\partial t} + \nabla \cdot \left(q^{h,adv} + q^{h,cond}\right) = Q^{h,well} + \sum_{k=1}^{n} H_{rk} \times Ae^{\left(-\frac{E_a}{RT}\right)} C_{fuel}^{a} P_i^{b}, \quad (15)$$

Current enhanced oil recovery (EOR) modelling techniques focus on optimizing recovery factors. Given field tests' economic inviability and technical complexity, initial experimental and numerical modelling becomes essential. Thus, to attain a thorough grasp and proficient application of ISC methods, conducting preliminary experimental work (i.e., via ramped temperature oxidation or combustion tube laboratory experiments) to establish a suitable kinetic reaction model and the corresponding kinetics parameters becomes crucial. Subsequently, utilizing a simulator, one can predict ISC technique performance within a modelled 3D cell through history matching the aforementioned kinetic model and parameters. After these kinetic parameters have been history-matched, they must be correctly up-scaled for a field-scale simulation (Kumar, 1987; Ado, 2020).

As explained by Storey et al. (2022), when dealing with reservoir simulation and model construction, there are two important elements to consider: the geological (static) model, which represents the solid volume of the reservoir, and the fluid (dynamic) model, which represents the fluid volume (oil, water, gas) that is found inside the reservoir. After creating the static model, the dynamic behaviour must be incorporated using production and injection wells. ISC simulations must include this step to capture the dynamics of the process adequately. Similarly, the modelling process entails meticulous numerical data input into a simulator to ensure accurate results. Static properties such as porosity, permeability, petrophysical, geological, and PVT properties can be derived from an analogous reservoir or obtained through laboratory experiments. Conversely,

obtaining thermodynamic and kinetic properties requires conducting combustion tests. This meticulous data collection and modelling process aims to develop an accurate ISC model, maximizing its efficacy when applied in the field.

ISC simulations typically demand high resolution to capture all relevant attributes, consequently slowing down the computational process. As previously mentioned, given the considerable expense and complexity of field tests, modelling ISC is a prerequisite. Figure 2.7 provides a comprehensive overview of the static and dynamic properties involved in the process.

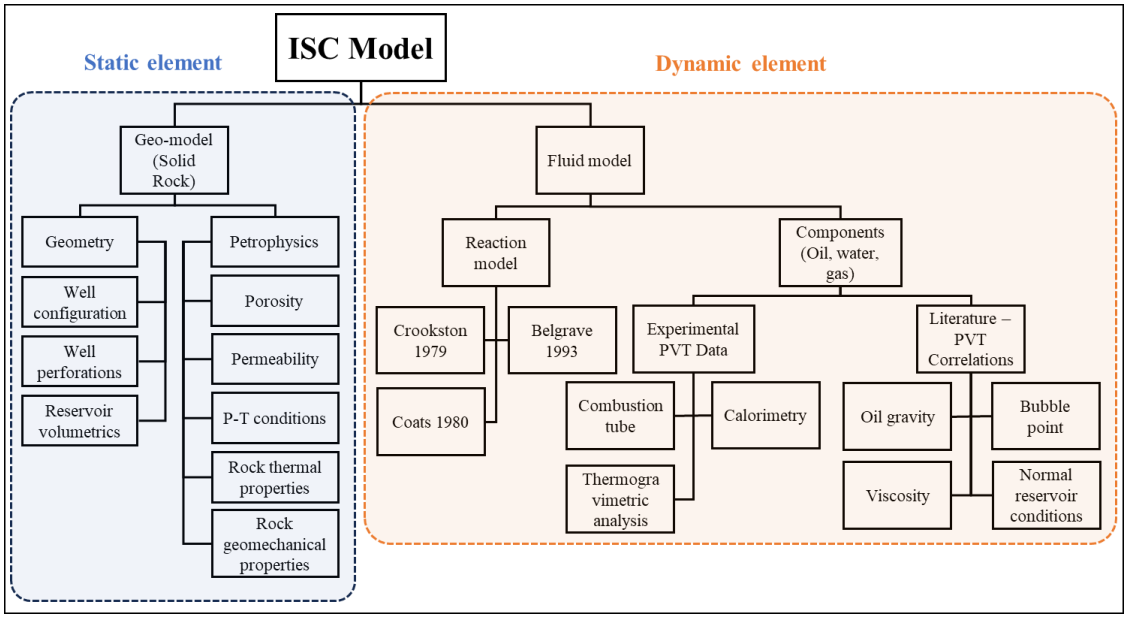

Figure 2.7 Constituent parts of an ISC model (Adapted from Storey et al. (2022))

2.6.1 Challenges in ISC Simulations

One of the main challenges when dealing with numerical simulations of the ISC process is that the data obtained from combustion tube history matching cannot be used directly for field simulations Zhu et al. (2021). This limitation stems from the narrow nature of the combustion front. To accurately capture the kinetics involved at play, it is necessary to model this region with small grid blocks in order to capture the kinetics involved. Therefore, if larger grid block sizes were employed, significant numerical errors would be observed, such as excessive amounts of fuel consumed, high temperatures in reaction zones, and slower movement of the reaction zone. As kinetic data estimated from the combustion tube history match are time and temperature-dependent, they will not produce similar results in large grid blocks. In order to avoid this issue, different techniques have been employed, such as dynamic gridding. However, it does not entirely

solve the grid size problem in field-scale simulation, as explained by Zhu et al. (2021). Nevertheless, more novel approaches, incorporating the use of the Damköhler number, are successfully used to solve the effects of the grid size effect in field-scale simulations (Nissen et al., 2015).

According to Gutierrez et al. (2009), some challenges must be addressed when modelling a dry combustion test. For instance, there is a tendency to operate a combustion tube test under ideal conditions, where the oxygen consumption rate in the combustion front controls the oxygen uptake. Therefore, the process is 100% efficient. Given such conditions, predicting whether the process will shift to the wrong oxidation mode is impossible. Another problem is that combustion tests do not provide kinetic information. Hence, it is vital to obtain this data from RTO experiments.

Neglecting the importance of minimum air flux: Trusting field-scale simulation models that have very low or even zero activation energy would yield misleading performance forecasts at lower air injection rates than those specified by the necessary minimum air flux to sustain combustion.

Numerical simulators must incorporate reaction schemes capable of predicting the negative temperature gradient region (NTGR) to become valid over a broad range of operating conditions. Therefore, being able to match combustion tube tests (Moore et al., 1992). For heavy oils and bitumen, the NTGR is a zone with low energy generation, so it acts as a barrier to the temperatures shifting from LTO mode to HTO mode. Conversely, if the energy generation in the HTO reaches below the energy level needed to offset the heat losses, the NGTR can promote the transition from HTO to LTO mode.

Simulation coupling of in-situ combustion involves combining numerical models of various aspects of the process, such as fluid flow, heat transfer, and chemical reactions, to create a comprehensive model of the in-situ combustion process. Critical comments and insight are found in the work by Gutierrez et al. (2009). Furthermore, Ado et al.'s (2017) research provides an instance of a model that forecasts operational factors, such as fuel accessibility and generated oxygen concentration, throughout in situ combustion procedures. This contribution enhances comprehension of the THAI technology. Another study, such as the research by Zhu et al. (2021),

focuses on evaluating the stability of the combustion front. They utilize a numerical simulation tool as an engineering resource to facilitate the planning and execution of real-world ISC projects.

2.7 Pilots and field experience

Since the 1920s, ISC has been employed extensively, with over 230 projects successfully executed in the United States, including notable ones like Bellevue, Midway Sunset, and Belridge. Additionally, several testing initiatives took place in Canada, including the Battrum, Eyehill, Tangleflags, Lindberg, and Countess projects. Subsequently, in the 1980s, numerous field projects were initiated in Europe, particularly in Romania, Hungary, and the former Soviet Union (now Russia and Kazakhstan), with the Suplacu de Barcau project being a prominent example.

2.7.1 Suplacu de Barcau, Romania.

This is the world's largest and most successful project of in situ combustion, continuously producing since the mid-1960s (Gadelle et al., 1981; Butler, 1991; Panait-Patica et al., 2006; Turta et al., 2007). The project employs dry-forward in-situ combustion from top to bottom at low pressures (200 psi). In this scenario, the oil viscosity reaches a substantial level of approximately 2,000 cp at a reservoir temperature of 64.4 ºF (18ºC). To enhance production, a peripheral direct line drive mechanism is implemented using vertical wells.

The field exhibits an anticline fold with an axial fault named Suplacu de Barcau. This fault serves as a boundary that confines the field to the South and East. The structure has a thickness ranging from 14 to 80 ft (4-24 m) and is situated at a depth of 115-660 ft (35-220 m) (Panait-Patica et al., 2006; Turta et al., 2007). Initially, in 1960, the reservoir operated under a solution gas drive mechanism, leading to an oil recovery rate of approximately 9%. The field experienced a modest peak production of 36 barrels per day during its early stages, gradually declining to 6 barrels per day per well in 1962 (Panait-Patica et al., 2006; Turta et al., 2007).

As a result, in order to confirm the theoretical models, a decision was made to test ISC and steam drive (SD) methods between 1963 and 1970. The successful performance in 1970 led to the decision to choose ISC for commercial exploitation. Also, given the high viscosity of 2,000 cp, cyclic steam stimulation (CSS) was selected as a necessary preheating procedure at this stage, and

the decision to switch from pattern to line drive exploitation mode was also made by Panait-Patica et al. (2006).

Two pilot projects were conducted, consisting of ISC patterns that spanned 4-5 years. One pattern focused on sweeping from the upper section of the anticline, while the other was implemented closer to the water-oil contact near the bottom. However, the data showed that the pattern at the bottom was not as efficient and controlled compared to the top pattern. Therefore, the decision was made to start sweeping the reservoir from the top in a downward manner to achieve better results (Panait-Patica et al., 2006).

The first linear ISC front was initiated in 1979 and gradually expanded, reaching zones in the western part of the reservoir. The initial well performance indicated a remarkable oil recovery rate of 55%. To sustain ISC propagation and maintain performance, another linear ISC front was introduced in the eastern part of the reservoir by 1983. However, despite efforts, the second ISC front was ultimately abandoned in 1996. Subsequently, starting in 1998, injection rates were reduced, leading to a progressive decline in oil production (Branoiu et al., 2021).

Between 1985 and 1991, oil production peaked, primarily attributed to the effective utilization of the maximum air injection rate. Nevertheless, a significant challenge throughout the implementation of ISC has been the leakage of some combustion gases to the surface, as highlighted by Turta et al. (2007). By 2007, it was estimated that an additional 20 years would be required to propagate the combustion front throughout the entire reservoir.

As of 2013, the field was producing approximately 8,000 to 10,000 barrels per day, as reported by Welch et al. (2013). Also, these authors claim that the sustained success of the project can be attributed to factors such as the reservoir geometry and the provision of adequate air injection to support the expansion of the combustion front in a linear manner.

2.7.2 Santhal and Balol projects

The Santhal and Balol fields are situated in the Mehsana heavy oil belt, located in the northwestern part of Gujarat, India. These fields were discovered in the early 1970s and have been under exploitation since 1974 in Santhal and 1985 in Balol by ONGC. The reservoir is found at an approximate depth of 1,000 m or 3,000 ft. It exhibits a strong lateral water drive, which poses challenges due to its unfavourable mobility ratio (Turta et al., 2007). Moreover, the oil extracted

from these fields through the wet ISC method had a viscosity of up to 200 cp for Santhal and 1,000 cp for Balol. The average porosity, permeability, and water saturation for both fields are approximately 28%, 5 darcies, and 30%, respectively (Dayal et al., 2010; Sur, 2022).

Initially, sucker rod pumps and screw pumps were installed for production purposes. However, in Balol, the water production increased while the oil recovery remained low at only 13% due to the unfavourable mobility ratio between oil and water. Consequently, the implementation of a thermal-enhanced oil recovery method became imperative. Initially, both steam injection and in situ combustion were considered potential approaches. However, steam flooding was deemed unfeasible due to the limited depth of 1,000 m, an average pay thickness of 5m, and the presence of a robust water drive (Turta et al., 2018). As a result, an initial pilot-scale ISC test was conducted in 1990 to evaluate its effectiveness, which yielded positive results indicating the significance of gravity in the movement of air and gases toward the up-dip portion of the reservoir (Roychaudhury et al., 1995).

Based on these findings, a specific oil layer within the field was developed using ISC with a crestal line drive in 1997. The expansion of this approach commenced from the south and gradually extended to cover the entire field in two phases. To confirm the continuity of the reservoir, N_2 gas was employed as a tracer (Roychaudhury et al., 1995).

Implementing the ISC technique in Balol significantly improved oil production and water cut reduction. From 1997 to 2004, the overall oil production increased from 350 m^3/day to 700 m^3/day, while the water cut decreased from 80% to 55% (Dayal et al., 2010). The recovery of the Balol reservoir varied across different regions, with approximately 55% recovery in the southern part and 12% in the northern part. The reduced mobility of viscous oil, low vertical sweep, early flue gas breakthrough in the producers, and front stalling were identified as factors contributing to the poor efficiency in the northern part (Sur, 2022).

To address this challenge, efforts were made to modify the displacement methodology by drilling more up-dip vertical injection wells and horizontal production wells from the flanks towards the injectors. This approach aimed to recover heavy oil over shorter distances, improving oil mobility. The optimization strategy offered significant advantages in overcoming oil mobility issues. In 2004, during a peak in air injection, the water cut decreased considerably to 58%. However, when air injection was halted for a period of three months, the water drive mechanisms regained

prominence by activating the aquifer. This observation suggests that the injected air has the necessary strength to halt aquifer encroachment, provided there is a proper balance between injected and produced fluids.

The Balol and Santhal projects provided compelling evidence of the benefits of implementing ISC processes with peripheral line drives for reservoirs characterized by a strong lateral water drive. These projects effectively controlled edge water and substantially reduced water cuts in production wells. Additionally, the utilization of wet ISC processes allowed for greater distances between wells, reaching up to 300 meters (980 feet), compared to the typical range of 50-100 meters (152-305 feet) observed in Suplacu de Barcau and BSOC Bellevue (Sur, 2022). Although the ultimate oil recovery may have been slightly lower, the wet ISC processes demonstrated the potential for improved well spacing and overall operational efficiency.

By 2013, the ongoing wet and dry combustion operations in Santhal and Balol led to approximately 15,000 barrels per day, further highlighting the success and impact of these ISC processes (Welch et al., 2013).

2.7.3 Bellevue Project

This ISC project utilizes dry in situ combustion at low pressure (less than 0.42 MPa or 60 psi) in a shallow reservoir with a low permeability of 700 mD. The oil viscosity in the reservoir is 676 cp, and the project employs a pattern system (Turta et al., 2007). The reservoir is divided into three distinct zones, with the upper zone consisting of sand varying in thickness from 15.3 to 21.4 m, the middle zone ranging from 3.1 to 6.2 m thick, and the lower zone varying from 9.3 to 15.3 m thick. Notably, only the upper and lower zones are productive.

This ISC project is situated northwest of Louisiana and stands as the largest ISC project in the United States. The reservoir, which exhibits a dome structure, was discovered in the 1920s, and production rates reached up to 1,115 m^3/day in 1923. In 1963, Getty Oil conducted an ISC test using an inverted 9-spot pattern. Later in the 1970s, Cities Service Oil and Bayou State Oil Corporation (BSOC) initiated an ISC experiment, which continued until the late 1970s. By 1982, 223 wells had been drilled, resulting in a production of approximately 2,750 bbl/day and an air-oil

ratio of 3,500 sm^3/m^3. However, CSO and Getty discontinued their projects in the mid-1980s, leaving BSOC as the sole operator in the field (Turta et al., 2007).

The ISC project, initiated by BSOC in 1970, initially operated in three inverted 7-spot pattern settings, achieving an oil recovery rate of 10%. In 1972, seven additional patterns were introduced to operate in the lower sand. Subsequently, in 1983, three more patterns were added to operate in the upper sand, transforming the operation into a simultaneous ISC process in both sands. By 2004, 15 well patterns were operating concurrently in the upper and lower zones. The project involved injecting 45,000 sm^3/day of air, resulting in a production rate of 50 m^3/day (Turta et al., 2007).

The ignition process in this project employs electrical heaters and has been enhanced by leveraging the reservoir's high heterogeneity. The objective is to inject a significant amount of heat during ignition and gradually increase the air rate at a controlled and slower pace once the front is established. This approach has proven highly effective, significantly improving performance, increasing oxygen utilization, and enhancing oil production.

2.7.4 Whitesands Project Pilot – First THAI pilot near Conklin, Alberta, Canada

Early pilots of conventional ISC in Canada typically involved vertical injectors and producers. The ignition of oil was performed either through downhole burners or steam injection. However, as noted by Welch et al. (2013), these pilots encountered several recovery challenges, including high sand production, erosion and corrosion of production well tubing strings, high lifting costs, and the formation of stubborn emulsions.

In response to these challenges, the Canadian operator- Petrobank- recognized the potential of the THAI technology for extracting heavy hydrocarbons in Alberta's Athabasca Oil Sands region. Consequently, in 2006, Petrobank and its subsidiary Whitesands Insitu Ltd launched their first-ever pilot using the THAI approach near Conklin, Alberta. The pilot comprised three well pairs, three air injector wells, and three production wells operating in a direct line drive configuration Welch et al. (2013).

According to Turta et al. (2023), the pilot was operated for five years, but it was observed that significantly less oxygen was injected than initially planned. Preheating through steam injection was carried out for 3-4 months, followed by ignition within 1-2 months. As the operation stabilized, the oil production per well peaked at 10-20 m^3/day. The project produced 180,000

barrels with an air-oil ratio of 5,000-6,000 sm^3/m^3. However, the pilot was eventually suspended due to unfavourable confinement in the pilot area, migration of combustion gases into the McMurray "A" formation, and communication with the bottom water zone from the start of steam injection. The project's failure was further compounded by factors such as sand influx and poor casing performance in the horizontal wells. Moreover, the lack of experience in handling projects of this nature exacerbated the operational challenges.

Another contributing factor to the project's failure was using a direct line drive (DLD). It was observed that the combustion front advanced less than 40 meters, less than half of the estimated distance from the toe to heel along the horizontal well. At the pilot's conclusion, only 7% of the oil was recovered, highlighting that the DLD configuration was unsuitable for achieving optimal sweep efficiency (Turta et al., 2023).

2.7.5 Kerrobert, Saskatchewan

Whitesands Insitu Ltd holds the rights and permits to operate in the Kerrobert lease, a 10 km^2 area situated 15 km southwest of Kerrobert, Saskatchewan. The lease contains a reservoir at a depth of 740 meters, housing heavy oil in the Waseca Formation along with a significant bottom water zone. Initially, conventional methods were employed to exploit these resources using two horizontal wells. Subsequently, in July 2009, approval was obtained for a THAI pilot consisting of two well pairs. Drilling and completion were successfully carried out in the same year, followed by the initiation of air injection in October 2009 (Welch et al., 2013).

By the end of 2010, oil production reached 150 barrels per day. The air-to-oil ratio between the two initial wells ranged from 1,000 to 2,000 sm^3/m^3 in 2010. According to Welch et al. (2013), the native oil was estimated to have a viscosity of 53,000 cp and an API gravity of 10º. However, the recovered oil was sold with a viscosity of 344 cp and an average density of 15.7º API, indicating that the THAI process effectively upgraded the oil.

Regarding reaction kinetics, gas analyses confirmed the occurrence of high-temperature oxidation reactions essential for sustaining a favourable in situ combustion mechanism. The produced gases exhibited a composition with only 0.5% oxygen, indicating complete oxygen consumption.

During the third quarter of 2010, the performance evaluation of the Kerrobert pilot demonstrated excellent results in implementing the THAI technique. Consequently, the operator proceeded with

the expansion of the pilot into a semi-commercial-scale project by drilling ten additional well pairs. By 2011, the construction of the THAI semi-commercial-scale project was completed. The preheating phase involved steam injection for 1-2 months, followed by ignition. However, the ignition process proved inefficient, resulting in a delay of 6 months. This delay led to low-temperature oxidations, which unfavourably mobilized the oil. Once the ignition phase passed, the in-situ combustion front became more apparent, as evidenced by the gas composition.

Regarding production, the well rates ranged from 7 to 14 m^3/day with a water cut between 30-50%. The total oil produced as of February 2015 reached around 50,000 m^3. The pilot confirmed an upgrade of about 7ºAPI, while the expansion project achieved approximately 5ºAPI. Additionally, the air-to-oil ratio was approximately 1,500 sm^3/m^3 for the pilot and around 2,400 for the semi-commercial project (Welch et al., 2013). For a detailed analysis of the operation at Kerrobert, the reader is directed to the work conducted by Wei et al. (2020).

2.7.6 China

China's heavy oil production faces significant challenges, mainly stemming from the late-stage use of conventional steam flooding methods. These methods are plagued by inefficiencies due to substantial heat losses during implementation. As a result, it is imperative to explore more effective alternatives, such as in situ combustion, which has undergone testing in oil fields including Shengli, Liaohe, Jilin and Xinjiang (Teng et al., 2017; S. Yang et al., 2018). A notable case presented by Zhu et al. (2021) involves the implementation of this technology in the D block (Du-66 reservoir) within Liaohe Oilfield, a project initiated back in 1986 (Teng et al., 2017).

The Du-66 reservoir, characterized by its monocline, exhibits a dipping angle of 5-10 degrees. The reservoir area spans 8.4 km^2 with an original oil in place of 5000 $x10^4$ tons (357 MMbbl). Depths range from 800 to 1300 meters, with a porosity of 0.25 and an average permeability of 800 mD within the poorly consolidated sandstone reservoir. Crude density is measured at 0.93 g/cm^3, while oil viscosity stands at 300-2000 cP at 50 degrees Celsius (Wang et al., 2016; Teng et al., 2017).

Initially, the block underwent cyclic steam stimulation; however, the results fell short of expectations. The recovery factor notably lagged behind the projected 27%, and the pressure plummeted from 11 MPa to 1.5 MPa. Consequently, in 2006, in situ combustion emerged as a post-CSS strategy to enhance recovery rates and economic viability. The ensuing pilot comprised

an inverted nine-spot well pattern involving over 90 ISC well patterns designed for air injection while the remaining wells still adhered to CSS (Teng et al., 2017).

The transformation from steam flooding to in-situ combustion, as detailed by Yao et al. (2018), yielded a substantial increase in single-well average daily production, rising from 0.5t/d (3.66 bbl/day) to 3.8t/d (27.85 bbl/day). The reservoir's total daily production surged to 619t/d (4424 bbl/day) by 2017 and an upgrading of 2-6 ° API (Liu et al., 2020).

Moreover, the application of THAI technology has seen three distinct pilots. A fire flooding pilot was conducted in 2008 in District Gao2-3 of the Liaohe oilfield. In it, a novel reusable igniter mechanism was used, which features a three-wire nickel chrome alloy coated in magnesia to produce enough heat for ignition (Wang et al., 2016).

The inaugural Shunguang Pilot, as outlined by Wang et al. (2016), underscores the prominence of Liaohe Oilfield as China's largest hub for heavy oil production. Over time, ISC has been effectively deployed across various reservoir types, including thin bed heavy oil, deep heavy oil, and bottom water reservoirs, showcasing its adaptability and impact (Yao et al., 2018).

2.8 Criteria for Selecting ISC

Screening criteria for field projects should be based on specific oil, water, rock, reservoir, and previous performance properties. According to Sarathi (1999), it is challenging to establish a definitive guideline for the application of ISC technology due to the diverse scenarios and rock characteristics encountered in previous applications. However, an effective screening guideline should consider rock type, oil type, and geological requirements. To provide useful insights, this paper compiles and summarizes commonly found screening guidelines from the literature pertaining to the commercial exploitation of heavy oil using ISC. Table 2.5 presents a summary of these informational screening guidelines.

Table 2.5 ISC screening guidelines based on information found in the literature.

Reference	Brigham et al. (2007)	Chu (1977)	Turta et al. (2007)	Turta (2013)	Taber et al. (1997)	Sarathi (1999)
Formation characteristics	The matrix/oil system is reactive enough to sustain combustion. Swelling clays may be a problem.	Relatively uniform sandstone reservoir		No presence of bottom water	High porosity sand/sandstone	Low clay content, low in minerals that promote increased fuel formation, such as pyrite, calcite and siderite. Extensive fractures and strong water drive should be avoided at all costs.
Reservoir depth	There is no depth limit as long as the reservoir contains the air injected.	>150 m (500 ft).			< 3,500 m (11,500 ft). Current field projects' average depth is approximately 1,070 m (3,500 ft).	90 - 3,800 m (300 - 12,500 ft)
Reservoir thickness	The reservoir has to be at least 4 m (15ft) in thickness to avoid excessive heat losses.	>3 m (10ft)		>3 m (10ft)	> 3m (10 ft)	1.5-15 m (5-50 ft)
Transmissibility	Air injectivity is favourable when the transmissibility is greater than 5md m/cp.			16 mD m/cP	> 20 md ft/cP	> 20 md ft/cP
Permeability		>100 mD		>100 mD	Average permeability > 50 mD*	Not critical
Porosity and oil saturation	The product, ϕS_o, should be more than 0.08 for combustion to be economically successful.	ϕ > 22%. The product, ϕS_o, should be more than 0.13. Oil saturation greater than 50 percent.		ϕ > 18%. The product ϕSo should be more than 0.07	Oil saturation greater than 50%	ϕ >18%. The product ϕSo should be more than 0.09
Oil gravity and viscosity	Viscosity has to be low enough to allow air injection, resulting in oil production at the design rate.	24 °API or less. μ_o < 1,000 cp	μ_o <1,000 cp (no need for CSS preheating) μ_o >2,000 cp (CSS becomes necessary)	μ_o: 60-10,000 cp	10-16 ºAPI. μ_o < 5,000 cp	μ_o < 5,000 cp. Oil gravity 10 - 40 °API
Oil Characteristics	The oil has to be readily oxidizable, as determined by laboratory experiments.				Some asphaltic components	Low asphaltic, low heavy metal content.

It is essential to mention that in cases where the initial oil saturation exceeds 50%, potential challenges arise due to the reduced availability of pore space for air injection and combustion reactions. This can lead to limited air penetration and hinder efficient combustion propagation. To optimize ISC performance, enhancing reservoir rock permeability, employing proper well placement, and adjusting injection strategies are crucial. These measures help ensure better air distribution, facilitate combustion front advancement, and ultimately improve recovery efficiency in reservoirs with high initial oil saturation (Taber et al., 1997).

In addition, Chu (1977) has postulated that the fuel content typically falls within the range of 0.8 to 2.8 lb/ft^3, with an average value of 1.45 lb/ ft^3. Moreover, they suggest that the air-fuel mass ratio for experimental and field-scale operations usually lies between 8 and 13, with an average of 9.65. Furthermore, the same author has proposed an average air-oil ratio of 12,400 scf/bbl for field-scale operations. In contrast, Turta et al. (2007) have presented differing findings, stating that this parameter oscillates within a broader range of 1,000 to 4,500 sm³/m³ (equivalent to 6,000 – 25,000 scf/bbl).

2.9 Future work

Further research is required to comprehend the environmental consequences associated with in situ combustion fully and to assess the economic viability of these processes. In addition, comprehensive studies are needed to evaluate the impact of ignition operations.

Since its initial field application in 2006, THAI technology has demonstrated its technical feasibility. The investigation and implementation of the direct line drive (DLD) configuration have already been conducted. However, a more extensive understanding of the implications of staggered line drive (SLD) in THAI technology is necessary. This can be achieved through dedicated 3D simulations, as such simulations have indicated the superiority of the SLD scheme in terms of fire front stability. Furthermore, systematic field testing of the SLD configuration should be conducted to validate its effectiveness (Ado, 2021a).

Research on in-situ combustion extensively investigates experiments and laboratory models. The kinetics behaviour of this technology, along with simulations of lab scale models, has been widely studied. The author believes that more emphasis should be placed on accurately upscaling from

lab to field scale models (Ado, 2020a; Zhu et al., 2021). This effort is crucial to comprehending this technology's intricate yet captivating nature.

Similarly, numerical models need to consider various factors including different completion settings, well design, injector and producer wellbore placement, injection of pure oxygen (Ado, 2021b), heterogeneities (Zamora et al., 2019) and the presence of bottom water and clays in the rock matrix (Pope et al., 2020; Anbari et al., 2023; Minakov et al., 2023; Zhang et al., 2023), all of which could significantly influence the technique's success.

Moreover, it is essential to place greater emphasis on comprehending the potential of ISC to generate hydrogen from bitumen. According to Song et al. (2023), the capacity of the oil and gas industry to play a substantial role in the energy transition by enabling extensive and economical hydrogen production from reservoirs is noteworthy. Equally important is the necessity to understand the pre-injection heating cycle (PIHC) to unravel the complexities of ignition prior to the commencement of air injection. Additionally, understanding the application of ISC in depleted conventional oil reservoirs to increase recovery factors and its integration with steam injection are essential aspects to consider (Yang, 2019; Harding, 2023).

2.10 Conclusions

In conclusion, the in-situ combustion technique is a promising method for enhanced oil recovery. The kinetics involved in the process are complex and require careful consideration when designing and implementing the method. Using laboratory tests is essential in optimizing the process and predicting its performance in the field. Additionally, it is necessary to incorporate and history-match the kinetics attributes with numerical simulations to predict the process's behaviour accurately. Upscaling the simulation to field conditions is another challenge that requires further research and detailed analysis.

The success and effectiveness of ISC projects vary depending on various factors such as reservoir characteristics, operational parameters, and project design. To ensure precise and appropriate implementation of the ISC technology at the field scale and to offer valuable insights, this paper presents and condenses screening guidelines for its application.

The case studies highlighted the importance of understanding the specific reservoir conditions and tailoring the ISC approach accordingly. Projects like Balol and Santhal demonstrated that

implementing ISC techniques in peripheral line drives can significantly reduce water cuts and control edge water, increasing oil production. On the other hand, projects like the Canadian Whitesands pilot using THAI technology faced challenges such as inefficient ignition and unfavourable combustion front advancement, which affected the overall performance. These experiences underscore the need for thorough reservoir characterization, operational optimization, and continuous monitoring to achieve successful ISC implementation.

Recent studies have highlighted the potential of the THAI and the Catalytic Upgrading Process in situ (CAPRI) combustion techniques as viable alternatives to traditional in situ combustion (Ado, 2022; Ado et al., 2022; Afanasev et al., 2023; Lopeman et al., 2023). These techniques have shown promising results in the laboratory and field. However, further research is needed to optimize their performance in terms of operational design and ignition initiation.

Overall, the development and optimization of the in-situ combustion technique and the continued research into novel approaches such as THAI and CAPRI will be critical for the continued production of hydrocarbons from unconventional resources. The successful implementation of these techniques will lead to increased hydrocarbon recovery and more efficient and sustainable production practices.

Chapter 3: Numerical model verification work

Summary

For the purpose of this research, the laboratory-scale model to be validated is based on the work conducted by Ado (2017). In order to validate the experimental-scale THAI model, it is crucial to utilize the results obtained from real-life physical combustion THAI tests. These specific tests were carried out at the Improved Oil Recovery Laboratory at the University of Bath. The tests, executed within a three-dimensional and low-pressure combustion cell, yielded crucial data on THAI performance parameters. These parameters include oil production rate, cumulative oil production, peak temperature, degree of upgrading, produced oxygen concentration, volumetric and areal sweep, temperature distribution, and air requirement, among others. The comprehensive results not only provided quantitative measures but also enhanced the understanding of the fundamental mechanisms governing the stability of THAI.

Most of the tests utilized Canadian oil sands or heavy oil sourced from the Alberta region, known for hosting the world's largest tar sands or heavy oil deposits. The most substantial of the three Canadian oil sand reserves is located in the northeastern part of Alberta and is commonly referred to as the Athabasca oil sands. However, only a fraction of this extensive reserve, approximately 10%, comprises bitumen, with the remaining composition being 4% water and 86% solid sediments deposited at a shallow depth of around 40 to 60 meters (Mossop, 1980; Hyne, 2012). Consequently, it becomes evident that employing in-situ oil recovery techniques is imperative for recovering at least 90% of the entire deposit. According to Ado (2017), to validate the numerical model, one of the chosen physical tests utilized Athabasca bitumen.

The lab experiment chosen for validation utilized a rectangular stainless steel combustion cell measuring 60 cm x 40 cm x 10 cm (Xia et al., 2002). The combustion cell's pressure ranged from 200 to 300 kPa. To monitor the combustion front, 85 thermocouples were strategically installed, and for adiabatic maintenance, nine computer-controlled electrical heating tapes were wrapped around the cell. These tapes ensured the cell wall temperature remained approximately 20 degrees Celsius below the average temperature inside the combustion cell, compensating for heat losses to

the surroundings. The cell was then enclosed in an aluminum box measuring 90 cm x 90 cm x 40 cm, filled with insulating material to minimize heat dissipation.

Additionally, the positioning and configuration of wells are noteworthy. For this THAI experiment, two wells were employed: a horizontal injector (HI) well and a horizontal producer (HP) well, arranged in a staggered line drive (SLD) pattern. The cell was completely filled with virgin Athabasca oil sand.

In the experimental model, an electrical heater at the sand pack face was activated until the air entrance temperature reached approximately 500 degrees Celsius. Subsequently, air was injected at a rate of 8000 m^3/min. After 190 minutes, the air injection rate was increased to one-third at a rate of 10667 m^3/min and sustained until the experiment's conclusion. Throughout the process, the numerical model calculated performance parameters such as oil rate, cumulative oil production, API gravity, produced oxygen concentration, and combustion peak temperature for historical matching.

3.1 Lab-scale Numerical Model

Ado et al.'s (2017) model employed the numerical simulator STARS by CMG. The thermal and flow simulator utilizes a fully implicit finite difference method to solve the discretized governing equations. Subsequently, the kinetic reactions equations are coupled with the transport equations to enable simultaneous solutions. Key input parameters were incorporated to address these equations, including porosity, saturations, permeabilities, initial pressure, and kinetic parameters.

3.1.1 Petrophysical parameters

The fluid saturations, porosity and permeabilities shown in Ado (2017) are as follows:

Table 3.1 Petrophysical parameters

So	Sw	Porosity	Vertical Permeability (mD)	Horizontal Permeability (mD)
0.85	0.15	0.34	3450	11500

Regarding the relative permeability curves (Figure 3.1), the model proposed by Ado (2017) used the data obtained from the work of Prowse et al. (1983). In order to gain more numerical stability, the curves were smoothened within the options of Builder.

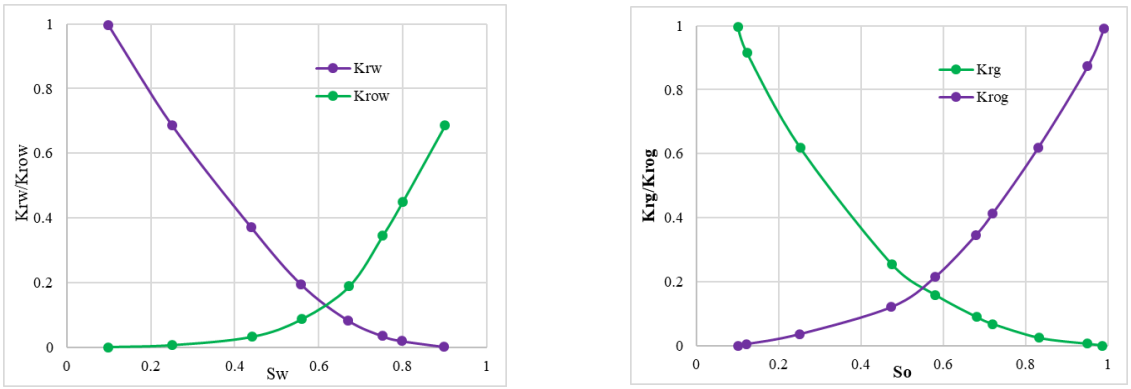

(a) (b)

Figure 3.1 (a) oil/water and (b) gas/oil relative permeability curves for the Athabasca bitumen (Prowse et al., 1983). Krw and Krow are the water and oil relative permeabilities at water saturation Sw, respectively, while Krg and Krog are the gas and oil relative permeabilities at oil saturation So, respectively. Adapted from Ado (2017).

3.1.2 PVT Data

To generate PVT data for the model, the equation of state Peng-Robinson available in the software Aspen HYSYS was used to form an oil blend with three Athabasca oil sands pseudo components. According to the model done by Ado (2017), three pseudocomponents were considered. These pseudocomponents and the PVT data are defined in the following table. The pseudocomponents are LC, MC and IC, light, mobile, and immobile components, respectively.

Table 3.2 PVT Data used in the study by Ado (2017).

Pseudo-components	LC	MC	IC
Fraction (mol%)	42.5	23.91	33.59
Molecular weight (g/mol)	210.82	496.81	1017.01
Pc (kPa)	1682.88	1038.46	729.22
Tc (°C)	464.68	698.53	940.36
ρ (kg m−3)	828.24	961.66	1088.04
Eccentricity	0.62	1.18	1.44
Boiling point temperature (°C)	281.47	549.67	785.78

In terms of the variation of Athabasca bitumen viscosities with respect to temperature (Figure 3.2), they were produced via the work by Mojarab et al. (2011). The viscosities for the LC and MC pseudo components were assigned to be the same as the ‘Light oils’ and ‘Heavy oils’ available in

STARS. On the other hand, the viscosity of the IC pseudocomponent was calculated using the viscosity nonlinear mixing rule equation as follows:

$$\ln \mu_{ph} = \sum_{j=1}^{n} x_{lm,j} \ln \mu_{lm,j} \tag{16}$$

where $x_{lm,j}$ and $\mu_{lm,i}$ are the linear mixing component mole fractions and viscosities, respectively.

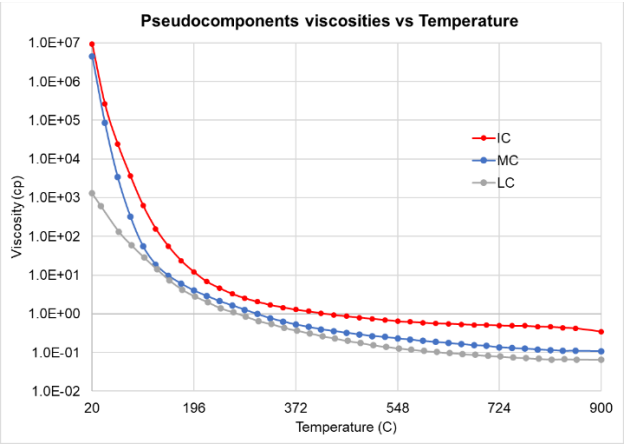

Figure 3.2 Pseudocomponents viscosities.

3.1.3 Kinetics

The kinetic scheme used in the study by Ado (2017) was taken from the work by Phillips et al. (1985). Given that the rate of coke deposition was not high enough to account for the coke deposition seen in the experiments and, therefore, the history match could not be correctly predicted, some tuning of the kinetic reactions of the coke depositing needed to be made. The frequency factors of reactions 3 and 4 were also slightly modified to match the experiments reported by Xia et al. (2002).

Table 3.3 Thermal cracking reactions kinetic data.

				Phillips et al. (1985)		Current Study	
No.	**Thermal cracking reactions**			**Frequency Factor (1/min)**	**Activation Energy (J/mole)**	**Frequency Factor (1/min)**	**Activation Energy (J/mole)**
1	IC	→	2.0471 MC	3.82E+20	2.39E+05	3.82E+20	2.39E+05
2	MC	→	0.4885 IC	3.37E+18	2.16E+05	3.37E+18	2.16E+05
3	MC	→	2.3567 LC	3.13E+15	1.81E+05	1.13E+15	1.85E+05
4	LC	→	0.4243 MC	1.22E+15	1.81E+05	1.52E+15	1.80E+05
5	IC	→	77.4563 COKE	6.96E+14	1.74E+05	2.32E+15	1.81E+05

In the coke combustion reaction (reaction #9), the frequency factor and activation energy were modified so that they matched the peak combustion temperature in the experiment. The coke undergoes a high-temperature oxidation combustion reaction, releasing heat to sustain an effective combustion front. The heat of this reaction has been adjusted to match the experimental peak temperature. Table 3.4 summarizes the main kinetic parameters for the involved combustion reactions.

Table 3.4 Combustion reactions kinetic data.

No.	Combustion reactions			Frequency Factor (1/min)	Activation Energy (J/mole)	Enthalpy (J/mole)
6	IC + 106.7 O2	→	78.9 CO2 + 4.2 CO + 46.9 H2O	1.81E+08	1.38E+05	4.00E+07
7	MC + 37.1 O2	→	28.1 CO2 + 1.5 CO + 22.4 H2O	1.81E+09	1.38E+05	1.60E+07
8	LC + 32.025 O2	→	11.2 CO2 + 0.6 CO + 14.5 H2O	1.81E+10	1.38E+05	4.91E+05
9	COKE + 1.22 O2	→	0.93 CO2 + 0.03 CO+ 0.57 H2O	1.00E+10	1.23E+05	3.90E+05

3.1.4 Boundary conditions

In order to simulate the model, it was assumed that there was a no-flow condition at the reservoir boundary, except in the horizontal injector and production well. The air injection rate started at 8000 cm^3/min, then increased to 12000 cm^3/min from 190 to 320 minutes. The constraints for the producer well were 270 kPa as minimum bottom hole pressure (BHP) and a total liquid production rate of 25 cm^3/min. It is also important to note that during the simulation, the heat loss only occurred via conduction from both overburden and underburden.

In reservoir modeling using CMG STARS, a no-flow boundary condition is commonly assumed for several reasons. First, it simplifies the model by treating the reservoir as a closed system, where fluids cannot flow in or out of the boundaries, ensuring that all dynamics are contained within the reservoir. This is particularly useful when focusing on internal processes, such as fluid movement near wellbores or the advancement of a combustion front in a THAI or in situ combustion (ISC) process, without external influences. Additionally, a no-flow boundary condition prevents unrealistic fluid gain or loss from outside the modeled area, ensuring more accurate predictions of pressure, saturation, and temperature. Since reservoir simulations typically represent a finite portion of the subsurface, applying no-flow boundaries isolates the model while allowing for more efficient computational resource usage. This assumption is also appropriate when the model

represents an isolated or sealed reservoir, or when the reservoir is large enough that flow across its boundaries would have negligible effects on the internal dynamics of the system.

3.1.5 Grid sensitivity

According to Ado (2017), different simulations were run to decide which mesh size to choose and to determine which one yielded the best resolution, taking into account computer efficiency. The method used by Ado (2017) was to use the dynamic gridding option (DYNAGRID) in CMG. The criteria used were that when the global mole fraction of any component was less than 3%, the oil mole fraction was <2%, pressure variation was within 20 kPa, and cell temperature was within 30 °C, the cell size would be restored to its original dimension. More on the grid sensitivity is found in the work by Ado (2017). Due to the results obtained with the variations of different gridblock numbers, the fine dynamic mesh of 38,000 gridblocks was used because it captured the most accurate results compared to the ones obtained in the original test. According to the physical experiment, there is no oil production from 18 to 30 minutes.

3.1.6 Results

3.1.6.1 Oil production

According to authors like Sur (2022), the start-up procedure is one of the most critical parameters for achieving good results in in situ combustion. An important thing notable in this model created by Ado (2017) is that no oil is present at the start of the simulation inside the horizontal producer before the pre-ignition heating cycle (PIHC). Figure 3.3 represents the results of the oil production throughout the whole duration of the simulation.

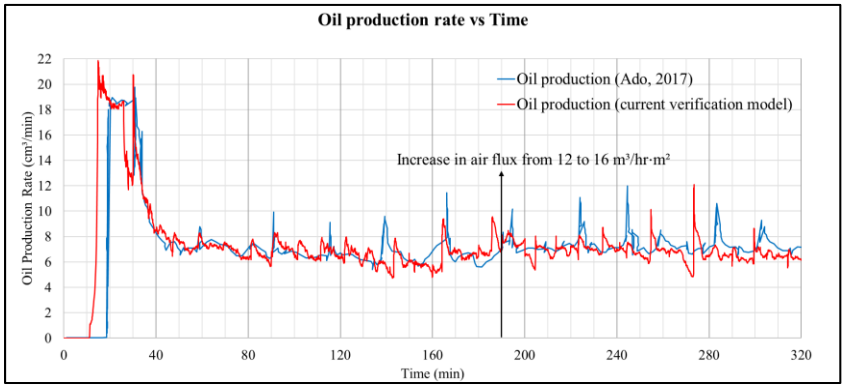

Figure 3.3 Comparison of oil production over time between Ado's (2017) numerical model (in blue) and the current study's verification model (in red).

The figure above shows a surge in oil production within the initial 20 minutes, as seen in Ado's (2017) model. This surge is attributed to the thermal generation of gases, leading to pressure buildup around the horizontal producer. This pattern is faithfully mirrored by the verification model in the current study. However, a notable difference lies in the timing of oil production onset: approximately 14 minutes in the validated model (in red) compared to 19 minutes in the original model (in blue).

Furthermore, while the maximum oil production recorded in the original model was 20 cm^3/min, the validated model achieved a maximum of 22 cm^3/min. Regarding average oil production, the original Ado's (2017) model reported an average rate of 8.89 cm^3/min, compared to 7.5 cm^3/min in the verification model. This variance can be attributed to an increased steam generation during the pre-ignition heating cycle, resulting in a pressure peak of 1553 kPa around the producer well, causing a pronounced spike in oil production.

It is worth noting that from 40 to 320 minutes, the oil production trend closely parallels that of the original model.

3.1.6.2 Peak temperature

As depicted in Figure 3.4, there is a notable alignment in the peak temperatures between the verification model and the original lab-scale model. Post-ignition, the maximum temperature reached is 900°C for the original model and 946°C for the verification model.

However, the simulation conducted by Ado (2017) presents a deviation from the replicated results. Unlike in the original model, there is no temperature spike at 160 minutes in the verification model simulation. This disparity could be attributed to the potential accumulation of coke in the original model, which was not observed in the replicated model. It is essential to recognize that this discrepancy may stem from numerical uncertainties, given that the parameters used in the numerical sections of both models were not identical. Moreover, differences in the versions of the STARS simulators used could have influenced the results.

During the initial 40 to 120 minutes, the replicated model exhibits higher temperatures, surpassing the original model by up to 100°C at 60 minutes. However, it is important to note that the

temperature of the replicated model was under-compensated compared to the original model from 250 to 320 minutes, with a difference of 50°C.

In summary, upon comparing the results obtained in this study, it is evident that the temperatures closely match throughout the simulation runtime, with an average peak temperature of 677°C and 667°C for the original and verification models, respectively.

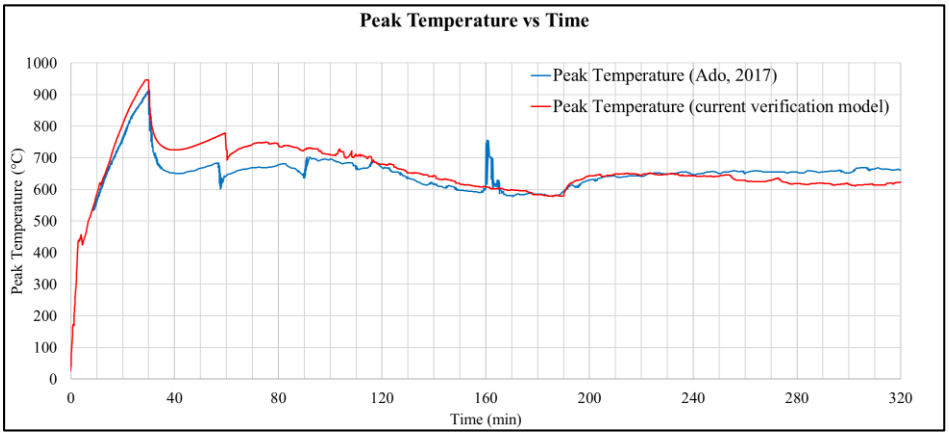

Figure 3.4 Peak temperature vs Time.

3.1.6.3 Oxygen production

The comparative analysis indicates a generally favourable correlation between the oxygen production simulations by Ado (2017) and those conducted in the current study. A significant difference is observed in the timing of the onset of oxygen production: it begins at approximately 130 minutes in the current research, in contrast to Ado's (2017) findings, which show a later start at around 180 minutes before increasing the air injection rate. Such findings are at odds with the hypothesis proposed by Greaves et al. (2012), who associate the start of oxygen production with the increase in air flux. Still, this increase in air flux did not occur until 190 minutes after the beginning of the simulation. The premature initiation of oxygen production could potentially be attributed to oxygen channelling. Further exploration into the mechanisms involved may provide insights into the early onset of oxygen production observed in this study.

Furthermore, the predicted oxygen concentration exhibits an oscillatory pattern, as seen in Figure 3.5. This behaviour is not attributed to numerical stability issues, as demonstrated through various mesh systems/types (Ado, 2017), which all indicated an oscillatory trend in oxygen concentration. This observation is corroborated by Kovscek et al. (2013), who reported a similar oscillatory trend. A comparable oscillatory behaviour is noted, albeit not as pronounced as in the predictions made

by Ado (2017). The oscillations are closely linked to the variations in coke concentration and the volume of oxygen along the horizontal producer (HP) well. The coke distribution along the vertical mid-plane alternates between high and low concentrations along the HP well, influencing oxygen consumption. According to Ado (2017), high coke concentrations lead to significant oxygen consumption at the HP well's toe, whereas lower concentrations of coke result in reduced oxygen consumption.

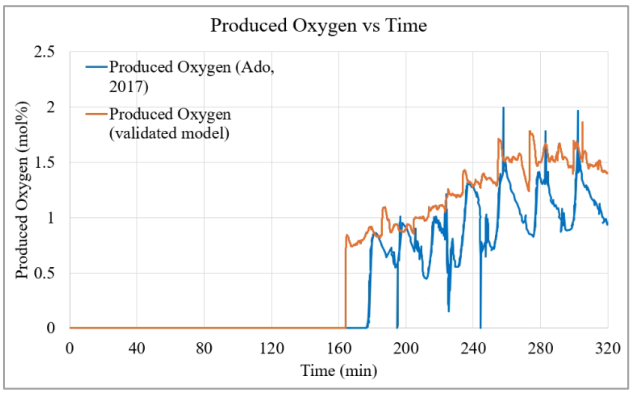

Figure 3.5 Produced Oxygen vs Time.

3.1.6.4 Fuel Availability

Given the vital role of fuel availability in ISC, the ability to accurately forecast it is a crucial indicator of a numerical model's reliability. The fuel consumption rate per reservoir volume serves as a critical metric for assessing the ISC process's stability and economic feasibility. Greaves et al. (2008) emphasized the importance of achieving an optimal fuel deposition during the initial phase of the THAI process, which is crucial for the successful advancement of the combustion front. It is essential that the deposited fuel level is balanced to prevent hindering the combustion front's progress or necessitating an excessively high air injection rate.

The fuel availability forecasted in this study aligns closely with the empirical data observed at the conclusion of the experiment, which spanned 320 minutes. In their experimental work, Greaves et al. (2012) recorded a fuel availability (coke) value of 85.4 kg/m³. Comparatively, as seen in Figure 3.6, the verification model presents an average predicted fuel availability of 93 kg/m³, situating it comfortably within the anticipated range for Athabasca Oil Sands, known for their unique

geological and compositional characteristics. This minor discrepancy between the observed and predicted values underscores the reliability of the simulation methodologies employed.

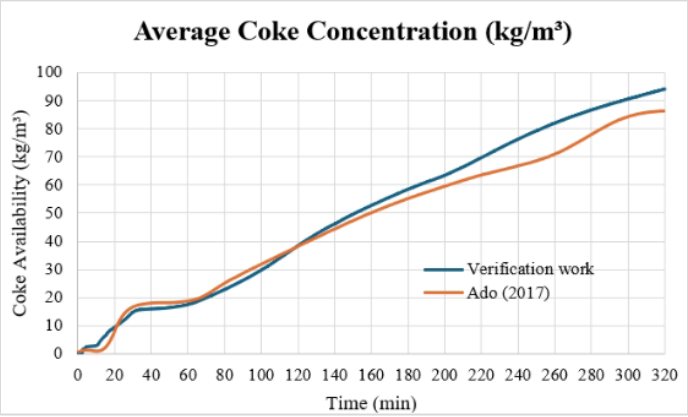

Figure 3.6 Comparison of Average Coke Concentration: Ado (2017) Model vs. Verification Model.

Additionally, coke deposition predominantly takes place ahead of the advancing combustion front. This spatial distribution of coke is critical, as it influences the dynamics of the combustion process, potentially affecting both the efficiency and sustainability of the in-situ combustion operation. Understanding this pattern is essential for optimizing the THAI process and ensuring its successful application in the Athabasca Oil Sands, where such techniques hold significant potential for enhanced oil recovery.

3.1.6.5 Fuel availability profiles

The results reveal differences in fuel concentration profiles between the original experimental and verification models. Specifically, Figures 3.7.a and 3.7.e illustrate that at the top of the original model at 150 minutes, the fuel concentration near the combustion front remains relatively steady, ranging from 35 to 40 kg/m³. In contrast, the validated model exhibits slightly higher concentrations, ranging from 40 to 50 kg/m³.

However, at 320 minutes, the validated model's fuel availability concentration profile (Figure 3.7.f) indicates a more uniform distribution at the leading edge of the coke deposition zone compared to the original model (Figure 3.7.b). While the original model's profile tends to narrow in the center, both models demonstrate similar fuel availability values of 30-38 kg/m³.

Figures 3.7.c and 3.7.g show that at 150 minutes, the fuel availability profiles of both models are remarkably similar in shape, having progressed only about 8 cm from the toe with concentrations

ranging from 59 to 78 kg/m³. Notably, both models demonstrate a significant accumulation of fuel inside the producer well, with the original model showing a concentration of 98 kg/m³ and the validated model exhibiting a higher concentration of 117 kg/m³.

At the end of the simulation (320 minutes), as shown in Figures 3.7.d and 3.7.h, both models reveal increasing fuel concentration below the horizontal producer well, with the coke zone advancing about one-third of the total axial length in the original model and about half the length in the validated model.

Furthermore, both models indicate that the fuel concentration in the vertical mid-plane (J layer: 10) at the end of the combustion period is around 59 kg/m³ in the original model and 70-90 kg/m³ in the replicated model. This suggests that although the replicated model shows slightly higher values of coke concentration due to numerical parameters, simulation tools, and computer efficiencies, the coke concentration profile remains comparable and falls within the expected realistic range.

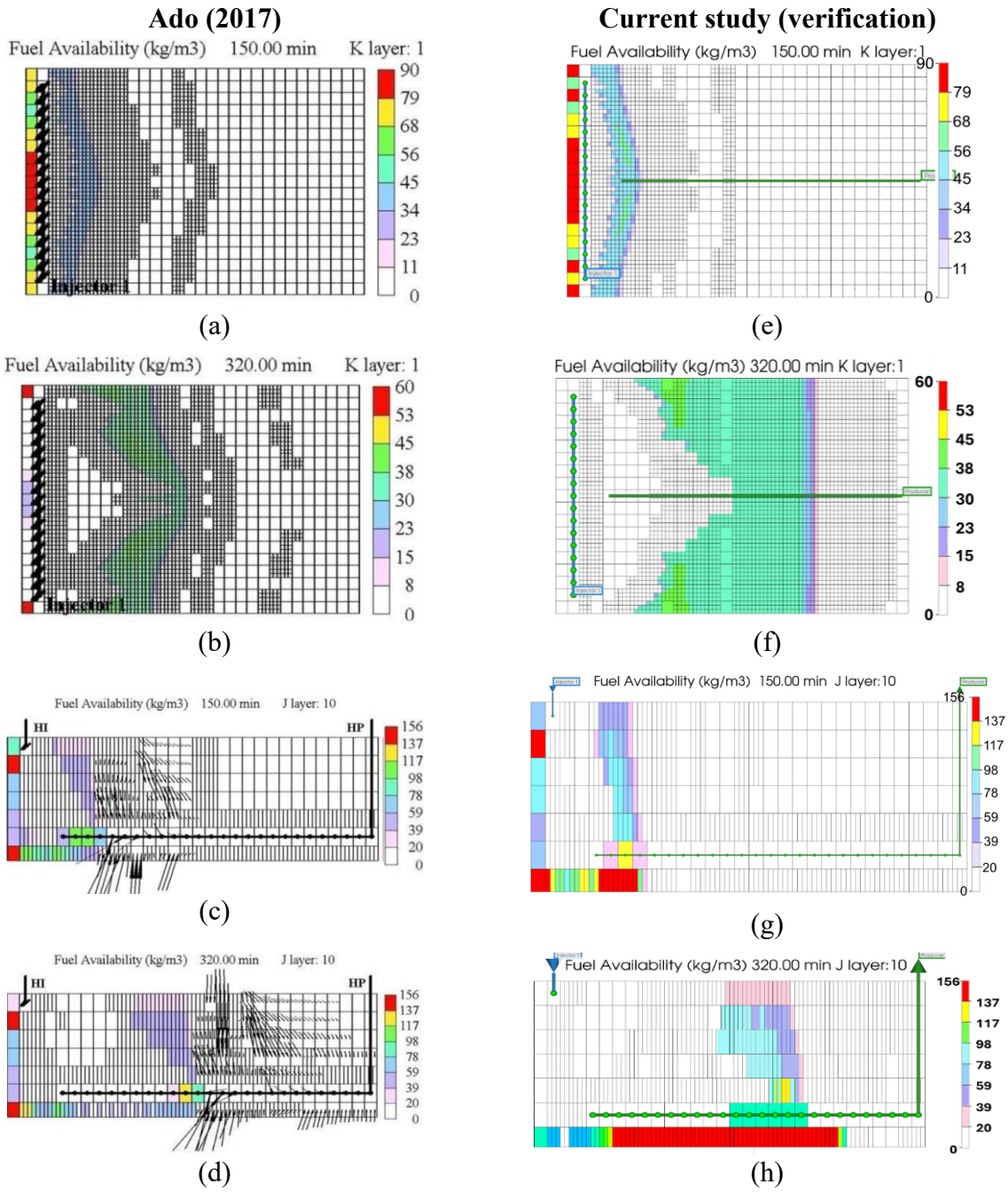

Figure 3.7 Fuel concentration profiles for Ado (2017) lab scale model at the top horizontal plane (K layer 1) at (a) 150 min, (b) 320 min; along vertical midplane (J layer 10) at (c) 150 min and (d) 320 minutes. Fuel concentrations obtained for the validated model at the top horizontal plane (K layer 1) at (e) 150 min, (f) 320 min, along vertical midplane (J layer 10) at (g) 150 min and (h) 320 minutes.

3.1.6.6 Temperature distribution

Figures 3.8.a through 3.8.h compare the temperature distributions in the original and validated models. These temperature maps are crucial for identifying where High-Temperature Oxidation (HTO) reactions occur. The maps highlight temperatures in the top layer and along the vertical

mid-sections. A key observation is the temperature around the coke combustion zones, which is approximately 400°C, signifying the occurrence and completion of HTO reactions. Notably, the combustion front in the verified model progresses more consistently and uniformly. However, it is crucial to recognize that the advance of the combustion front in the verification model is 20% slower than the original model. This discrepancy could stem from differences in stability and the methodologies used for dynamic gridding calculations by the simulator, potentially leading to varied outcomes. Despite these differences, both models effectively demonstrate the presence and forward movement of the combustion front over time.

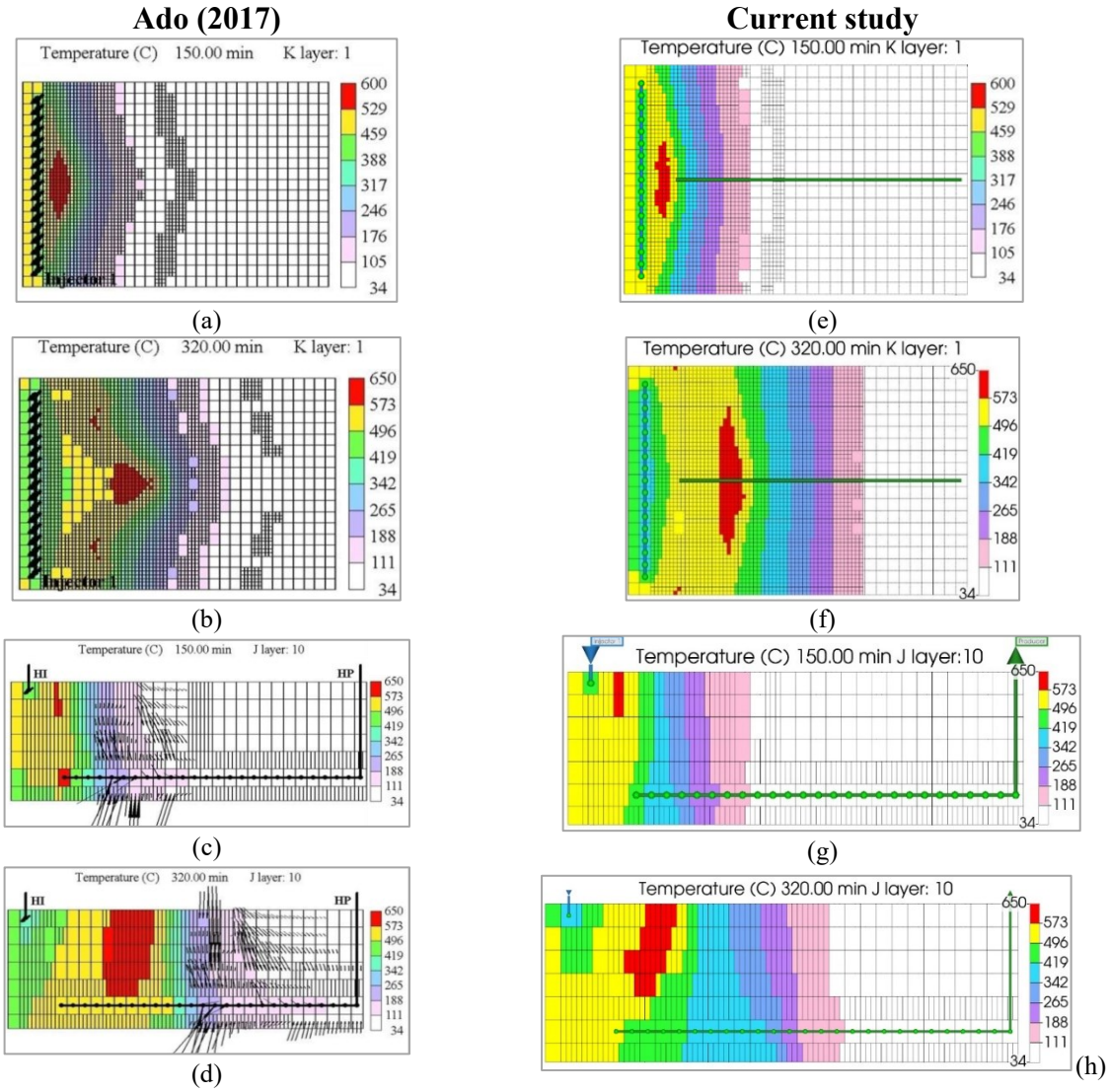

Figure 3.8 Temperature distribution profiles for Ado's (2017) lab scale model at the top horizontal plane (K layer 1) at (a) 150 min, (b) 320 min; along vertical midplane (J layer 10) at (c) 150 min and (d) 320 minutes. Temperature distribution profiles obtained for the validated model: at the top horizontal plane (K layer 1) at (e) 150 min, (f) 320 min, along the vertical midplane (J layer 10) at (g) 150 min and (h) 320 minutes.

3.1.6.7 Oil saturation

As depicted in Figures 3.9.a through 3.9.d, the mobile oil zone is visually represented by the red zone, indicating the accumulation and movement of oil propelled by the combustion front and flue gases. By 150 minutes, Figure 3.9.a illustrates that the trailing edge of the mobile oil zone has extended to approximately half of the axial length of the horizontal producer (HP). Comparing this with the verification model, Figure 3.9.b demonstrates that oil displacement has reached around 46% of the total axial well length.

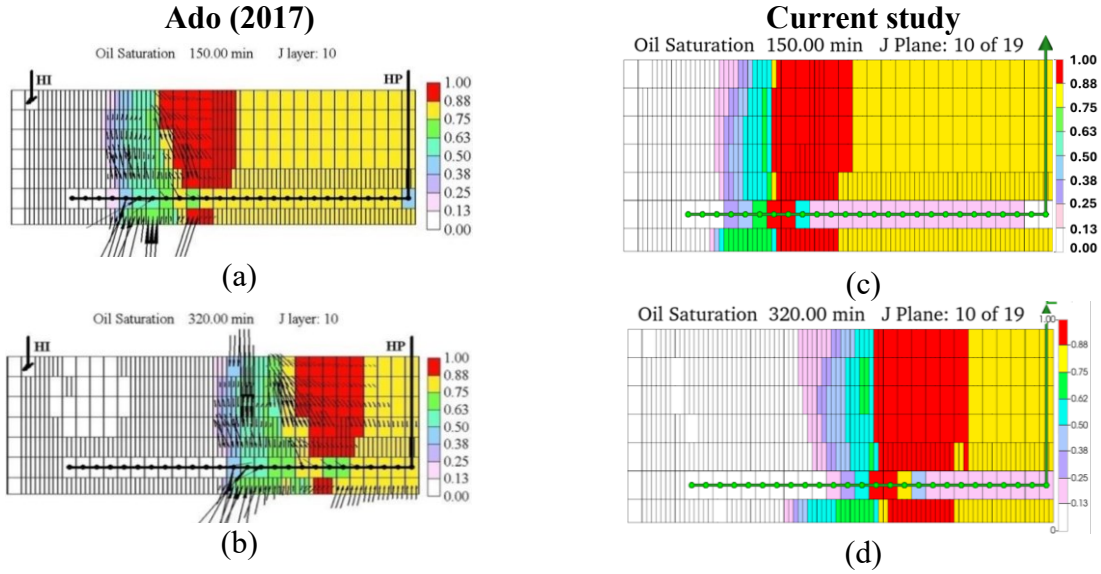

Figure 3.9 Oil Saturation profiles for Ado's (2017) lab scale model along the vertical midplane at (a) 150 minutes and (b) 320 minutes. Oil Saturation profiles for the current verification model along the vertical midplane at (c) 150 min and (d) 320 minutes.

At the conclusion of the combustion period, as observed in Ado's (2017) model, there is a notable advancement of the mobile oil zone along the axial length of the wellbore, reaching approximately 85% of the total horizontal wellbore length. This behaviour is in accordance with expectations, as demonstrated in the experimental work by Greaves et al. (2008). Comparatively, the verified model exhibits a similar trend, with the mobile oil zone extending to about 77% of the total horizontal production well length.

This significant alignment between the two models indicates a robust agreement in the behaviour of the oil saturation maps. Furthermore, the oil displacement in the models correlates closely with the temperature distributions observed in the temperature maps. It is noteworthy that higher

temperatures facilitate greater oil mobility, causing it to travel further down to the horizontal producer.

Interestingly, while both models demonstrate the expected movement of the mobile oil zone along the producer well, the replicated model showcases a more expansive and stable oil sweep toward the producer's heel. This broader sweep suggests enhanced oil displacement and recovery efficiency in the replicated model.

In summary, the consistent behaviour of the mobile oil zone in both models, coupled with the broad and stable sweep observed in the replicated model, underscores the robustness and reliability of the simulation results.

3.2 Field Scale Simulation of the THAI Process

3.2.1 Upscaling to Field Scale

When scaling from the lab scale to the field scale, it is crucial to understand that the kinetics employed in the lab scale cannot be used directly in the field scale model because of the grid block sizes (Zhu et al., 2011). In the lab scale, the length of each grid block is on the order of centimeters, while in the field scale, it is on the order of meters, several orders of magnitude higher. This suggests that the grid resolution may be insufficiently fine to accurately capture the combustion, typically within a two-centimetre thickness. The occurrence of reactions that produce coke, coupled with the fact that the reaction times are significantly longer than those in a lab-scale model, results in excessive fuel deposition. Therefore, the rate of this fuel deposition is many times higher than it should be in the field scale (Ado, 2017). This part of the thesis validates the upscaling method proposed by Ado (2017) by replicating the upscaled model.

3.2.2 Upscaling methodology

As seen in Ado's (2017) study, it was observed that an increase in grid block size without adjusting kinetic parameters leads to excessive fuel accumulation and consumption. The reported average fuel availability noted as 287 ± 135 kg/m³, coupled with inefficient oil displacement in front of the combustion zone, underscores the necessity of modifying kinetic parameters. This adjustment is vital for accurately depicting the underlying physicochemical processes.

First, in order to modify the kinetic parameters, a new material balance approach has to be adopted, as seen in Figure 3.10.

Figure 3.10 Grid block side view for material balance

The general material balance can be written as:

$$\text{Flow in } (F_{ijo}) + \text{Generation } (G_{ijo}) = \text{Flow out } (F_{ij}) + \text{Accumulation } (A_{ij}) \quad (17)$$

or as:

$$F_{ijo} + \int_0^V R_{ij}\,dV = F_{ij} + \frac{dN_{ij}}{dt} \quad (18)$$

where F_{ijo} and F_{ij} are the inlet and outlet molar flow rates of component i in phase j, respectively, R_{ij} is the rate of generation or consumption of the i-th component in the j-th phase, N_{ij} is the accumulated amount of component i in phase j inside the grid block, and V is the volume of the grid block (Ado, 2017).

Some assumptions can be made:

- The process is in a steady state. The accumulation term is zero.
- There is perfect mixing, and the temperature at every point is the same
- The reaction rate is uniform and independent of the reservoir volume

Therefore, Eq. 18 can be written as:

$$F_{ijo} - F_{ij} = -R_{ij} \int_0^V dV \quad (19)$$

Integrating the equation 19 gives:

$$(-R_{ij})V = (F_{ijo} - F_{ij}) \quad (20)$$

As the fuel availability determined in a lab cell should be the same at the field scale (Kovscek et al., 2013), the fraction of the i-th component converted to fuel at the experimental scale is the same as at the field scale.

$$\text{Fraction converted} = \frac{(-R_{ij})V}{F_{ijo}} = \frac{F_{ijo}-F_{ij}}{F_{ijo}} \tag{21}$$

Thus,

$$\left(\frac{-R_{ij}V}{F_{ijo}}\right)_{lab} = \left(\frac{-R_{ij}V}{F_{ijo}}\right)_{field} \tag{22}$$

Further information on performing upscaling for cracking and combustion reactions is provided below.

3.2.2.1 Downscaling the cracking reactions

In the context of the thermal cracking reaction, the coke formation rate from component i within phase j, also referred to as IC, adheres to a first-order reaction dependent on the concentration of component i. Therefore, the consumption rate of the pseudo-component IC is determined by:

$$-R_{ij} = kC_{ij} \tag{23}$$

in this scenario, "k" represents the frequency factor (expressed in min^{-1}), and "C_{ij}" denotes the concentration of component i. It is assumed that the component, whether within or surrounding the reaction area, maintains a steady temperature, leading to a uniform density, which implies:

$$C_{ij} = \frac{F_{ijo}(1 - X_{ij})}{q} \tag{24}$$

X_{ij} is the conversion of component i, and q is the volumetric flow rate. The equation 23 then becomes

$$-R_{ij} = \frac{kF_{ijo}(1 - X_{ij})}{q} \tag{25}$$

Substituting equation 25 into equation 22 results in

$$\left(\frac{kF_{ijo}(1 - X_{ij})}{q}\frac{V}{F_{ijo}}\right)_{lab} = \left(\frac{kF_{ijo}(1 - X_{ij})}{q}\frac{V}{F_{ijo}}\right)_{field} \tag{26}$$

As the conversion is the same, $(1 - X_{ij})$ is independent of the scale, and the above equation reduces to:

$$\left(\mathrm{k}\frac{\mathrm{V}}{\mathrm{q}}\right)_{\mathrm{lab}} = \left(\mathrm{k}\frac{\mathrm{V}}{\mathrm{q}}\right)_{\mathrm{field}} \tag{27}$$

the ratio V/q is called the space time, which is the time it takes to process a certain volume or gridblock based on the feed entrance condition. Therefore, the equation can be written as:

$$(\mathrm{k}\tau)_{\mathrm{lab}} = (\mathrm{k}\tau)_{\mathrm{field}} \tag{28}$$

where $k\tau$ is a dimensionless number called the Damkhöler number, which estimates the extent of conversion achievable. The left-hand side of the equation is known; however, for the field scale, neither k nor τ is known. In this case, the frequency factor is the adjustable variable, as it has to be included as an input parameter in the simulation:

$$\mathrm{k}_{\mathrm{field}} = \frac{(\mathrm{k}\tau)_{\mathrm{lab}}}{(\tau)_{\mathrm{field}}} = \frac{\mathrm{k}_{\mathrm{lab}}}{\mathrm{S}_{\mathrm{t}}} \tag{29}$$

here, St is the time scaling factor. In the field scale, the time is many times bigger than in the lab scale, so this leads to saying that in order to achieve the same representation at the field scale as in the lab scale, the frequency of the coke deposition reactions must be decreased by the same factor as the lab scale time was increased.

3.2.2.2 Downscaling combustion reactions

In the combustion reactions, oxygen consumption occurs at a rate that is first order in relation to the partial pressure of oxygen, making it second order in total. Consequently, the Damkhöler number, as outlined in Eq. 30, depends on the partial pressure of oxygen within the reservoir, as detailed by Fogler (2006), and can be expressed as

$$(\mathrm{k}\tau\mathrm{P})_{\mathrm{lab}} = (\mathrm{k}\tau\mathrm{P})_{\mathrm{field}} \tag{30}$$

where P is the reservoir pressure. Because air is used as the oxidizing fluid, the mole fraction cancels out.

Rearranging the equation 30 gives:

$$k_{field} = \frac{(k\tau P)_{lab}}{(\tau P)_{field}} = \frac{k_{lab}}{S_t \cdot S_p} \quad (31)$$

where S_p is the pressure scaling factor, which is the ratio of the field reservoir pressure to the experimental cell pressure. The experimental model was run at a pressure of 200 while in the actual reservoir, the pressure was 2800 kPa, which made the S_p=14.

3.2.3 Results and Discussion

In Ado's (2017) work, the upscaling method was implemented in the lab scale model, and the cracking and combustion reactions were successfully downscaled using a time scaling factor (S_t) of 4670, obtained through trial and error (further detailed in Ado (2017)). Additionally, a pressure scaling factor (S_p) of 14 was applied. Following these adjustments, a numerical field scale model named P1 was created with dimensions of 150 m × 100 m × 24 m (as shown in Figure 3.11). These dimensions are similar to those of Petrobank's THAI project near Conklin, Alberta.

The model has two vertical injectors (2VI), which are perforated only at the top of the reservoir and one horizontal producer (HP) arranged in a staggered line drive pattern (SLD). In his thesis, Ado (2017) names this model as 'Model P1', which was operated at a steady air injection rate of 20,000 m³/day over a two-year combustion period to evaluate fuel availability and oil extraction rate.

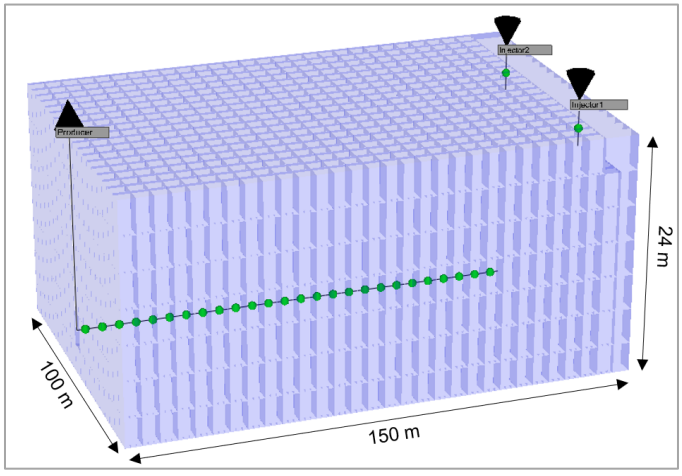

Figure 3.11 Dimensions of the field scale model.

Some operating parameters of this model are presented in the following table:

Table 3.5 Key Properties of the P1 Field Scale Model by Ado (2017).

	I	J	K
Reservoir Dimensions, m	150	100	24
Number of refined grid blocks	90	57	7
Total number of grid blocks	35910		
Well Arrangement	2VIHP		
Initial reservoir temperature and pressure	25°C and 2800 KPa		
Initial oil and water saturations	0.8 and 0.2		
Porosity	34%		
Absolute permeability	6400 mD	3450 mD	
Well internal diameter	178 mm (7 in)		
Producer back pressure	2800 kPa		
Steam injection pressure	5500 kPa		
PIHC duration	104 days		
Steam injection rate	78 m^3/day		
Air Injection rate	20000 m^3/day		

Considering the aforementioned properties and the downscaling of thermal cracking and combustion reactions, the verification of Ado's (2017) field-scale Model P1 was conducted as part of the current research objectives. This model, hereafter referred to as Model A1, represents the verification of the field-scale model. The comparison between the original study results and those obtained from the verification model, constructed using the thermal simulator STARS, is presented herein.

3.2.3.1 Oil production.

For both the models P1 and A1, the simulation commenced with steam injection (Pre-Ignition Heating Cycle or PIHC) into each of the two injector wells, continuing for 104 days at a rate of 39 cubic meters per day (equivalent to a total of 500 barrels per day) through each well. The injected steam was maintained at a temperature of 271.3°C with a quality of 0.8.

Following this initial 104-day period of steam injection, air injection commenced at a rate of 10,000 cubic meters per day for each injector well. Notably, in model P1, oil production commenced 58 days post-initiation of the steaming process, contrasting with model A1 where oil production was delayed until day 473, marking a significant 415-day discrepancy between the two models, as seen in Figure 3.12. Therefore, to facilitate a consistent comparison between both models, a time difference of 415 days will be used to account for the discrepancy in the timelines

of the two models. This is why the end of the combustion time for Model A1 was considered to be 1247 days.

Unlike model P1, the verification model's oil production ramped up at a considerable amount of time after the end of the PIHC. This disparity might be attributed to unidentified changes in parameters or properties during the upscaling from the lab-scale model. Oil production in model P1 commenced significantly earlier than the actual field pilot, which began 90 days after the initiation of steam injection.

In model P1, oil production started nearly two months after the PIHC started, reaching a peak production of 170 m³/day, then dropped to under 75 m³/day within an additional week. During the combustion phase, the average oil production was approximately 36 m³/day for model P1 and 27 m³/day for model A1, indicating a close match as illustrated in Figure 3.12. The consistent slope of the cumulative oil production curve throughout this period suggests a stable oil extraction rate.

The cumulative oil production reached 28420 cubic meters by day 834 (and 30.5% OOIP) in the P1 model, while model A1's total production was nearly 26500 cubic meters, this gives a difference of only 7 %. This is indicative of a close match.

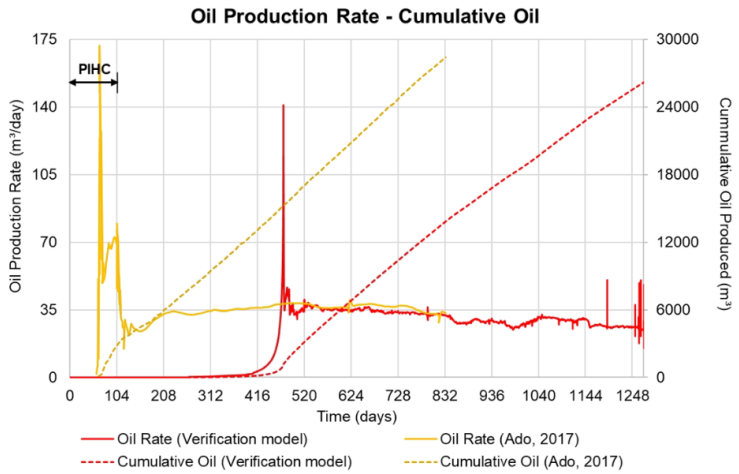

Figure 3.12 Comparative Analysis of Oil Production Rate and Cumulative Oil: Original vs. Validated Models

3.2.3.2 Fuel availability

Fuel availability is a critical parameter in sustaining the optimal performance of the in-situ combustion method. As previously seen, the oil that is thermally converted to coke acts as a fuel that is deposited on the sand face. As the coke is being deposited, it is burned off simultaneously,

so there has to be an optimal ratio of deposition to disappearance of this coke to avoid an effect called ‘overcoking.’ Overcoking is detrimental to the correct behavior of in situ combustion, as stated by Stosur (1977).

According to the results presented in Ado's (2017) study, the fuel availability at the end of the combustion period (834 days) at the horizontal midplane ranged from 18 to 24 kg/m³, as shown in Figure 3.13.a. Comparatively, model A1 exhibited a fuel availability at the horizontal midplane at the end of the simulation period (1247 days) ranging from 30 to 54 kg/m³, as depicted in Figure 3.13.d.

The distribution of fuel availability along the vertical midplane at the end of the simulation indicates a uniform coke distribution in model P1, as illustrated in Figure 3.13.b. For model A1, the average fuel concentration ranged between 10 to 24 kg/m³ at the end of the combustion period. Notably, a more pronounced accumulation of coke was deposited at the bottom of model A1. Some parts of the horizontal producer show an indication of overcoking. A possible explanation for this phenomenon is the influence of thermal conduction, which becomes the dominant heat transfer mechanism in the scenario described. As oil flows down to the horizontal well, some heat is transferred to the underlying oil beneath the horizontal producer. According to Marjerrison et al. (1992), in this region, only thermal cracking reactions tend to occur, leading to the consumption of the immobile pseudo-component (IC) and resulting in a high concentration of coke. Given the specific geometry of the area and the limited ability of oxygen to reach this zone, the coke does not combust, thus accumulating over time.

Figures 3.13.c and 3.13.f show the fuel availability profiles at the base of the reservoir for model P1 and model A1. The validated model showed a much higher coke concentration compared to the original model because the validated model presented values greater than 24 kg/m³ compared to the maximum values of 0.55 kg/m³ for the original model, which aligns with the results obtained in the experimental model carried out by Greaves et al. (2012).

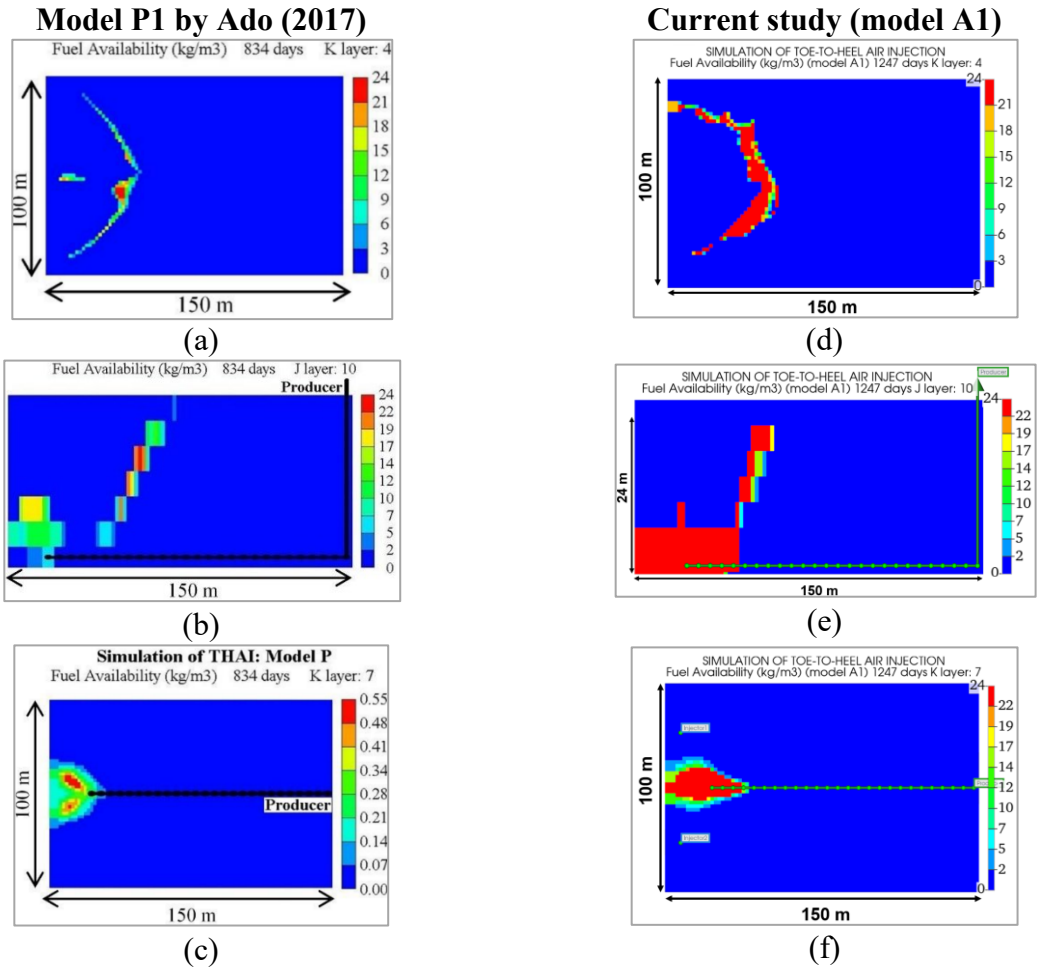

Figure 3.13 Fuel Availability Profiles Comparison between Original (Model P1) and Replicated (Model A1) Field-Scale Models. Model P1 at 834 days at (a) aerial view on K layer 4, (b) vertical midplane J layer 10, (c) aerial view on K layer 7. Model A1 at 1247 days at (d) aerial view on K layer 4, (e) vertical midplane J layer 10, (f) aerial view on K layer 7.

3.2.3.3 Oil Saturation

Oil saturation profiles are depicted in Figures 3.14.a through 3.14.f. Notably, Figures 3.14.a and 3.14.d illustrate the aerial view of the oil saturation profiles, revealing an oil sweep that gradually narrows down at the center of the model. Within model P1, distinct oil saturation regions are observable, with the mobile oil region represented in red. However, this zone is less prominent compared to replicated model A1, where a significantly higher fraction of oil has been swept, resulting in the formation of a more uniform oil saturation zone ahead of the combustion front.

Upon comparing both oil saturation profiles, it is evident that the oil sweeping front has advanced 45% and 52% for models P1 and A1, respectively. In model P1, a connection between the injectors and the producer wells is established by the end of the post-ignition heating cycle (PIHC) on day 104, as seen in Figure 3.14.b. During this time, the oil in the affected zone is displaced due to

steam expansion, thereby mobilizing oil to the horizontal producer well. Conversely, this communication does not occur in replicated model A1 until day 517 (Figure 3.14.e).

In Figure 3.14.c, the oil flux vectors along the vertical mid-plane visually represent the mobile oil zone. These vectors delineate two distinct groups: those oriented vertically, pointing towards the horizontal producer well, and those slightly slanted, pointing towards the toe of the HP well. The latter group indicates that the oil is flowing in a direction opposite to that of the combustion front, while the former denotes oil drainage above the well, solely influenced by gravity.

This behaviour, along with the delineation of the two oil flux vector groups, is also evident in the replicated model (Model A1), as depicted in Figure 3.14.f. The consistent portrayal of these dynamics across both models underscores the reliability of the simulation results and provides valuable insights into fluid dynamics and reservoir characteristics during oil recovery processes.

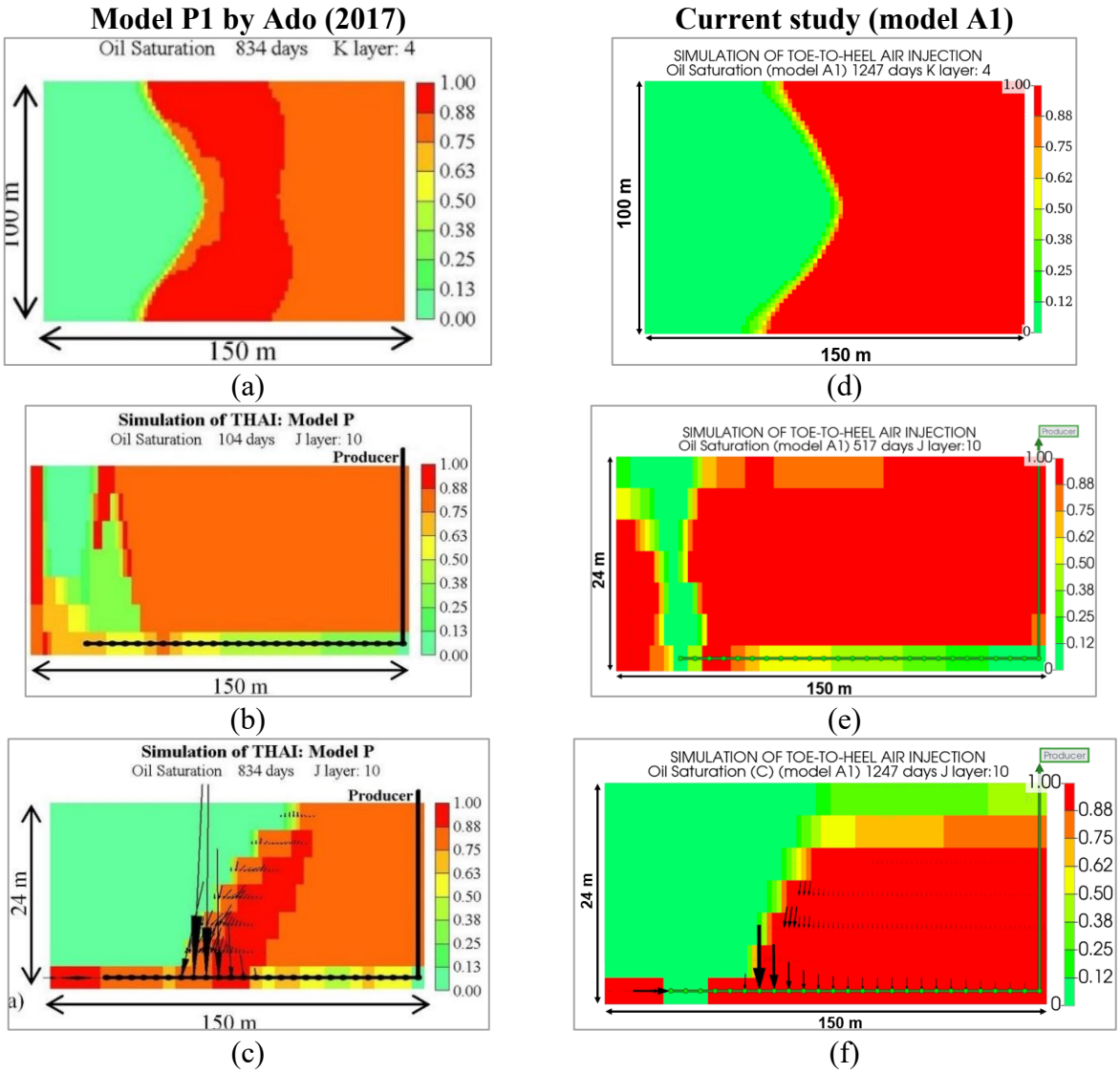

Figure 3.14 Oil saturation profiles for model P1 by Ado (2017) are shown for (a) day 834 at the horizontal midplane, (b) day 104 at the vertical midplane, and (c) day 834 at the vertical midplane. The oil saturation profiles for the verification model A1 are shown for (d) day 1247 at the horizontal midplane, (e) day 517 at the vertical midplane, and (f) day 1247 at the vertical midplane.

3.2.3.4 Temperature

As previously detailed, the pre-ignition heating cycle (PIHC) involved steam injection during the initial 104 days of simulation for models P1 and A1. This process aimed to establish communication between injector wells and the horizontal producer. After the PIHC, the vertical midplane temperature profile of model P1, as depicted in Figure 3.15.a, indicates that the area affected by steam injection had already attained a steam saturation temperature of 230°C.

In contrast, for the replicated model (Model A1), this temperature threshold and subsequent well communication were only achieved by day 517. While both temperature profiles exhibit

similarities, Model P1 illustrates complete saturation of the horizontal producer's toe with steam, resulting in its temperature reaching 230°C. Conversely, in the replicated model, only one perforation of the horizontal producer well achieved this temperature.

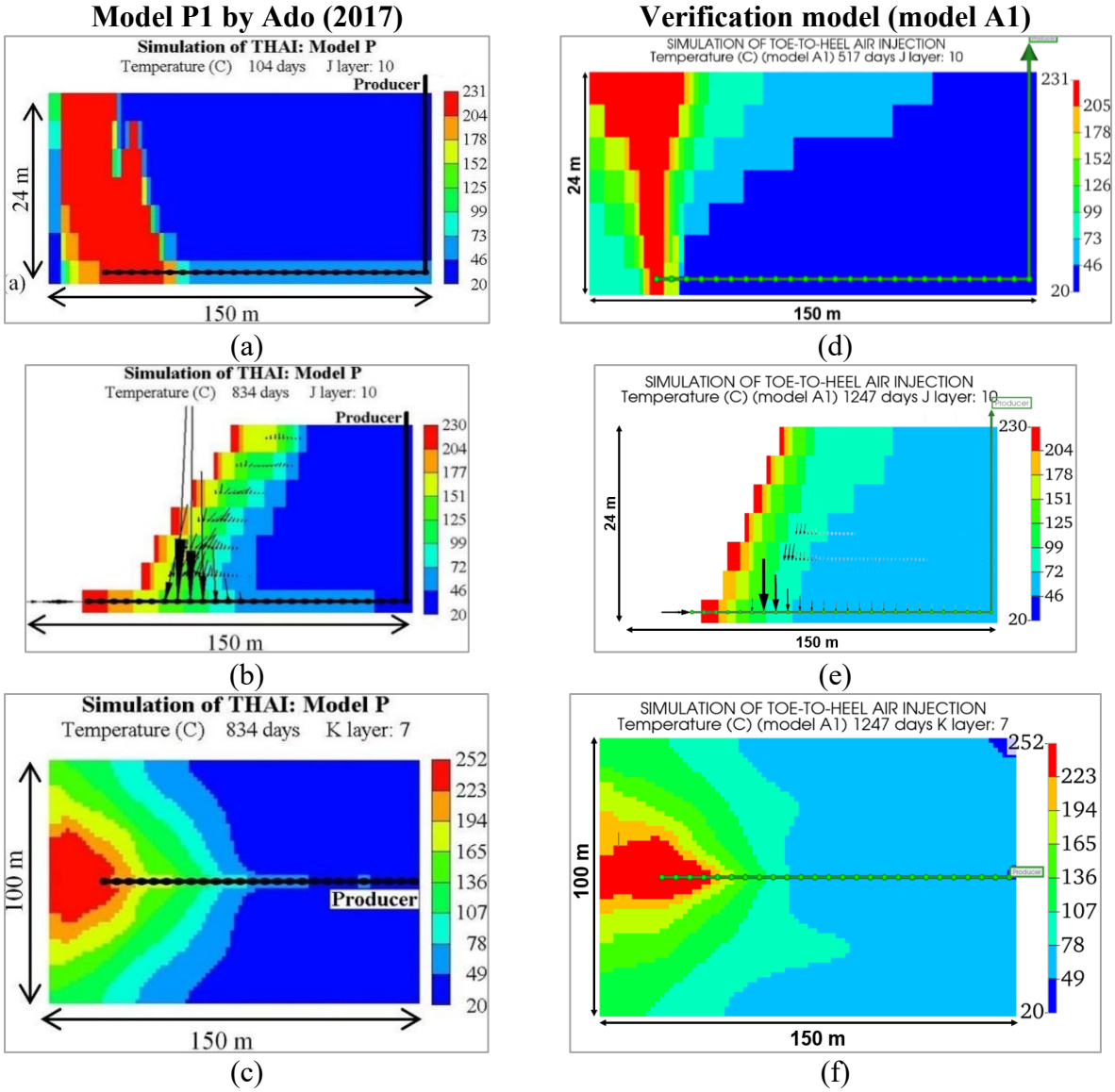

Figure 3.15 Temperature (°C) profiles for model P1 by Ado (2017) are shown for (a) day 104 at the vertical midplane, (b) day 834 at the vertical midplane, and (c) day 834 at the horizontal midplane. The temperature (°C) profiles for the verification model A1 are shown for (d) day 517 at the vertical midplane, (e) day 1247 at the vertical midplane, and (f) day 1247 at the horizontal midplane.

In Model P1, temperatures along the vertical mid-plane at the simulation's conclusion span from 72°C near the cold oil region to 150°C in proximity to the combustion front. Similarly, the temperatures in the replicated model align with those observed in Model P1, with one notable

exception: a region in the upper part of the reservoir where temperatures tend to rise, reaching around 78°C. This discrepancy is not present in the original field-scale model, Model P1.

The explanation for this discrepancy lies in the channelling of steam in the horizontal top layers, a phenomenon absent in the original field-scale model.

A significant accumulation of oil is observed at the toe of the horizontal well, accompanied by substantial production activity. According to the original field-scale model, temperatures in this area reach up to 250°C, whereas in the replicated model, the temperature peaks at 290°C. Moving farther downstream, approximately halfway along the horizontal producer well, the temperature drops to 72°C. This temperature trend is consistent with Model A1, indicating robust replication of thermal behaviour.

Moreover, in alignment with the findings from oil saturation maps, the mobile oil zone exhibits major oil flux vectors situated roughly one-third of the distance from the well's toe. According to Ado (2017), the longest oil flux vectors extend over a distance of 60 meters, constituting approximately 45% of the total well length. In contrast, the replicated model's results suggest that the mobile oil zone spans approximately 40 meters, accounting for roughly 30% of the total well length.

3.3 Conclusions

The verification of the numerical lab-scale and field-scale models found in the thesis carried out by Ado (2017) was successful, and this verification was based on the available information found in the original work. The Phillips et al. (1985) kinetic data and the PVT data made available were used to successfully verify the lab scale model proposed by Ado (2017), which originally intended to history match the 3D combustion cell experiment carried out initially by Xia and Greaves (2002). The kinetic upscaling methodology employed by Ado (2017), based on the downscaling of the frequency factors used in the thermal cracking and combustion reactions of the kinetic model, was successfully done to account for the bigger grid size in the field-scale scenario.

In the numerical lab-scale model verification work, there was a close match of the oil production rate, peak temperature (average temperature), and the oxygen production rate, which was also comparable. The fuel availability results closely matched the real values obtained from the post-mortem analysis of the 3D combustion test experiment conducted by Greaves et al. (2012) and

were more accurate than the results from the lab-scale numerical model conducted by Ado (2017). Although there were some differences in the values of the fuel availability profiles, the values predicted in the verified numerical lab-scale model were still within the acceptable range.

The numerical lab-scale model results included temperature maps that identified where high-temperature oxidation reactions occurred. Temperature profiles in the verified model showed increased temperatures around coke zones and a more consistent advancement compared to the results obtained by Ado (2017). However, the lab-scale model by Ado (2017) demonstrated a 20% more rapid temperature advancement than the verified model.

The numerical lab-scale model results, in terms of oil saturation at the end of the simulated period and the advancement of the mobile oil zone (MOZ), indicate that the verification work shows oil has travelled 77% of the total horizontal well length, compared to 85% in the original work conducted by Ado (2017).

Chapter 4: Applicability of Toe to Heel Air Injection under different configurations

4.1 Introduction

After successfully verifying Ado's (2017) lab scale and field scale numerical models against the current research numerical models, the focus of this chapter shifts to evaluating various alternatives for the THAI process. Initially, it is observed that the injection points in model A1 (field scale model) are positioned very close to the left (inlet) boundary, suggesting that air is predominantly directed towards the producer well—a scenario that does not entirely reflect real-world conditions. To enhance the accuracy and validity of the model, more realistic modifications have been implemented. Specifically, expanding the boundaries of the model allows the fluids to flow more freely, not just being funnelled directly toward the producer well. This adjustment provides a more flexible and realistic simulation of fluid dynamics within the reservoir.

Another significant modification implemented is the use of deeper injector wells that extend throughout the entire depth of the reservoir. In the verified field scale Model A1, the injector wells were only perforated at the top of the reservoir. By extending the perforations to the bottom, the model could achieve a more comprehensive oil sweep, resulting in improved performance and oil recovery.

Later in this chapter, a model is introduced that employs a single well to serve both as an injector and a producer. This dual-purpose approach is a central innovation of this thesis and a novel methodology in its field. It uniquely enables air injection at the toe of the well while oil is produced along the heel. While this method poses specific challenges, its potential to significantly enhance recovery efficiency is considerable and justifies the detailed exploration proposed in this chapter. The chapter discusses both models: one using a single wellbore with a stationary injection interval at the toe and another where the air injection interval progresses along the single wellbore, shifting every 18 and 24 months.

4.2 Models design

The numerical models were constructed and analyzed using CMG's thermal simulation software STARS. These simulations were designed to replicate the conditions of the toe-to-heel air injection

processes, adhering to the same parameters established during the verification stage of both the lab-scale and field-scale models proposed by Ado (2017).

Regarding grid dimensions, two distinct setups were employed: the first maintained the dimensions used in the verified field-scale model A1 (150 m x 100 m x 24 m), while the second expanded these boundaries. Specifically, the expansion increased the dimensions in the J direction threefold to 450 meters, in the I direction by 2.57 times to 257 meters, while the dimensions in the K direction remained constant at 24 meters. This expansion was critical to assess the effects of a larger spatial scale on the process dynamics.

Petrophysical parameters, PVT data, and kinetic rates were consistent with those used in model A1. Notably, the kinetic data employed had been previously upscaled, as detailed in Chapter 3. This consistency was crucial for ensuring the reliability of the simulation outcomes by comparing them across different scales and setups.

Regarding boundary conditions, the simulations adhered to a no-flow boundary condition for all external boundaries to mimic a closed-system environment. Similarly, wellbore constraints regarding flow rate and bottom hole pressure were aligned with the specifications outlined in Chapter 3.

The primary assumption underpinning these models was the absence of material flow into or out of the underburden or overburden, implying that heat loss within these models occurred solely through conduction. This assumption is vital as it influences the thermal dynamics within the system, impacting the overall efficiency and effectiveness of the heat management strategy in the simulated toe-to-heel air injection process.

This chapter explores a series of models designed to refine and expand our understanding of the THAI process. Each model introduces specific variations to enhance oil recovery through strategic modifications in well design, boundary expansion, and injection protocols.

Model B: This iteration extends the depth of the injector wells from the initial design found in Model A1 to the final layer, specifically layer number 7. This extension is intended to explore the effects of air injection through multiple perforations along the injector well rather than the single perforation in layer one used in Model A1. This model aims to advance the combustion front more

effectively by injecting air across these additional K layers and potentially increasing oil production.

Model C: Operating at the field scale, this model retains the wellbore positioning of Model A1 but extends the boundaries of the model. Air is injected from the top (i.e. from K layer 1), with the injection rate experimentally varied between 20,000 and 40,000 m^3/day. This modification is designed to assess the impact of increased air volume on the efficiency of the combustion process and oil recovery.

Model D: This model introduces a novel approach by featuring a single horizontal well situated at the bottom of the reservoir, acting as an injector and producer. The air is injected solely through the last perforation at the toe of the well, and this injection point remains stationary throughout the simulation period. This setup tests the efficacy of a fixed injection point in maintaining a stable and controlled combustion front.

Model E: Similar to Model D regarding injection behaviour, Model E also features a stationary injection point through the last perforator at the toe of the single horizontal well. However, this model includes expanded boundaries in the I and J directions to examine how increased spatial dimensions affect the distribution and efficiency of the injected air.

Model F: This model retains the original dimensions of Model A1 (150 m x 100 m x 24 m) and employs a single horizontal wellbore configuration that serves dual functions as both injector and producer. Unlike Model D, the air injection point in Model F is not static but is strategically moved along the horizontal well every 18 months to optimize air injection locations, thus enhancing control over the combustion front propagation.

Model G: Utilizing the same input parameters and moving injection interval of 18 months as Model F, Model G extends the boundaries to match those of Model E. This adjustment investigates how larger spatial domains, coupled with dynamic injection strategies, influence overall process efficiency and oil recovery.

Model H: This field-scale model mirrors the configuration of Model G but adjusts the air injector interval movement every 24 months. This variation aims to evaluate the effects of a slower

progression of the injection point on the combustion dynamics and the potential benefits in terms of oil recovery and operational flexibility.

Each model addresses specific research questions related to optimizing the THAI process, focusing on how variations in well design, injection strategies, and field dimensions can collectively enhance oil recovery efficiency.

4.3 Case-by-Case Analysis of THAI Variations: Results Overview

4.3.1 Model B: field-scale model with two vertical wellbores perforated throughout the reservoir's depth, paired with a horizontal producer well

4.3.1.1 Model description

Model B was developed to explore whether extending the depth of injector wells could enhance the effectiveness of the process. In this modification, both injector wells were perforated from the first to the seventh layer of the original reservoir, contrasting with the previous well configuration in model A1, where the injectors only perforated the first layer at the top of the reservoir. All other operational parameters and wellbore configurations outlined in Table 3.5 were kept identical to the previous setup. Both models utilized a staggered line drive pattern, allowing for a direct comparison to determine the impact of the extended well depth on the overall process efficiency.

4.3.1.2 Oil production

As depicted in Figure 4.1, oil production in Model B began just before the conclusion of the PIHC at 100 days, reaching an initial peak of 370 m^3/day. This notable peak can be attributed to the accumulation of high pressure from the steam injected during the pre-ignition heating cycle, which coincided with the steam's arrival at the production well during this period (Figure 4.2).

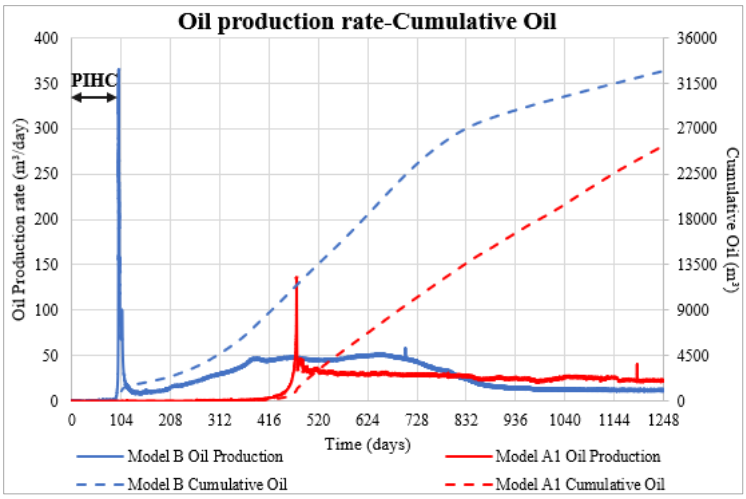

Figure 4.1 Oil production compared Model A1 and Model B

Subsequently, the production rate followed an upward trend, stabilizing at an average of 48 m³/day over the next 350 days. Following this period, there was a decline in production, with the rate dropping to an average of 8.5 m³/day, which persisted until the end of the simulation at 1248 days. The cumulative production rates initially displayed a steady incline, indicative of stable oil production during the first 800 days. However, this trend experienced a slight downturn due to the subsequent reduction in the oil rate. Ultimately, the extension of the injector wells in Model B resulted in a cumulative oil production of 32,700 m³, representing a 23.4% increase over Model A1.

The increase in oil production from day 365 until 670 can be attributed to oil accumulation at the toe of the well. The gas ahead in the horizontal well pushes this oil bilaterally, increasing pressure at the well's base. Consequently, the air does not start sweeping the oil from the last perforation at the toe of the well; instead, it begins sweeping approximately 40 meters ahead of the last perforation. From this point, it continues sweeping toward the toe of the well, a behaviour not observed in Model A1. After sweeping the portion between the toe of the well and the initial

sweeping point, production declines because the accumulated oil at the toe has already been produced.

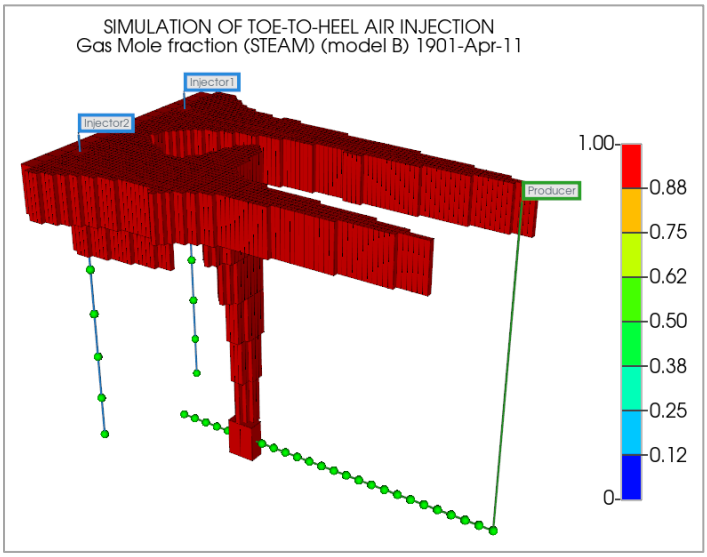

Figure 4.2 Steam mole fraction for model B at 100 days (1901-Apr-11)

4.3.1.3 Fuel Availability

Fuel availability is one of the most crucial aspects of determining the success of an in situ combustion project (Greaves et al., 1997; Turta et al., 2018; Storey et al., 2022). Its accurate prediction could be considered one of the most robust predictions of a numerical model (Ado, 2020). Authors like Greaves et al. (2008) suggest that the amount of fuel consumed per unit volume of the reservoir is an excellent parameter to evaluate the stability of the ISC. In the same regard, obtaining the right fuel laydown during the start-up phase of ISC is one of the main requirements for successful combustion front propagation. So, the amount of fuel should not be so high that it stalls the combustion front or needs an excessive air injection.

In this model, as the steam that was injected established direct communication with the producer well on the 100th day within the pre-ignition heating cycle, then this heat released to the surrounding bitumen triggered the occurrence of the thermal cracking reactions and thus provoked the accumulation of coke as shown in Figure 4.3.a. Figure 4.3.b shows that the average fuel

availability at the end of the combustion period (1248 days) was of 53 kg/m³, which closely match the average fuel availability obtained in the lab-scale model simulation performed by Ado (2017).

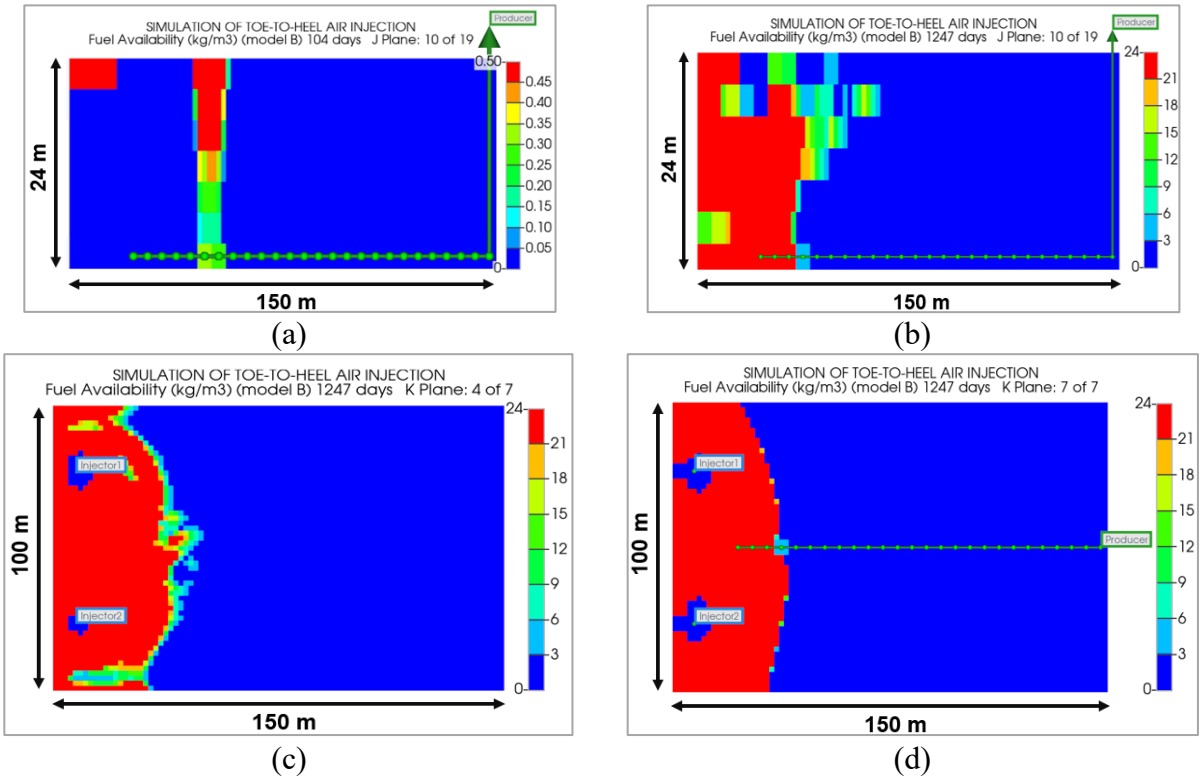

Figure 4.3 Fuel Availability (kg/m³) at different time points and perspectives. a) Side View at 104 Days: J Plane 10 of 19 b) Side View at 1247 Days: J Plane 10 of 19 c) Aerial View at 1247 Days: K Plane 4 of 7 d) Aerial View at 1247 Days: K Plane 7 of 7

Figures 4.3.c and 4.3.d show the fuel availability profiles at the end of the simulated period for the aerial views located at layers four and seven, respectively. A significant difference is evident when comparing the fuel availability in the horizontal midplane between Model A1 (Figure 3.13.d) and Model B (Figure 4.3.c). In Model A1, there is a defined narrow coke deposition zone advancing, whereas in Model B, there is no such thin zone of coke. This absence indicates an imbalance between the coke being deposited and the coke being burned. This imbalance could lead to suboptimal performance of the operation, necessitating further investigation to adjust the oxygen flux and sustain an optimal in-situ combustion performance.

Similarly, continuing with the same analysis, the coke deposition profile at the base of the reservoir in model B (figure 4.3.d) indicates a high density of coke which means overcoking. Given the high oxygen flux, in this model, we can see how detrimental the elongation of the injection wells is for

the combustion front. Fuel availability reaches a very high and unrealistic value of 1366 at the base of the reservoir compared to the same plane in model A1, as shown in Figure 3.13.f.

4.3.1.4 Oil saturation

Oil flux vectors indicate a high drawdown caused by the injected steam during the PIHC, as seen in figure 4.4.here is a clear advancement in the current model compared to model A1 and because in the model B the oil starts to flow towards the producer in a record time of 100 days compared to a delay of producing hydrocarbons in the model A1 at the day 473.

In Figure 4.4.b, the oil saturation profile in the aerial view shows that the oil displacement has reached about 61% in the center of the reservoir, where oil saturation seems to narrow down in the middle, while in model A1, this oil sweep only reached 52%. Similarly, comparing the oil displacement from oil saturation profiles obtained in model A1 and the ones obtained in model B, we can see how model B shows a better oil sweep in the vertical midplane view (figure 4.4.c) with approximately 70% of the longitudinal distance of the model being swept.

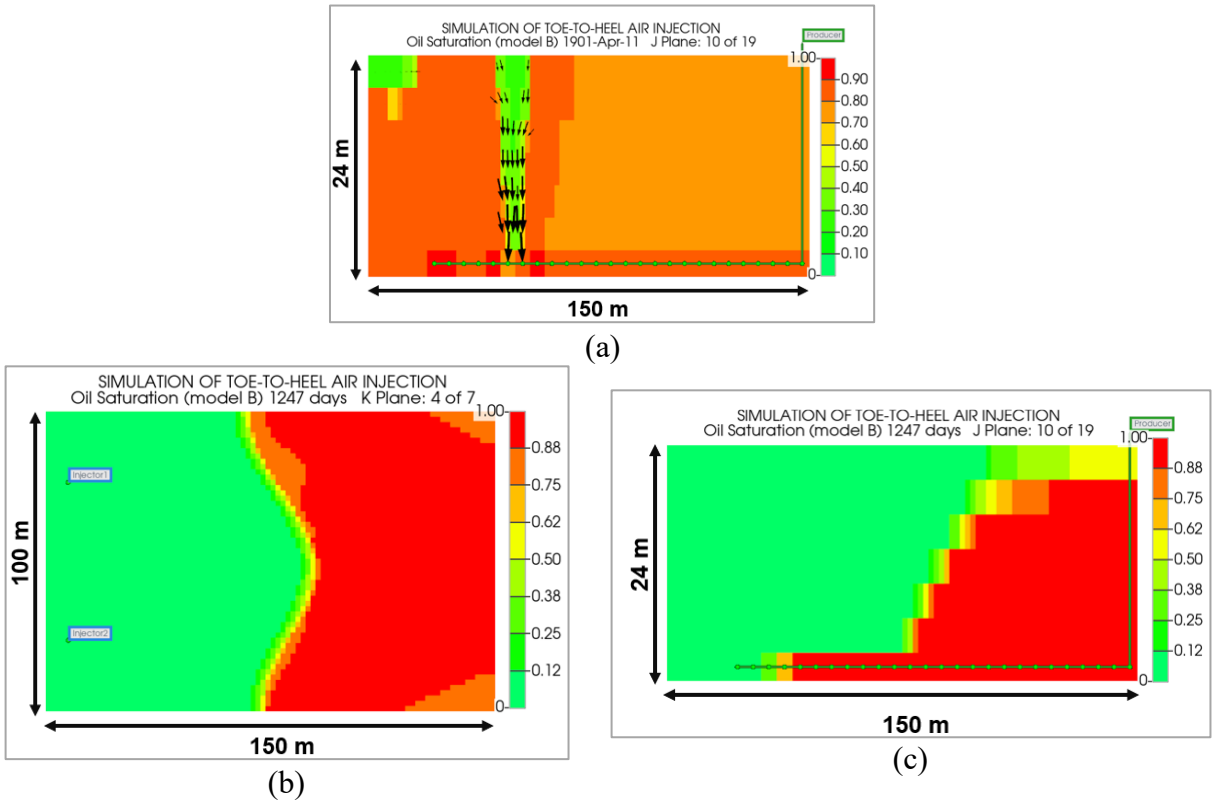

Figure 4.4 Oil Saturation profiles at different views. a) Side View at 100 days: J Plane 10 of 19 b) Aerial View at 1247 Days: K Plane 4 of 7 c) Side View at 1247 days: J Plane 10 of 19.

4.3.1.5 Temperature

Regarding temperature, results show that air injection wells contact the producer well by day 100, as depicted in Figure 4.5.a. When the steam reaches a saturation pressure of 230°C, the oil around the steam path is displaced due to the expansion of the moving steam, subsequently mobilizing towards the producer well. By the end of the 1247-day simulation period, the combustion front is observed advancing, as illustrated by the temperature profile in the vertical midplane shown in Figure 4.5.b. High temperatures extend to 11% of the total wellbore length at the base of the reservoir and 46% at the top. However, as seen in the oil saturation results, by the end of the simulation, the oil has been swept approximately 70% of the distance of the producer well. This finding aligns with Greaves and Turta's (1997) observation that the oil is being mobilized well ahead of the combustion front.

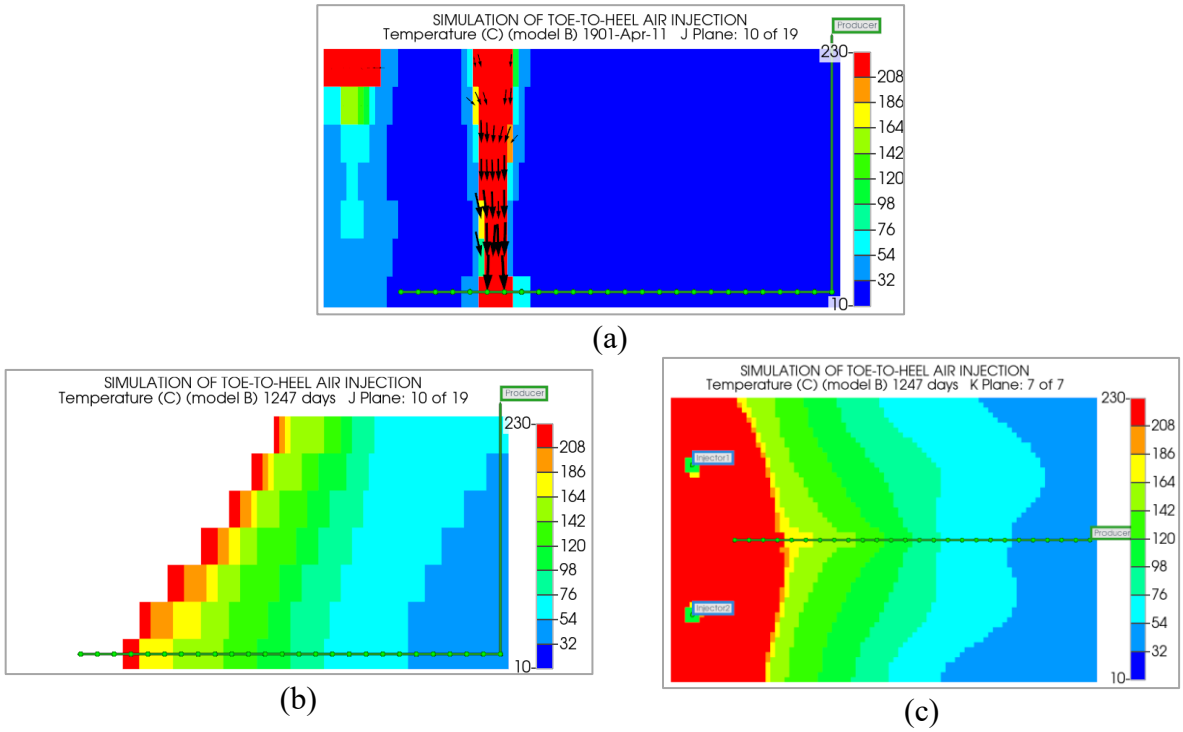

Figure 4.5 Temperature (°C) profiles at different views. a) Side View at 100 days: J Plane 10 of 19 b) Side View at 1247 days: J Plane 10 of 19. c) Aerial View at 1247 Days: K Plane 7 of 7

4.3.2 Model C: Original field scale model (Model A1) with extended horizontal boundaries

4.3.2.1 Model Description

This model was created to accurately capture the behaviour of the fluids and the chemical reactions occurring in increased dimensions in the I and J directions. Initially, in the validated field-scale

Model A1, the I direction consisted of 30 blocks of 5 meters each, totalling 150 meters long. The J direction had 19 blocks of 5.26 meters each, approximately 100 meters. Model C's boundaries were extended to 90 blocks of 5 meters each in the I direction, totalling 450 meters, and 49 blocks of 5.26 meters in the J direction, totalling 257 meters. The simulation was run for 1520 days (4.16 years.). The remaining input parameters used in the simulation were identical to those in Models A1 and B simulations. This includes the PVT data, viscosities, relative permeability curves, petrophysical properties, heat capacities, numerical settings, dynamic gridding parameters, wellbore constraints and placement within the model. For a 3D view of this model's dimensions and wellbore configuration, please refer to Figure 4.6.

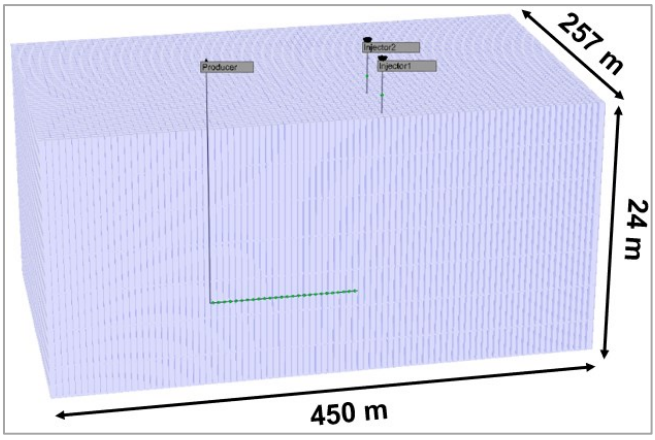

Figure 4.6 3D Representation of Model C

First, Model C, which featured a SLD configuration, was simulated with two vertical wells perforated at the top of the reservoir, each injecting air at a rate of 10,000 m³/day. A second simulation evaluated the benefits of doubling the air injection rate to 20,000 m³/day in each well. The producer well was placed at the seventh layer, at the bottom of the reservoir, consistent with Models A1 and B.

4.3.2.2 Oil production

As seen in Figure 4.7, the oil production for model C with air injection of 20,000 m³/day and 40,000 m³/ day commenced at approximately 500 days. In the case where the model was run with an air injection of 20,000 m³/day, we can see that from December 1901 to January 1902 (from 334 to 365 days), the oil saturation in the last perforation located at the toe of the producer well increased from 0.7 in December 1901 to 1 in January 1902. As the relative permeability is maximum at this time, The injection of gas results in an increase in pressure within the grid block,

leading to the compression and displacement of the oil, thereby causing the observed rise in oil saturation in this grid block. There is a gradual increase in oil production to peak around 1157 days, reaching close to 78 m³/day. Following this peak, the green curve shows a decline decreasing towards the end of the observed period.

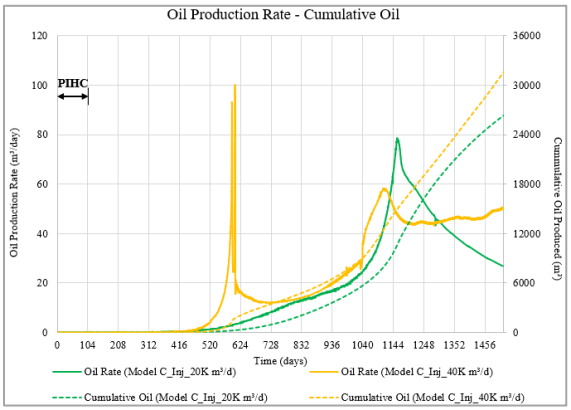

Figure 4.7 Oil production rates and cumulative oil production for Model C.

In the case where 40,000 m³/day of air is injected, the yellow continuous line suggests an initial sharp increase in oil production. This happens because the injected air creates a pathway between the injection sites and the production well, pushing the oil toward the producer. This causes oil production to peak sharply around 600 days at a rate of 100 m³/day. After this peak, production quickly drops but then increases again around day 1120, reaching up to 58 m³/day, and continues to rise until the end of the simulation. This pattern shows how effectively the injected air moves the oil within the reservoir.

4.3.2.3 Oil saturation

Figure 4.8.a shows that on September 1, 1902 (608 days since the beginning of the simulation), the model where the injection was 20,000 m³/day did not generate communication between the injectors and the producer well. However, the model where the injection rate was 40,000 m³/day did let this communication occur, which is why, on day 600, there was a spike in oil production for this case, as previously seen in Figure. 4.7.

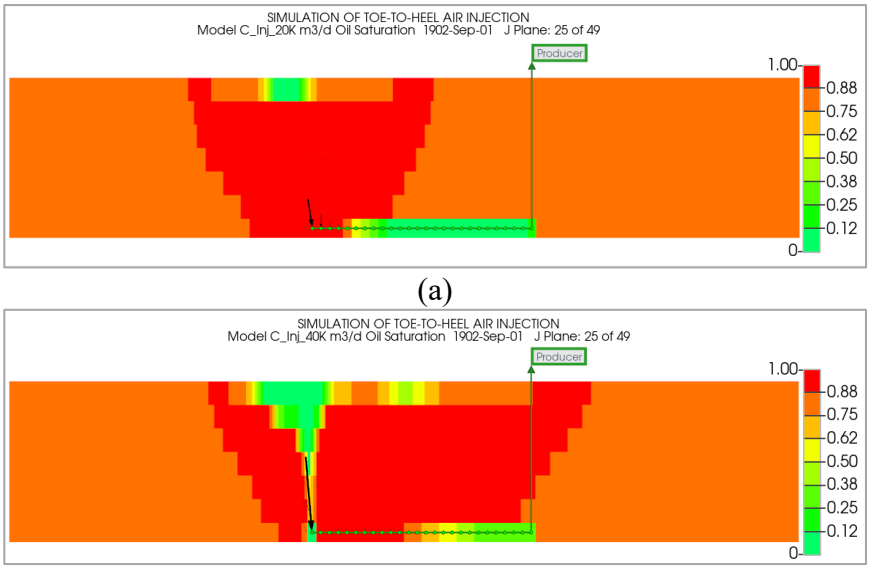

Figure 4.8 Oil saturation profiles for model C with (a) an air injection of 20,000 m³/day and (b) 40,000 m³/day at day 608.

For the oil saturation at the end of the simulation time of 1520 days, as seen in Figure 4.9, we can see that for the case of the air injection is 20000 m³/day, the oil does not fill the entirety of the wellbore. However, in the case where the air injection is doubled, the wellbore is filled with oil, which means that the path for the oil to flow is much better. Also important are the oil flux vectors that, in the case of the air injection of 40000 m³/day, appear more robust than the ones in the model where 20000 m³/day of air is injected.

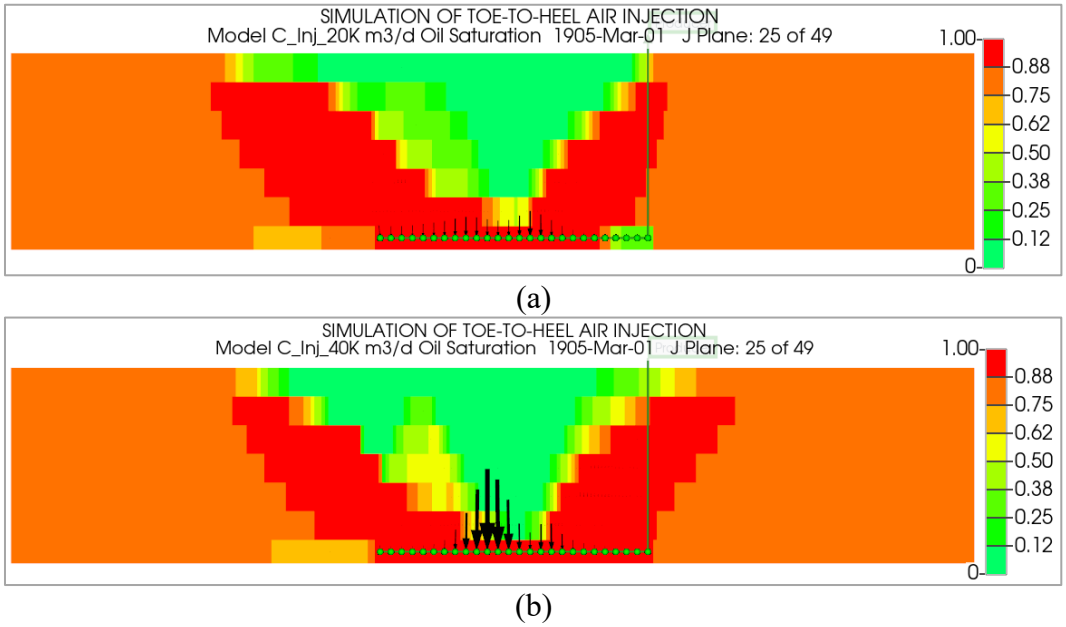

Figure 4.9 Oil saturation profiles (J plane 25 of 49) for (a) Model with air injection of 2000 m³/day and (b) Model with air injection of 40000 m³/day. At the end of the simulation time of 1520 days.

As seen in Figure 4.10, the differences in the sweep areas between the two models are pronounced by the end of the simulation for the horizontal midplanes. In the model with a lower air injection rate of 20,000 m³/day, the swept oil area is noticeably narrower and smaller, taking on an oval shape. In contrast, the model with a higher air injection rate of 40,000 m³/day exhibits a much larger sweep area that resembles a bean shape. This indicates a more extensive oil displacement, covering a broader area and showing less elongation along the J axis.

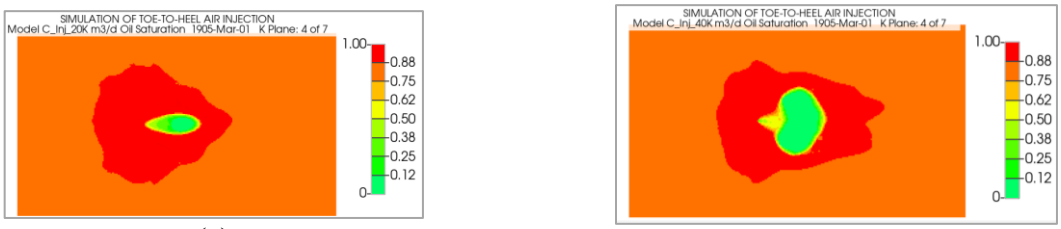

(a) (b)

Figure 4.10 Oil saturation profiles (K plane 4 of 7) for (a) Model with air injection of 2000 m³/day and (b) Model with air injection of 40000 m³/day. At the end of the simulation time of 1520 days.

4.3.2.4 Fuel Availability

Figure 4.11.a shows that by the end of the simulation, the model with an air injection rate of 20,000 m³/day exhibited fuel availability in the first horizontal layer ranging from 33 to 55 kg/m³. These values are consistent with those reported for Athabasca bitumen by Alexander et al. (1962). However, the fuel concentration diminishes significantly, moving toward the bottom of the reservoir becoming virtually nonexistent.

In contrast, the model with an air injection rate of 40,000 m³/day presents a more favourable scenario. In layers 2, 3, and 4, the fuel concentration forms a backward-leaning shape with values ranging from 12 to 49 kg/m³ (Figure 4.11.b), which falls within the acceptable range of 25-50 kg/m³ according to Alexander et al. (1962). Despite this, coke deposition is absent in the remaining layers, preventing the formation of a stable coke zone.

Examining the horizontal midplane (layer 4 of 7), we observe that with an air injection rate of 20,000 m³/day, the fuel availability peaks at a low 4e-3 kg/m³, indicating an underprediction. Conversely, with an air injection rate of 40,000 m³/day, the fuel availability ranges from 20 to 140 kg/m³, indicating excessive coke deposition and an overprediction.

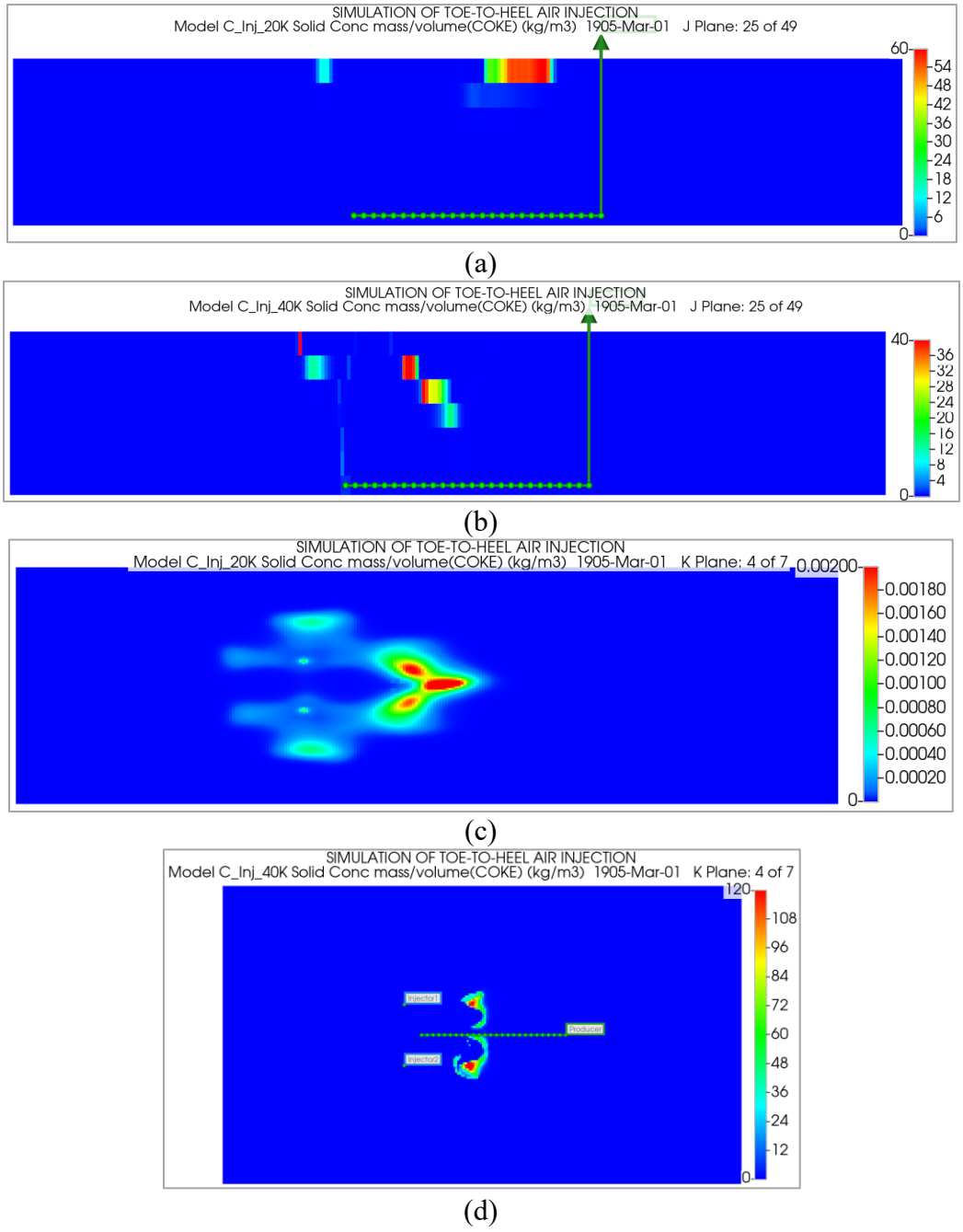

Figure 4.11 Predicted fuel availability profiles in kg/m³ at simulation end time (1520 Days, 1 March 1905) for (a) vertical midplane (Plane 25 of 49) for model with 20,000 m³/day air injection, (b) vertical midplane (Plane 25 of 49) for model with 40,000 m³/day air injection, (c) horizontal midplane (Plane 4 of 7) for model with 20,000 m³/day air injection, and (d) horizontal midplane (Plane 4 of 7) for model with 40,000 m³/day air injection.

Similarly, 3D views of the fuel availability distribution after the time simulated for both cases are presented in Figure 4.12. As it can be seen, the model with a higher air injection rate shows that a higher amount of coke is deposited because there will be more oxygen. With more oxygen, the combustion temperatures increase, accelerating the thermal cracking of hydrocarbons. The higher temperatures facilitate the breaking down of more complex hydrocarbons into simpler molecules

more rapidly, resulting in more coke formation. Higher temperatures can also cause the thermal decomposition of oil components that would not typically crack at lower temperatures.

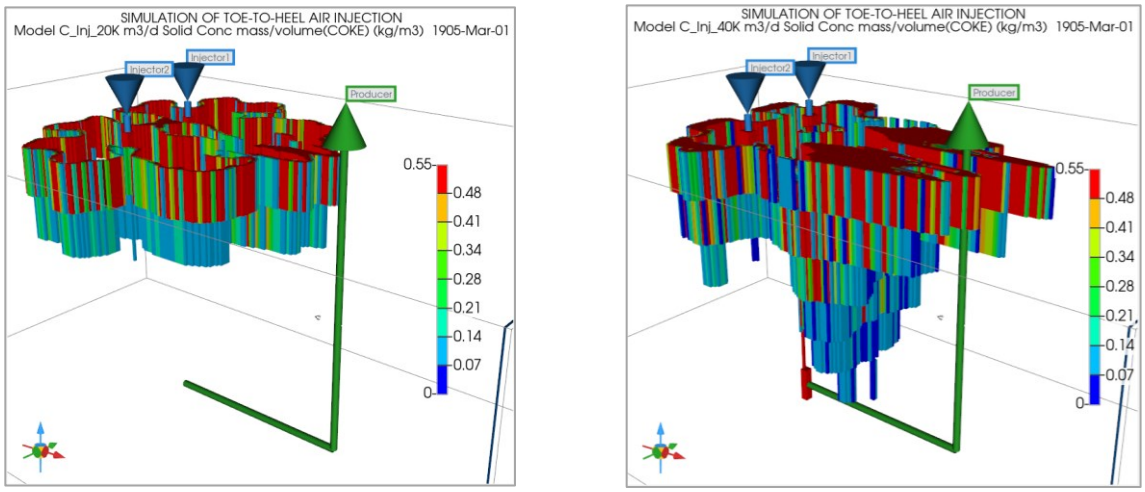

(a) (b)

Figure 4.12 3D View of Coke Availability Maps at the End of the 1520-Day Simulation for Model C with Air Injection Rates of (a) 20,000 m³/day and (b) 40,000 m³/day

As observed, by the end of the simulation, the model with an air injection rate of 40,000 m³/day predicts significantly more coke deposition. The coke is deposited across all seven layers of the reservoir model, even extending near the horizontal wellbore. This indicates that the heat generated from the coke formation reaction can influence the creation of less viscous oil components, thereby enhancing oil mobilization.

This is evident in the oil production rate plot (Figure 4.7) and the temperature and oil saturation profiles. The model with the higher air injection rate demonstrates improved oil mobilization. A key contributing factor is that this model has generated 14.8 times more coke than the model with an air injection rate of 20,000 m³/day.

4.3.2.5 Temperature

At the end of the simulation, the model with an air injection rate of 20,000 m³/day indicated that only low-temperature oxidation reactions occurred, with observed temperatures reaching approximately 158°C (Figure 4.13.a). This temperature is insufficient for burning coke and sustaining an effective combustion front. In contrast, the model with an air injection rate of 40,000 m³/day exhibited temperatures exceeding 400°C, which are conducive to maintaining ongoing combustion operations.

These temperature behaviours are depicted in Figure 4.13, where the higher temperature profiles in the model with air injection of 40000 m³/day (C_Inj_40K) are prominent across the mid-horizontal plane of the model (Figure 4.13.b). These higher temperatures cover a larger area and significantly impact the reservoir, effectively reducing oil viscosity and enhancing its flow toward the horizontal production well.

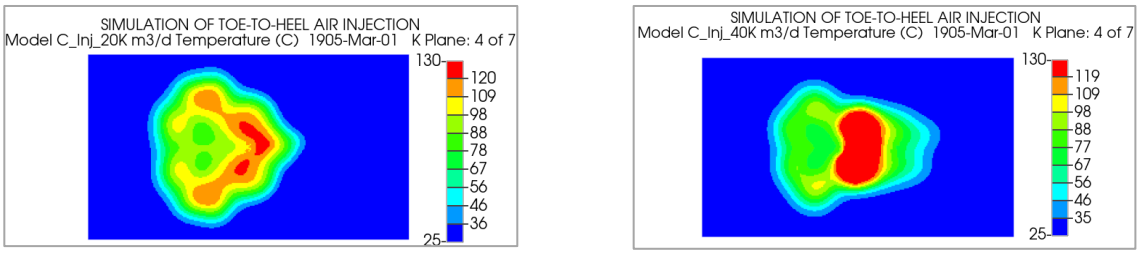

(a) (b)

Figure 4.13 Temperature maps for the horizontal midplanes of (a) the model with an air injection rate of 20,000 m³/day and (b) the model with an air injection rate of 40,000 m³/day

Figure 4.14 displays the temperature profiles in the vertical midplanes for both models at the end of the simulation period. According to Figure 4.14.a It is evident that the model with an air injection rate of 20,000 m³/day experienced suboptimal combustion reactions, with the highest temperatures reaching only between 120-150°C. This model's temperature coverage is broader but primarily concentrated behind the injector wells. Conversely, the model with an air injection rate of 40,000 m³/day achieved significantly higher temperatures, surpassing 450°C, which indicates effective coke combustion. This temperature distribution underscores the enhanced combustion efficiency in the higher air injection model.

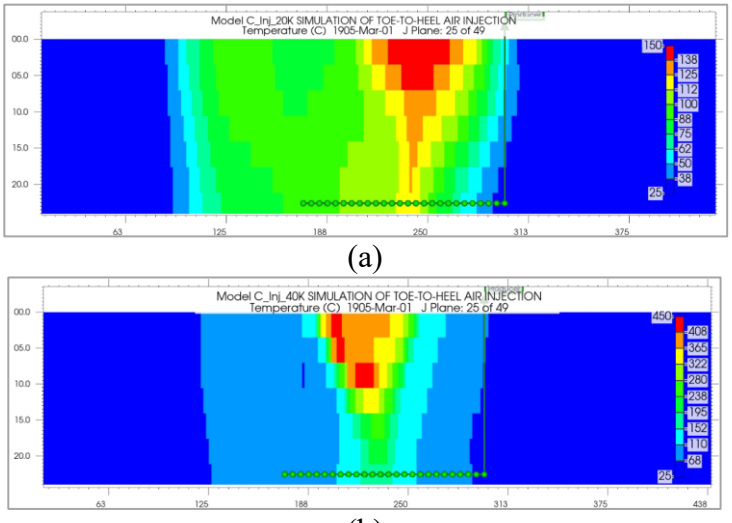

(a)

(b)

Figure 4.14 Temperature maps for the vertical midplanes of (a) the model with an air injection rate of 20,000 m³/day and (b) with an air injection rate of 40,000 m³/day after 1520 days of combustion.

Similarly, the 3D views presented in Figure 4.15 illustrate the temperature distribution in both models, with a cutoff value set above 100°C, displaying only temperatures higher than this threshold. This visualization supports earlier observations that temperatures are advancing more effectively toward the heel of the well in the model with an air injection rate of 40,000 m³/day. This model's efficiency is further evidenced by the significantly higher fuel deposition, which is nearly 14.8 times greater than in the model with an air injection rate of 20,000 m³/day.

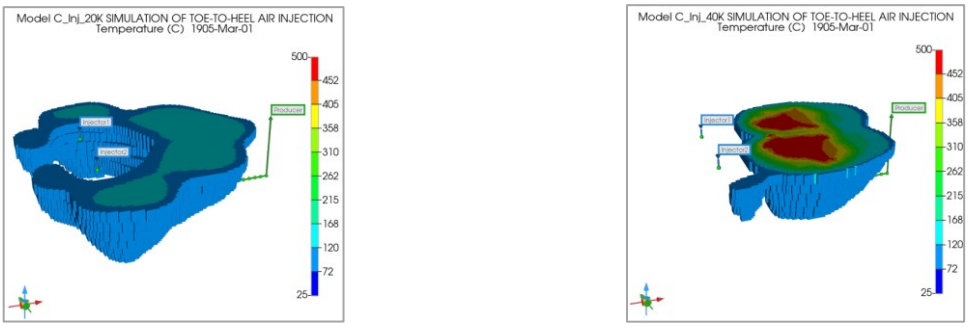

(a) (b)

Figure 4.15 3D temperature maps of (a) the model with an air injection rate of 20,000 m³/day and (b) the model with an air injection rate of 40,000 m³/day after 1520 days of combustion.

This assertion is corroborated by the oxygen production metrics in the 40,000 m³/day model, where oxygen accounted for 6% of the gas produced, compared to 21% in the 20,000 m³/day model. These figures were derived from the plot of gas volume fraction versus time, highlighting the differing efficiencies and combustion dynamics between the two models.

4.3.3 Model D: Single Injector-Producer Wellbore with Injection Only through the Last Perforation at the Toe (Dimensions: 150 m x 100 m x 24 m)

4.3.3.1 Model Description

The innovative aspect of this research lies in developing a novel in situ combustion method that modifies the THAI technology. This variation utilizes a single well for both the simultaneous injection of air and the production of hydrocarbons. Specifically, Model D is designed based on the field-scale reservoir dimensions Ado (2017) provided in his thesis. Unlike Ado's approach, which used one horizontal producer well located at the bottom of the reservoir and two vertical injectors at the reservoir's top, Model D integrates both functions into one wellbore. This well is strategically positioned along the vertical midplane of the reservoir, specifically in the J-plane at location 10 of 19.

Additionally, it is situated at the reservoir's base in the vertical K layer number 7. The horizontal section of this well matches the length of the producer well in the field-scale model A1, which is 125 meters. The simulation for this model spanned 3012 days or approximately 8.25 years.

4.3.3.2 Pre-ignition heating cycle (PIHC)

The pre-ignition heating cycle used in this study mirrors that of Model A1, which aligns with the verified field-scale model P1 described by Ado (2017). To elevate the temperature across a substantial area near the toe of the horizontal well, steam was injected into the reservoir through the final three perforations of the injector well over 120 days. This procedure was designed to heat a sufficient reservoir volume to the target temperature, facilitating adequate coke deposition necessary to initiate the ignition process.

4.3.3.3 Oil Production

According to Figure 4.16, during the pre-ignition heating cycle, which lasted the first 120 days of the simulation, oil production rates began as early as day 9, peaking at 180 m^3/day. Subsequently, the rates declined to approximately 60 m^3/day by the end of February 1901 (day 60). After this period, production rates stabilized, maintaining an average of approximately 54-64 m^3/day until the conclusion of the pre-ignition heating cycle.

The initial surge in production is attributed to the direct contact between the injected steam and the oil. The steam injection mobilizes the surrounding oil and transports heat that promotes the conversion of heavier hydrocarbons into lighter ones. This transformation significantly increases the pressure near the toe of the horizontal well. The resultant increase in pressure enhances the drawdown effect, thereby explaining the initially high production rates observed during the pre-ignition heating cycle.

From the end of the PIHC until the conclusion of the 3012-day simulation, the production stabilized at an approximate rate of 6.3 m^3/day, resulting in a cumulative oil production of 29,946 m^3.

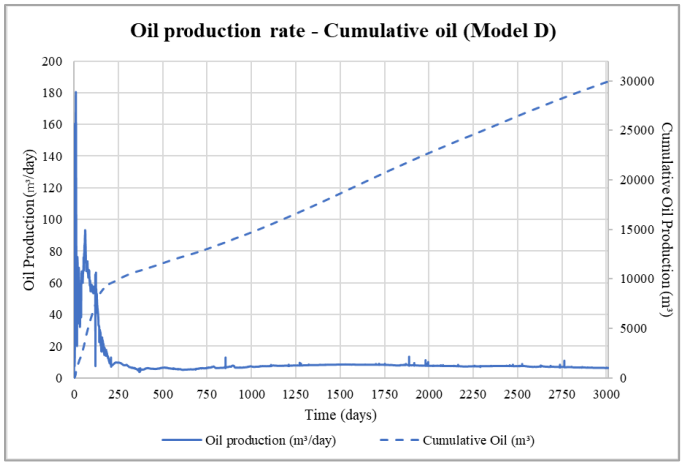

Figure 4.16 Oil production rate and cumulative oil production for model D.

4.3.3.4 Oil Saturation

According to Figure 4.17, the oil saturation profile at the conclusion of the simulation reveals a significant gravity-driven flow of the mobile oil zone towards the horizontal producer. This is evidenced by the forward-leaning and vertical oil flux vectors observed in the profile. The oil displacement has covered approximately 80% of the total axial length of the wellbore. This extensive displacement is attributed to the transport of heat through conduction and convection and the 'bulldozing effect' created by the advancing combustion front.

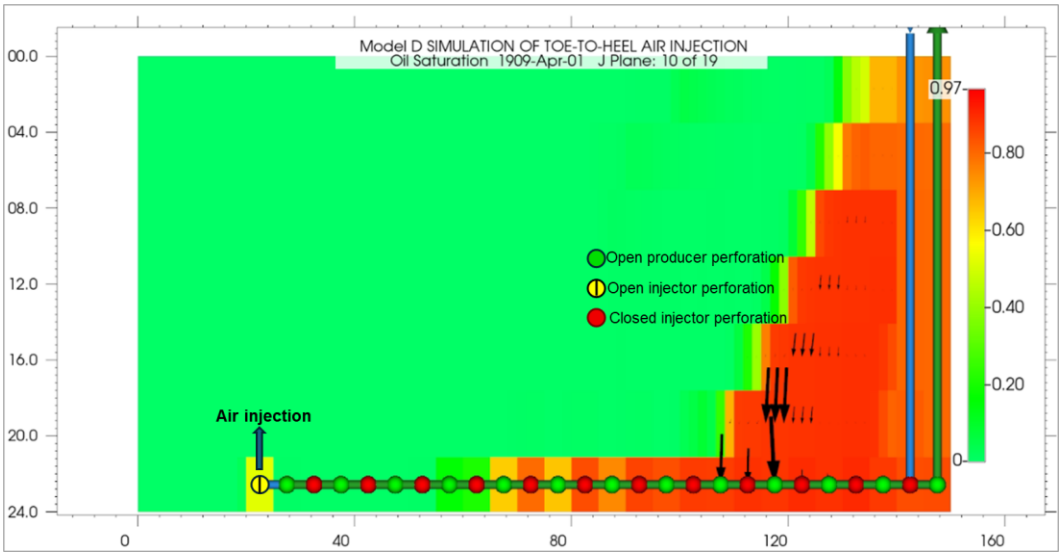

Figure 4.17 Vertical midplane view (plane 10 of 19) of oil saturation profile in Model D at the end of the simulated time (1520 days).

4.3.3.5 Fuel Availability

As seen in Figure 4.18, the concentration of fuel (kg/m³) at the end of the simulation in the vertical midplane of the reservoir ranges between 5 and 386 kg/m³. This range indicates a behaviour of overcoking, namely an excessive concentration of coke at the base of the reservoir. This phenomenon aligns with the findings of Greaves (2002), who noted that a more significant amount of oil is transformed into coke as the bitumen gravitates downwards due to intrinsic processes occurring at that location. It is also important to emphasize that there is an inadequate displacement of coke, which could be explained by oxygen distribution within the reservoir. Unwanted oxygen production in certain areas can extinguish the combustion front in the upper layers, leaving traces of coke in the middle and lower zones of the model. This analysis suggests that managing oxygen flow and understanding combustion dynamics are crucial for optimizing hydrocarbon recovery and minimizing undesired coke formation.

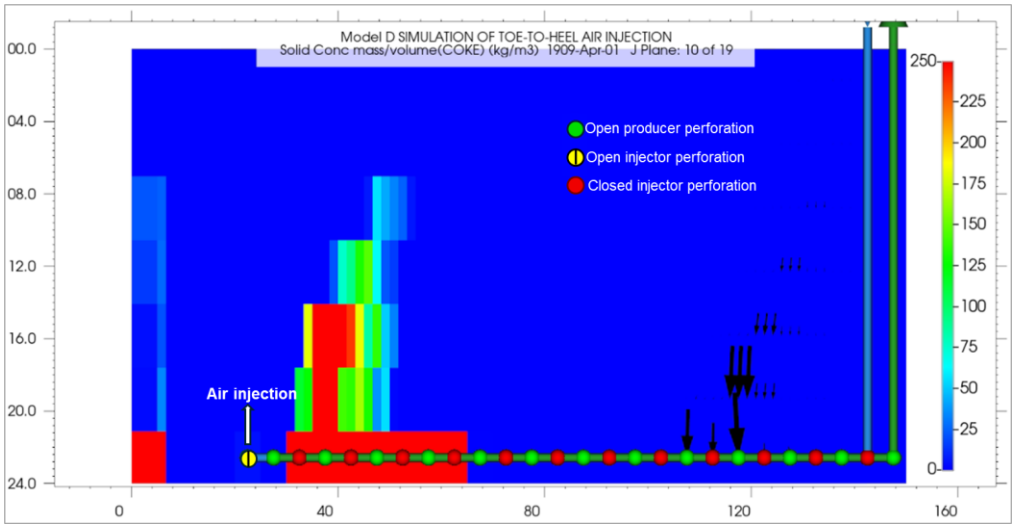

Figure 4.18 Fuel availability profile in kg/m³ at the end of the simulated time (1520 days).

As illustrated in Figure 4.19, overcoking at the base of the reservoir at the end of the simulated period is well-documented in the literature and results from a complex interplay of physical and chemical factors. Gravity segregation causes heavier components like bitumen to migrate downwards, concentrating hydrocarbon material at the reservoir's base. Despite oxygen being injected at the reservoir's base, it is often insufficient to combust all the deposited coke fully. This leads to incomplete combustion due to barriers or oxygen consumption in the upper layers. Fluid and gas dynamics within the reservoir can further hinder the effective mixing of oxygen with hydrocarbons, exacerbating areas of incomplete combustion. Similarly, increased pressure from

the combustion process can impede the movement of gases, limiting oxygen's reach to lower zones. Additionally, the rate of chemical reactions can vary, with cooler, less oxygenated areas at the base favouring coke formation over complete combustion to carbon dioxide and water.

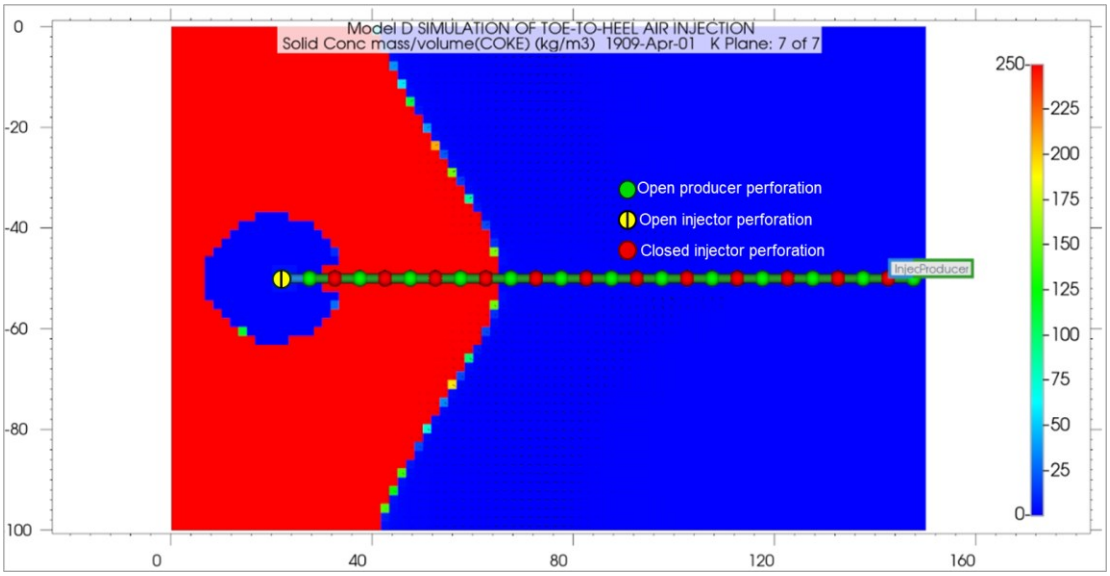

Figure 4.19 Fuel availability profile at the base of the reservoir at the end of the simulated time.

4.3.3.6 Temperature

Measured from the toe of the well, combustion temperatures (HTO temperatures) are predicted to occur 46 meters ahead at the reservoir's top, representing 36% of the total wellbore length. In contrast, at the bottom of the reservoir, these temperatures reach 33 meters ahead of the toe, equating to 26% of the total well's length. Thus, it is reasonable to approximate that combustion occurs along 31% of the total well's length if the injection point remains static at the toe throughout the 3012-day simulation period. See Figure 4.20 and Figure 4.21 for reference.

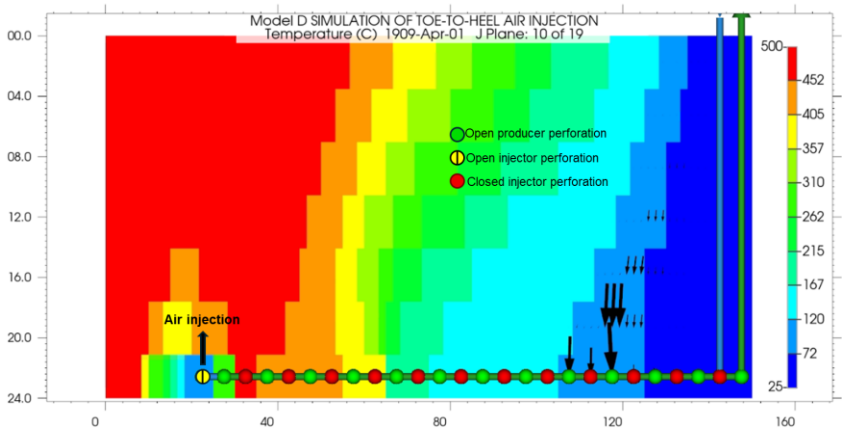

Figure 4.20 Temperature profile at the vertical midplane (J plane, 10 of 19) at the end of the 3012-day simulation period.

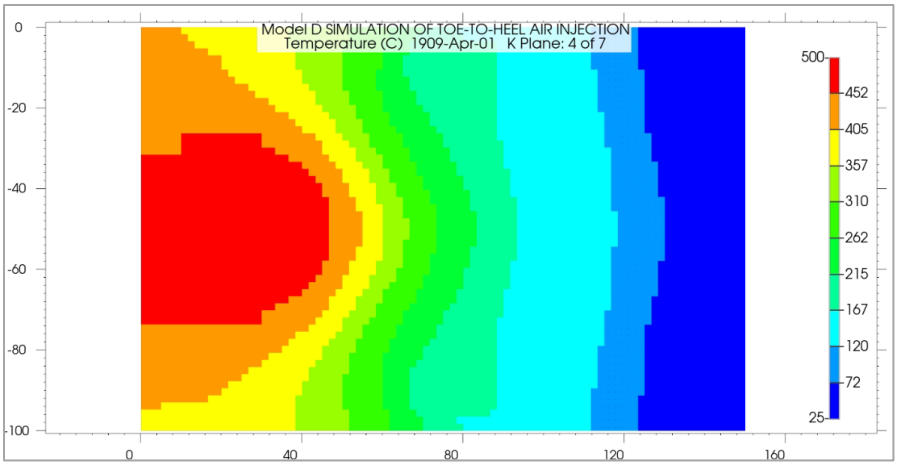

Figure 4.21 Temperature profile at the horizontal midplane (K plane, 4 of 7) at the end of the 3012-day simulation period.

4.3.4 Model E: Single Injector-Producer Wellbore with Injection Only through the Last Perforation at the Toe (Dimensions: 450 m x 257 m x 24 m)

Model E serves as an advanced exploration tool designed to investigate the same parameters as Model D but with expanded boundaries in the I and J directions. This adjustment allows for a more comprehensive analysis of the combustion front behaviour in a typical Athabasca bitumen reservoir without the constraints of the original field scale dimensions. Table 4.1 shows the key parameters of the model E.

Table 4.1 Key parameters of the model E.

	I	J	K
Reservoir Dimensions, m	257	450	24
Number of refined grid blocks	147	270	7
Total number of grid blocks	277830		
Well Arrangement	1 HI + 1HP		
Initial reservoir temperature and pressure	25°C and 2800 kPa		
Initial oil and water saturations	0.8 and 0.2		
Porosity	34%		
Absolute permeability	6400 mD		3450 mD
Well internal diameter	178 mm (7 in)		
Producer back pressure	2800 kPa		
Steam injection pressure	5500 kPa		
PIHC duration	120 days		
Steam injection rate	80 m³/day		
Air Injection rate	20000 m³/day		
Air Injection temperature	50, 150 and 300°C		
Simulated time	7305 days (20 years)		

By expanding the boundaries in the I and J direction, Model E provides a more accurate representation of reservoir dynamics and combustion front behaviour, offering valuable insights

into the potential impact of boundary conditions on reservoir performance. This approach helps better understand how the expanded boundaries influence the efficiency and effectiveness of bitumen extraction processes. In this model, there is a static interval air injection through the last perforator for the entire simulation period. The air injection temperatures to be evaluated will be 50, 150 and 300 °C.

4.3.4.1 Oil Production

During the first four months of PIHC, for the three air injection temperatures of 50, 150 and 300 C, oil production oscillated between 40 and 90 m^3/day, with peaks reaching up to 157 m^3/day. This spike in production is caused by the fact that when steam is first injected into the reservoir, the temperature around the injection well rises rapidly. This elevated temperature reduces the viscosity of the surrounding oil, making it more fluid and more accessible to produce. Additionally, the heated oil and reservoir rock's thermal expansion helps push the oil toward the production wells. The increased reservoir pressure from the steam injection further enhances this effect by driving the oil more efficiently towards the wellbore.

- *Air injection temperature of 50 °C*

In the case where the air injection temperature was 50C, production fell to 8 m^3/day at 286 days after air injection commenced. From 290 until 740 days, production stabilized at approximately 13 m^3/day. There was a sudden increase in production from day 760 to 1651, with production stabilizing at about 16.5 m^3/day. Later, on day 2021, production declined to around 10 m^3/day and remained stabilized at that value, between 10 to 12 m^3/day, until the end of the simulation.

As seen in Figure 4.22, there was a drop in production from day 1650 (July 1905) to 2021 (July 1906) in the model with air injection of 50C because there was an increase in the oxygen production rate, which could indicate that there is not effective combustion of the bitumen in place, significantly affecting oil production. Additionally, it is observed that the oil flux vectors near the toe of the well change direction from pointing towards the toe of the producer well to rotating and pointing in the opposite direction towards the heel of the well. This also shows that as combustion is not being carried out effectively in the direction needed to advance the combustion front towards the heel of the well, the oil will now have to start flowing from other areas of lower resistance, specifically starting to migrate from the area just below the last open perforation of the injector

well. These factors contribute to increased gas production, and the well will begin to fill with gas instead of oil.

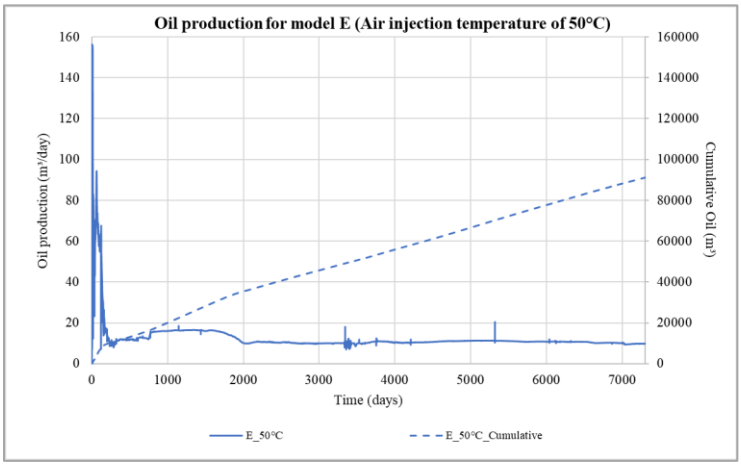

Figure 4.22 Oil production rate and cumulate oil produced for model E (Air injection rate of 50 °C)

- *Air injection temperature of 150 °C*

As seen in Figure 4.23, the model variant with an air injection temperature of 150°C showed improved oil production results as expected. In this case, oil production began to increase around day 1940, peaking at about day 2020 with a production rate of 18 m³/day. This spike was due to the accumulation of flue gas, which increased pressure and pushed the oil toward the perforations located at the toe of the well. Subsequently, the oil production stabilized, maintaining an average rate of approximately 14 m³/day until the end of the simulation.

- *Air injection temperature of 300 °C*

As shown in Figure 4.23, the oil production with an air injection temperature of 300°C demonstrated significantly better results due to the favourable combustion kinetics and thermal cracking reactions within the reservoir model. Oil production increased steadily from day 1774 to day 2880, reaching a peak of 30 m³/day. The reason for the increase in oil production is relatively straightforward: there was a combustion of oil pseudocomponents, specifically a portion of the immobile component (IC) and light component (LC). These reactions release heat, activating thermal cracking reactions and producing coke opposite the HP toe. This also results in a more significant pressure drawdown in the area, causing a larger quantity of oil to decrease its viscosity and be displaced towards the toe of the HP well. Following this period, the production rate declined to 19 m³/day and maintained this level for the remainder of the simulation.

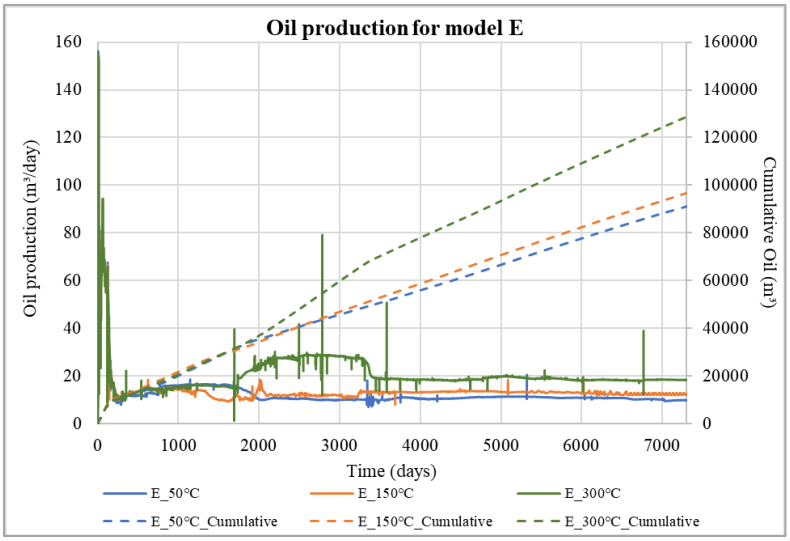

Figure 4.23 Oil Production and Cumulative Oil Produced Over Time in Model E at Air Injection Temperatures of 50°C, 150°C, and 300°C.

4.3.4.2 Oil Saturation

- *Air injection temperature of 50 °C*

By the end of the 20-year simulation, we see how the oil is displaced by the gas injected into the reservoir, and the oil flows as the reservoir temperature gradually increases as the mobile oil zone moves towards the heel of the HP. At the bottom of the reservoir, in layer 7, we observe a bank of accumulated oil, which is the oil that has been displaced from higher parts of the reservoir and is being recovered by the HP well. In terms of reservoir recovery, at the end of the twenty years of simulation, the model predicted a recovery of 93% of the Original Oil In Place (OOIP).

- *Air injection temperature of 150 °C*

The oil saturation profiles between the models with injection temperatures of 50°C and 150°C are quite similar. At the end of the simulation, the recovery factor of the reservoir is 94%, compared to 93% of the OOIP in the model with an injection temperature of 50°C. The Mobile Oil Zone (MOZ) is identified by the oil flux vectors superimposed on the oil saturation profile. They indicate the relative magnitudes of the oil flow rate. Similarly, it is observed that the mobile oil zone is advancing, and the oil flux vectors are leaning backward.

- *Air injection temperature of 300 °C*

According to the oil saturation profile from the vertical midplane (Figure 4.24), the oil saturation is quite similar to the behaviour observed in previous models with injection temperatures of 50°C

and 150°C. The oil flux vectors point towards the heel of the HP well, indicating the mobile oil zone, which suggests effective sweeping. This is evident in the oil production, which is higher than in previous models, and consequently, the recovery factor tends to be higher.

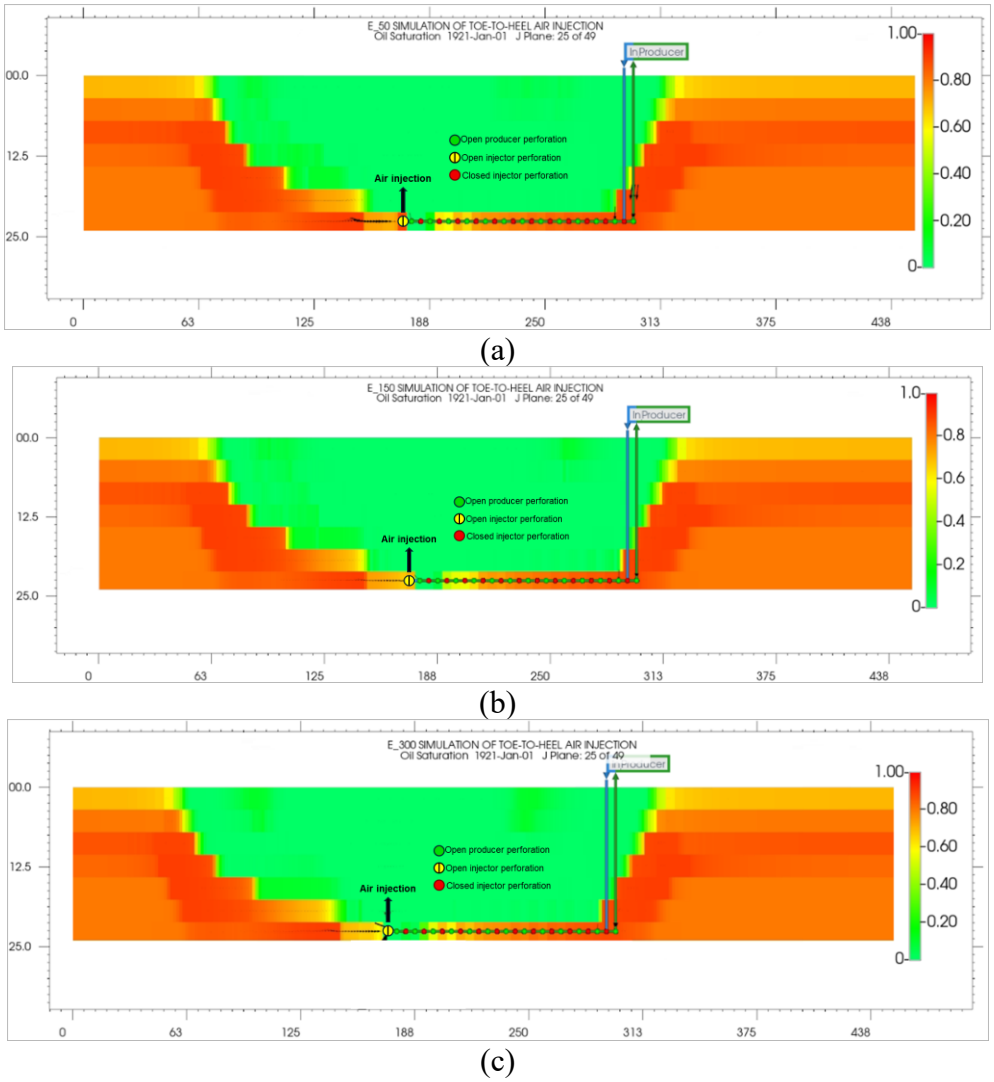

Figure 4.24 Vertical midplane view (J Plane 25 of 49) of Oil Saturation profiles at the end of the 20-year simulation period for Model E with Air Injection Temperatures of (a) 50°C, (b) 150°C, and (c) 300°C

4.3.4.3 Fuel Availability

- *Air injection temperature of 50 °C*

According to Figure 4.25.a, the coke availability concentration ranges from 90 to 300 kg/m³ at the end of the pre-ignition heating cycle. While these values are unrealistic, they serve as a preliminary setup to facilitate combustion once air enriched with oxygen begins to be injected. It is also noted that the coke-rich zone spans approximately 25 meters and progresses more rapidly at the top of

the reservoir (layer number 1) than at the base. Additionally, it is essential to mention that there is not a clearly defined coke zone, suggesting that the process may be unstable, likely as a result of the tuning of kinetic parameters in the original work by Ado (2017). Although the coke deposition profile aligns with the post-mortem examinations of the 3D THAI combustion cell experiment (Greaves et al., 2012), where little coke deposition occurs in the midplane due to it being the area with the most significant drawdown, it is observed that the top of the reservoir exhibits a significant accumulation of coke. As it descends through the vertical profile of the reservoir, this concentration decreases.

- *Air injection temperature of 150 °C*

In the model with an injection temperature of 150°C, Figure 4.25.b shows that the coke deposition zone appears to be more stable compared to the model with an injection temperature of 50°C. The 150°C injection maintained a more defined coke zone in the reservoir for a significantly longer period than the 50°C injection model. Until mid-1905, the average coke concentration in both models was the same. However, from that year onwards, the model with a 150°C injection temperature consistently maintained a coke deposition level that was 30% higher. This is reflected in the average coke concentration throughout the simulated period.

- *Air injection temperature of 300 °C*

At the end of the simulated combustion and according to Figure 4.25.c, we observe a relatively stable combustion front, evidenced by the consistent coke deposition along the J plane in the reservoir (vertical midplane). The coke concentration varies, similar to what was previously observed in the models with 50°C and 150°C air injections. Notably, at the top of the reservoir, coke availability ranges from 200 to 1300 kg/m³, indicating a potential overprediction of coke in this layer. Moving downward to the reservoir's base, the coke zone's forward-leaning shape displays values from 39 to 400 kg/m³, which appears to be more realistic. In terms of the advancement of this coke zone, in the upper regions, we see that it has advanced around 75 meters, and at the base, it has advanced 30 meters.

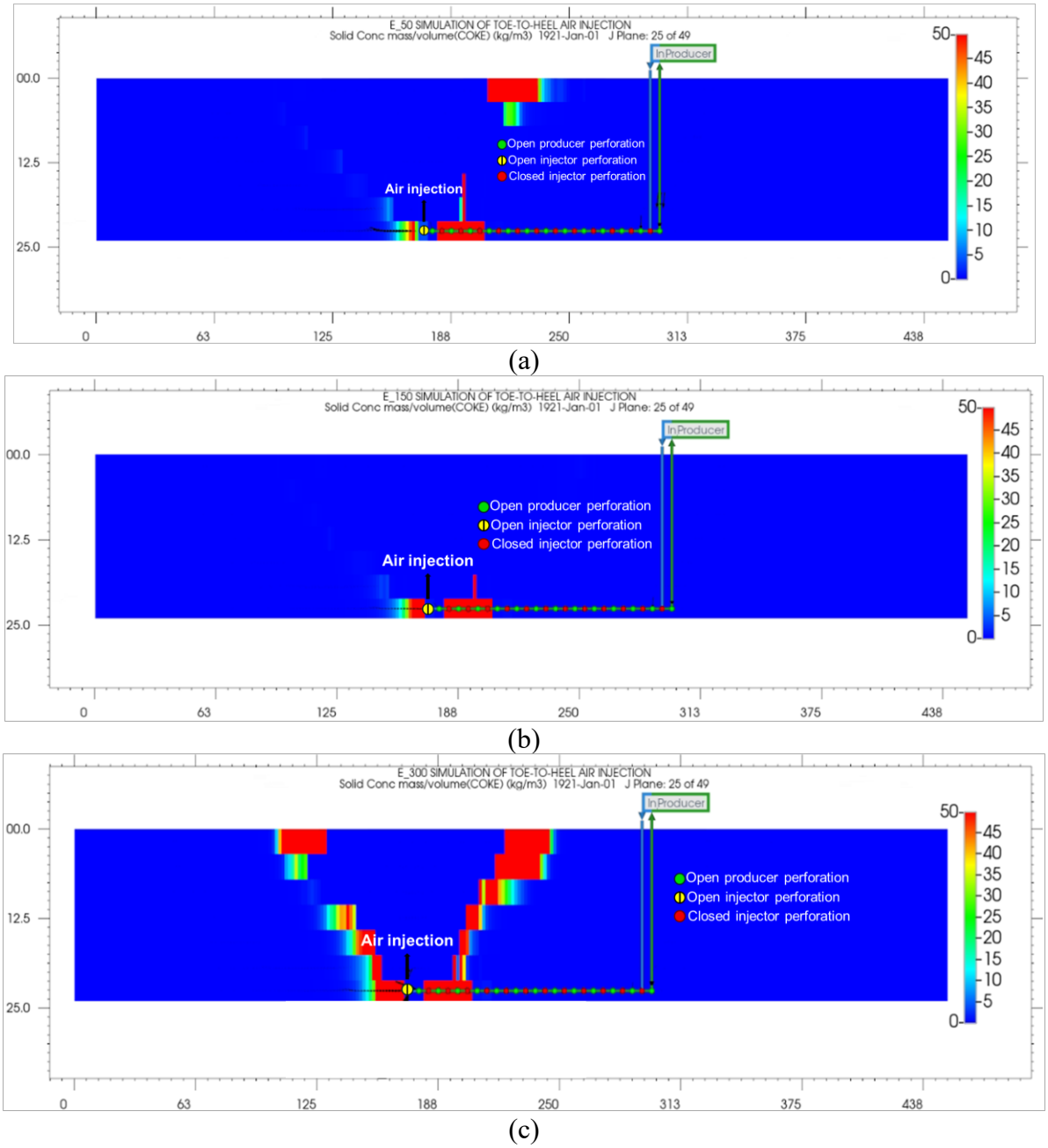

Figure 4.25 Vertical midplane view (J Plane 25 of 49) of coke availability profiles at the end of the 20-year simulation period for Model E with air injection temperatures of (a) 50°C, (b) 150°C, and (c) 300°C.

4.3.4.4 Temperature

- *Air injection temperature of 50 °C*

For the case of an air temperature of 50° C in the vertical midplane at the end of the 20-year simulation, Figure 4.26.a shows that the model generates combustion in the direction of the heel of the production well and also in the opposite direction. We observe that on this date, in layer number 1, which is higher up in the reservoir, the temperature reaches values of 580°C. However,

as it moves deeper into the reservoir, this temperature stabilizes between 450 to 480°C. The temperature has reached values above 400°C up to 46 meters from the toe of the well in the first layer and up to 25 meters from the toe in the sixth layer. Temperatures above 400 degrees indicate the combustion front, which, in this case, appears to be leaning forward. However, it seems it is not moving continuously but staying static, as it has only travelled 35 meters.

It is also observed that the oil flow vectors indicate that oil drainage is much ahead of the combustion front, and these vectors are primarily vertical. However, horizontal vectors can also be seen, which point towards the horizontal producer (HP).

- *Air injection temperature of 150 °C*

After the 20-year in situ combustion simulation, Figure 4.26.b shows that the combustion front has propagated along the horizontal production well, extending 66 meters in layer one at the top and 30 meters at the base of the reservoir. Compared to the model where the injection temperature is 50°C, we can observe that the temperature is higher at the top of the reservoir. In contrast, in other parts, the temperatures appear very similar. In the horizontal plane (aerial view) number 1, i.e., at the top of the reservoir, by the end of the twenty-year simulation, the model with an injection temperature of 150°C the combustion front has travelled 66 meters from the toe of the HP compared to the 46 meters in the model with 50°C injection temperature. However, this occurs only in horizontal plane number 1 (at the top of the reservoir), as the temperature profiles appear quite identical when viewing the other horizontal layers.

- *Air injection temperature of 300 °C*

Regarding temperature, according to Figure 4.26.c, by the end of the simulated period, the combustion front has reached 60 meters from the toe at the top of the reservoir. This is based on a temperature above 400°C cutoff parameter for coke combustion. As we move vertically down to layer number 7, we see that the shape of the combustion front is leaning forward, with the upper end pointing more toward the heel of the HP well.

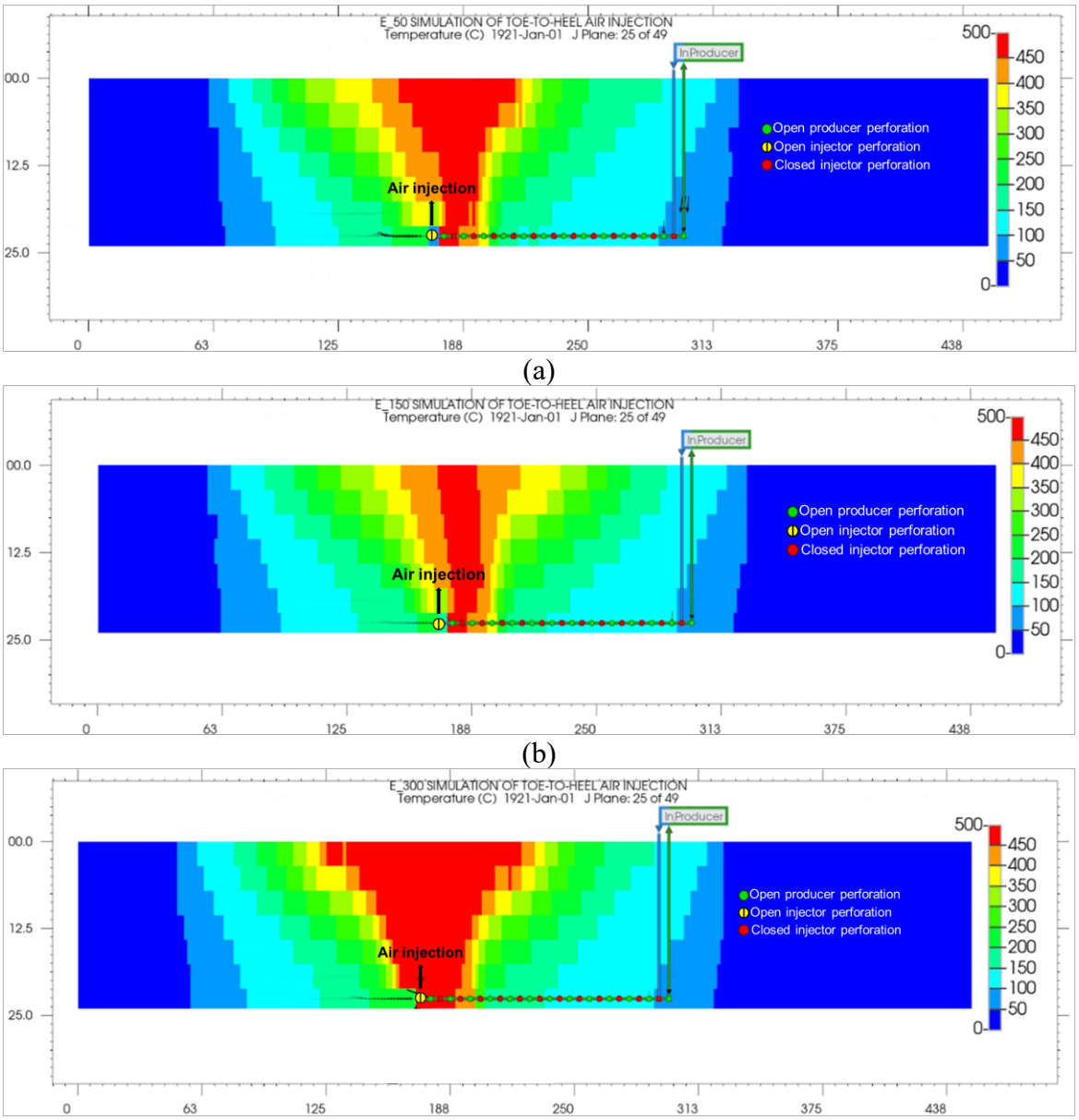

Figure 4.26 Vertical midplane view (J Plane 25 of 49) of temperature profiles at the end of the 20-year simulation period for Model E with air injection temperatures of (a) 50°C, (b) 150°C, and (c) 300°C

4.3.5 Model F: Single Injector-Producer Wellbore with Advancing Injection interval every 18 months (Dimensions: 150 m x 100 m x 24 m)

4.3.5.1 Model Description

This model shares similar dimensions with those used in Model D, which is based on the upscaled dimensions from Ado (2017). As previously outlined in this study, the goal is to develop a model utilizing a single injector-producer well that can sustain in situ combustion with toe-to-heel air

injection over an extended period. Model F introduces a novel approach by incorporating a moving air injection interval within a single wellbore, allowing air to be injected into specific areas to propagate combustion toward the heel of the well. This method includes an 18-month delay for shifting the injection interval, aimed at enhancing oil recovery by advancing the combustion front. For consistency, the simulation for Model F uses the same duration of 3012 days (approximately 8.25 years) as Model D.

For the implementation of the proposed THAI variant, a specialized engineering design is required. This model incorporates a wellbore configuration that supports simultaneous parallel injection and production within a single wellbore, allowing for the dynamic shifting of the air injection interval while ensuring controlled and efficient advancement of the combustion front in the reservoir. In Model F, the horizontal section of the well extends 125 meters. Based on Ado's (2017) proposed field-scale THAI model, 26 perforators were spaced laterally along the wellbore at 5-meter intervals. In the proposed well configuration in this research, there are 13 designated perforations for injection and 13 for production. The process begins with a pre-ignition heating cycle lasting 120 days, during which steam is injected at a rate of 78 m^3/day. During this period, only the first three numerical perforations at the toe (#26, #24, #22) in the injection well are opened, while all production perforations remain fully open, as shown in Figure 4.27.

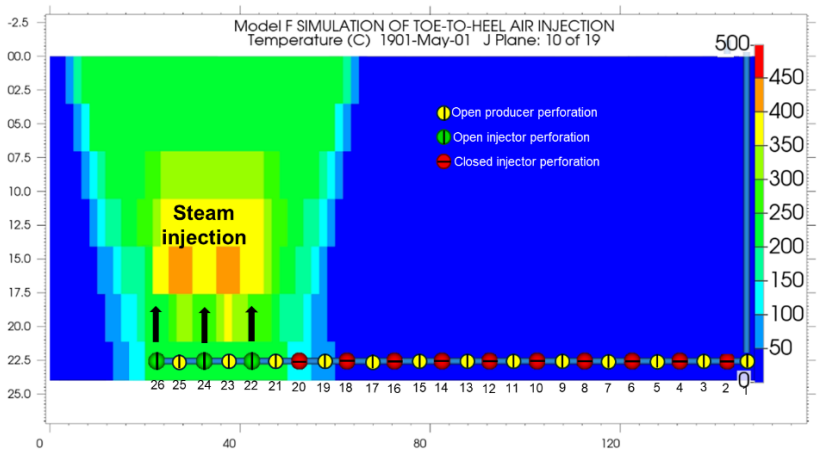

Figure 4.27. Temperature results at the vertical midplane illustrate the single injector/producer wellbore at the conclusion of the pre-ignition heating cycle (day 120), with the first three injection perforations (#26, #24, and #22) opened for steam injection.

On day 120 of the simulation, and for the following 18 months, injector perforations #24 and #22 are shut off, while all production perforations remain fully open. During this period, air is injected

solely through the numerical perforation #26 at a rate of 20,000 m³/day and a temperature of 50°C. This marks the first stage of air injection, as illustrated in Figure 4.28.

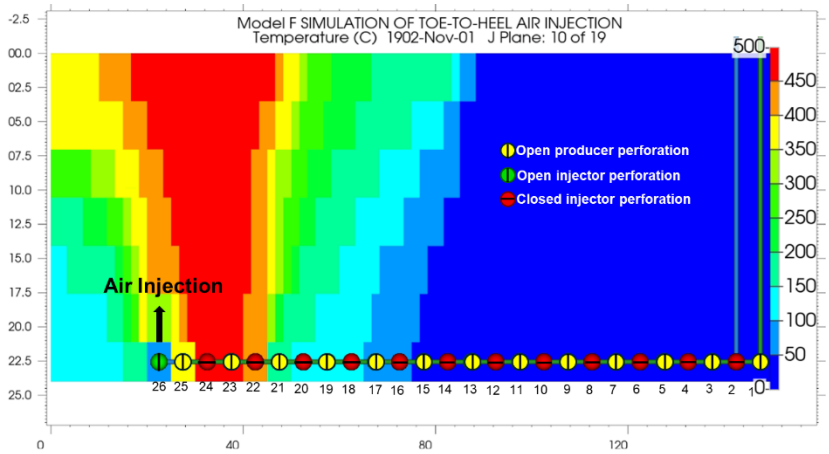

Figure 4.28 Temperature profile at the vertical midplane following the first 18-month air injection period (May 1, 1901 - November 1, 1902), with air injected exclusively through perforation #26 at the toe

After 18 months of continuous air injection through perforation #26, on November 1, 1904 (669 days since the start of the simulation), the injection point was shifted further up the horizontal wellbore. Consequently, perforation #26 was switched off, and perforation #24 was activated for air injection, while all production perforations remain fully open, as shown in Figure 4.29. This new air injection phase lasted another 18 months, until May 1904. The 18-month interval was selected as the optimal duration for air injection to ensure efficient advancement of the combustion front.

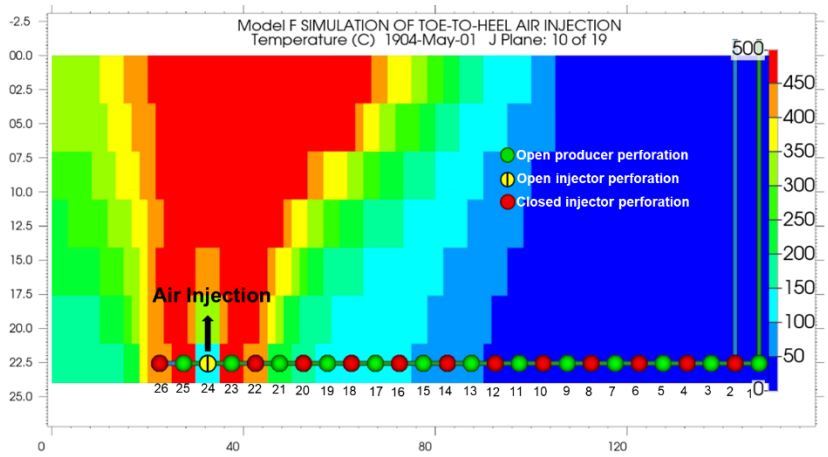

Figure 4.29 Temperature profile at the vertical midplane following the second 18-month air injection period (November 1, 1902 – May 1, 1904), with air injected exclusively through perforation #24.

To simplify the presentation and avoid displaying the schematics for each air injection interval location, it is important to note that the same injection shifting pattern was followed throughout the wellbore, while all production perforations remained fully open. The air injection interval was shifted every 18 months over the course of the 3012-day simulation. This systematic progression continued as air was injected further up along the wellbore, advancing the combustion front and mobilizing the oil in a toe-to-heel fashion.

It is important to note that the numerical models created with CMG STARS simulate one perforation every 5 meters to represent the injection or production of fluids as a source/sink term in the mass balance conservation equation. However, in practice, perforating guns can create a specified number of perforations per linear foot, with shot densities typically ranging from 13 to 39 shots per meter (SPM)(Lake & Clegg, 2007). The optimal shot density for a well is best determined using a nodal analysis simulator. For the case of models E through H, there are 26 numerical perforations in total—13 for injection and 13 for production—each covering a 5-meter span. Each numerical perforation in the model represents multiple actual perforations, depending on the shot density used during the operation.

4.3.5.2 Oil Production

Figure 4.27 depicts the oil production rate and cumulative oil production for Model F. Similar to Model D, the early stage of the simulation shows a comparable trend in oil production, influenced by the injection of hot steam during the PIHC. Consequently, the oil production values from the beginning of the simulation until the end of the PIHC are identical to those described for Model D.

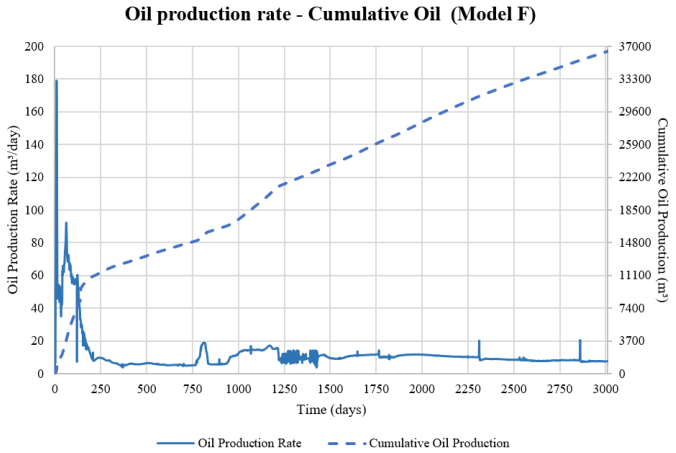

Figure 4.30 Oil production rate and cumulative oil production for model F.

Production experienced minor spikes due to possible coke accumulations from February to April 1903 (days 769 to 834), when oil production reached 20 m³/day. Subsequently, from 1903 to 1904 (days 916 to 1216), oil production increased and stabilized at approximately 15 m³/day. Following this period, until the end of the simulation, oil production ranged between 6 to 8.5 m³/day.

4.3.5.3 Oil Saturation

According to Figure 4.28, the profile of the residual oil saturation after the simulation period closely resembles the results from Model D (Figure 4.17). However, we observe a more pronounced reduction in oil saturation near the horizontal well in this case. This is attributed to the progressive and lateral advancement of the gas injection point. As the injection point is opened and closed every 18 months, the mobile oil front gradually moves towards the heel of the well, demonstrating an improvement in oil recovery due to the sequential injection strategy.

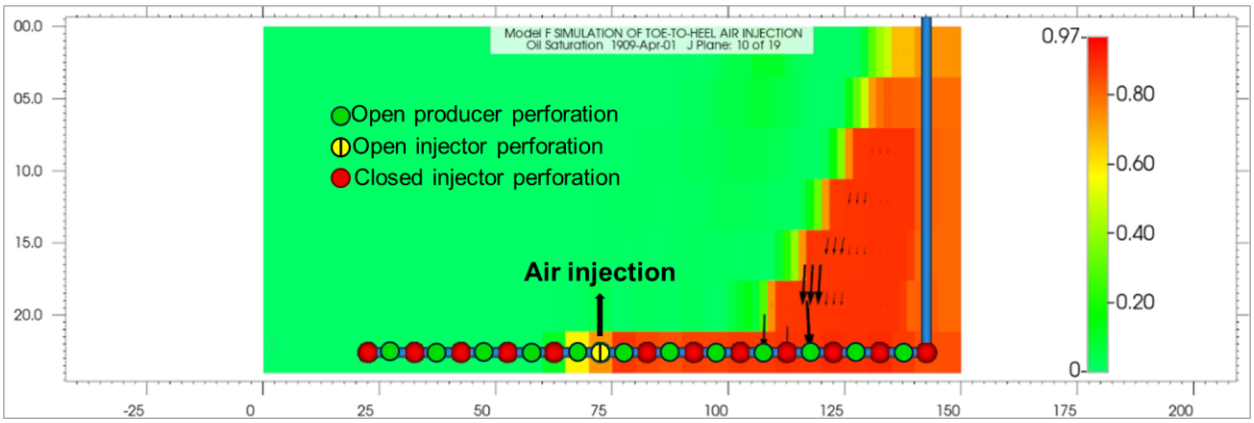

Figure 4.31 Oil saturation profile at the end of the simulated time for model F (3012 days) at the vertical midplane.

4.3.5.4 Fuel Availability

At the beginning of the simulation, during the pre-ignition heating cycle, coke formation was similar to that observed in Model D. The steam injection from the last three perforations at the toe heated the surrounding area, causing the oil to be pushed toward the producer perforations and fostering coke formation, which helped sustain the combustion front. One of the main differences is that by the end of the simulation, Model F exhibited a coke availability of 42 kg/m³, whereas Model D showed approximately 51 kg/m³. This difference is due to the greater coke consumption in Model F, leading to better production outcomes compared to Model D. This is evidenced by the total oxygen production, which was 7.14% lower in Model F than in Model D, indicating a more efficient combustion process in Model F. While the coke zone in Model F is not clearly defined in

the vertical midplane section, coke deposition extended further along the horizontal dimension of the reservoir compared to Model D. As seen in Figure 4.29, by the end of the simulation, the coke zone in Model F reached 73 meters ahead of the toe in one of the offset parallel planes to the vertical midplane, whereas in Model D, this extent was less pronounced.

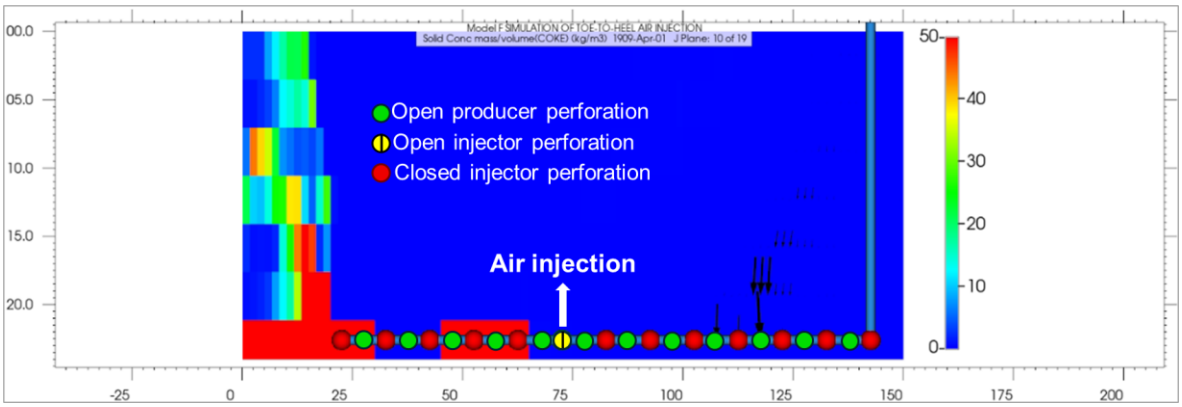

Figure 4.32 Fuel Availability (kg/m³) profile at the vertical midplane of model F at the end of the 3012-day simulation

4.3.5.5 Temperature

By the end of the PIHC (120 days, or May 1901), the temperature near the steam injection area, close to the last three perforations at the toe of the well, exceeded 500°C. This high temperature led to the formation of coke and the displacement of bitumen towards the producer well perforations. Eighteen months later, in November 1902, the air injection point was shifted from the last injector perforation to the second-to-last perforation, advancing the combustion front. This shift occurred because sufficient coke had been deposited ahead of the new injection point, acting as a barrier to prevent air channelling. As a result of this first shift, the combustion front maintained an average temperature of 650°C and advanced approximately 30 meters.

In May 1904, the injection point was moved again, surpassing the combustion region, and air was started to be injected into an area ahead of it. Injecting directly into the coke zone allowed the air to consume the fuel effectively. However, when the injection point shifted again, the absence of a coke zone to burn prevented the sustained propagation of the combustion front. During the shift in November 1905, the high temperatures observed until this point ceased to progress towards the heel, resulting in the high-temperature zone remaining almost unchanged for the rest of the

simulation and failing to advance further into the reservoir. Figure 4.30 shows the temperature profile for the vertical midplane at the end of the simulated time.

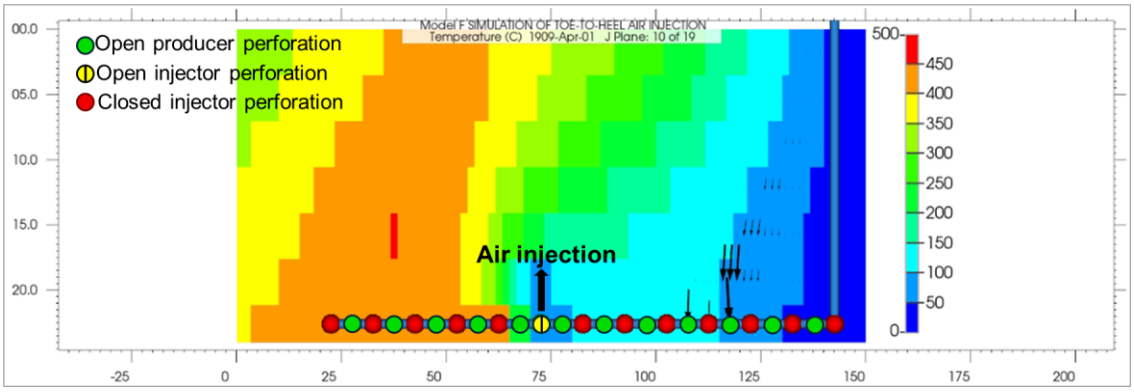

Figure 4.33 Temperature (°C) profile at the vertical midplane of model F at the end of the 3012-day simulation

4.3.6 Model G: Single Injector-Producer Wellbore with Advancing Injection interval every 18 months (Dimensions: 450 m x 257 m x 24 m)

Model G will be the primary focus for the remainder of this thesis, representing the innovative core of this research. It shares the dimensions and single wellbore configuration of Model E (450 m x 257 m x 24 m) but incorporates an advancing injection mechanism similar to what was observed in Model F. This selective, advancing injection mechanism is designed to optimize air injection to the most critical zones of the reservoir. Based on extensive research and analysis, a calculated interval of 18 months has been determined as optimal for closing one injector perforator and opening the next, facilitating the controlled movement of air injection along the well.

4.3.6.1 Oil Production

The oil production graph from the 20-year simulation of the THAI model with a single producer-injector horizontal wellbore offers valuable insights into the reservoir's performance and the effectiveness of the air injection process. According to Figure 4.31, oil production for Model G at injection temperatures of 300°C, 150°C, and 50°C exhibited a similar trend during the PIHC phase, with initial peaks around 155 m^3/day. This high production rate was due to steam preheating, which significantly enhanced the bitumen's mobility. As the simulation progressed, the production rates stabilized, averaging between 54-93 m^3/day.

For the case where the injection temperature was chosen to be 300, once the PIHC period concluded and air injection commenced, the production averaged 25-27 m^3/day for the remainder

of the simulation. These fluctuations included noticeable spikes and troughs, which corresponded to the moving air injection intervals as the injection switched from one perforator to the next downstream along the well. This pattern highlights the dynamic nature of the combustion front and its impact on oil recovery rates throughout the extended simulation period.

When air injection temperatures were 150°C and 50°C, oil production exhibited similar behaviour during the pre-ignition heating cycle, with the production curves displaying comparable patterns. However, around day 1765, a divergence in oil production occurred across the three cases. This change was primarily due to the model with an air injection temperature of 300°C, where the higher temperature facilitated greater oil mobility and reduced density. The elevated temperature induced thermal cracking reactions, generating less viscous components, which enhanced oil production.

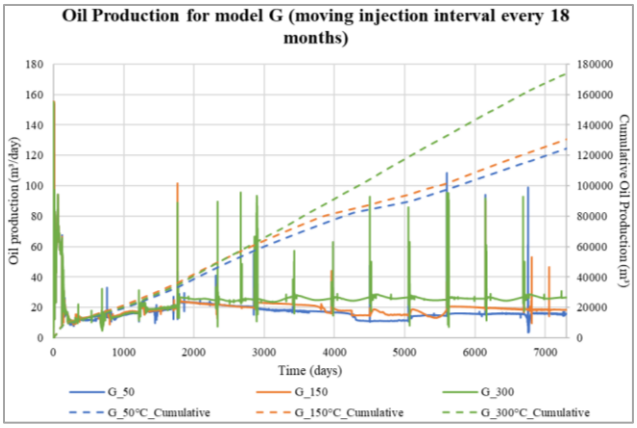

Figure 4.34 Graph of oil production rate and cumulative oil production for numerical Model G at air injection temperatures of 50°C, 150°C, and 300°C.

4.3.6.2 Oil Saturation

As mentioned previously, the oil production trend for the three cases with varying air injection temperatures was virtually the same until day 1765 (November 1905), the date when the fourth injector perforator was activated. Analyzing the oil saturation profile results, as soon as this perforator was opened, its surrounding oil saturation dropped to zero in the model with an air injection temperature of 300°C. However, when the injection temperature was 150°C and 50°C, the oil saturation in the grid block containing this perforator remained at 73% and 91%, respectively.

This explains why, on day 1765, the production in the model with a 300°C air injection temperature surpassed those with injection temperatures of 150°C and 50°C. Additionally, the oil sweep

efficiency in the model with a 300°C air injection temperature was significantly better compared to the models with 150°C and 50°C, as illustrated in Figure 4.32. The oil saturation profile indicates that higher air injection temperatures along the wellbore are directly proportional to the final oil recovery.

This is corroborated by the final oil recovery in Model G, where the air injection temperature of 300°C resulted in a 33% and 39% higher oil recovery compared to the models with air injection temperatures of 150°C and 50°C, respectively.

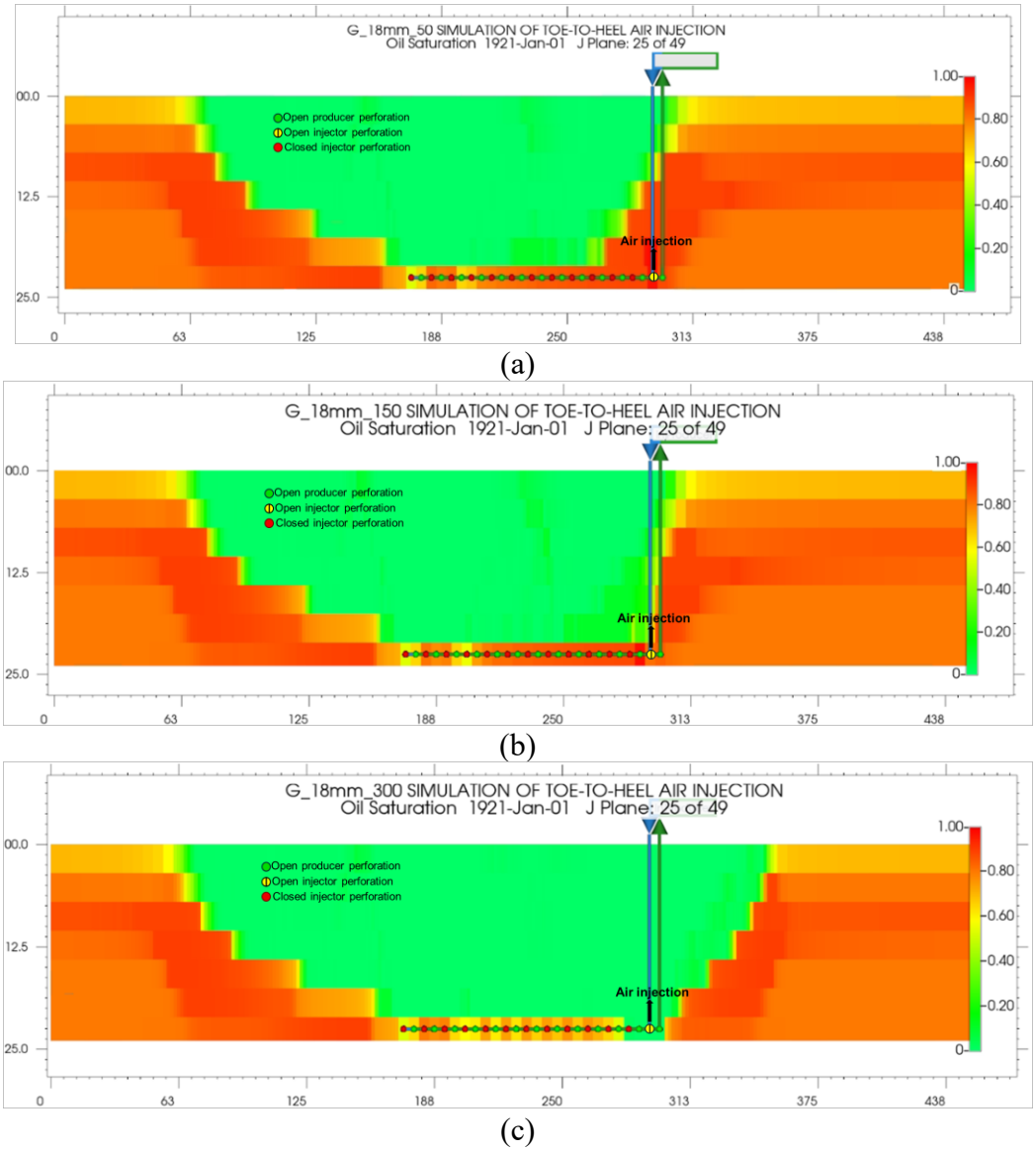

Figure 4.35 Oil saturation profiles along the vertical midplane (plane 25 of 49) of Model G at the end of the 20-year simulation for air injection temperatures of (a) 50°C, (b) 150°C, and (c) 300°C.

4.3.6.3 Fuel Availability

According to Figure 4.33.c, which depicts the results of fuel availability for Model G with an air injection temperature of 300°C, the coke availability ranged from 35 to 62 kg/m³. The Coke Zone exhibited a forward-leaning progression that advanced favourably from the beginning of the simulation until June 1906. At this point, when the air injection interval was opened at the fourth perforator, the coke zone was almost entirely consumed, leading to its disappearance. Consequently, oxygen production increased as the oxygen was not fully achieving its combustion function.

In 1909, the simulation indicated some coke deposition in the first two layers, which were combusted almost immediately. This was caused by the moving air injection interval. The air injection temperature of 300°C facilitated thermal cracking reactions, resulting in coke deposition in the reservoir. The pre-ignition heating cycle with steam left unburned coke near the toe of the well, while the area opposite the toe showed coke combustion as the air injection moved along the horizontal well.

It is unclear why coke deposition predominantly occurred in the upper layers of the reservoir rather than uniformly across its depth, given the homogeneity of the reservoir. Ideally, a contiguous, homogeneous coke zone should form throughout the reservoir. However, the periodic movement of the injection device every 18 months stimulated further coke production, enhancing oil mobilization and increasing overall oil production.

For the simulation model with air injection temperatures of 150°C and 50°C, it is observed that the coke front develops in the area adjacent to the toe of the well during the pre-ignition heating cycle. This is favourable as it ensures sufficient coke deposition to support the progressive advancement of in-situ combustion during the simulation. However, the coke front in the vertical midplane disappears between April and June 1905 for both models with injection temperatures of 50°C and 150°C. This occurs because the oxygen bypasses the coke zone, subsequently injecting into areas where coke had not yet been deposited.

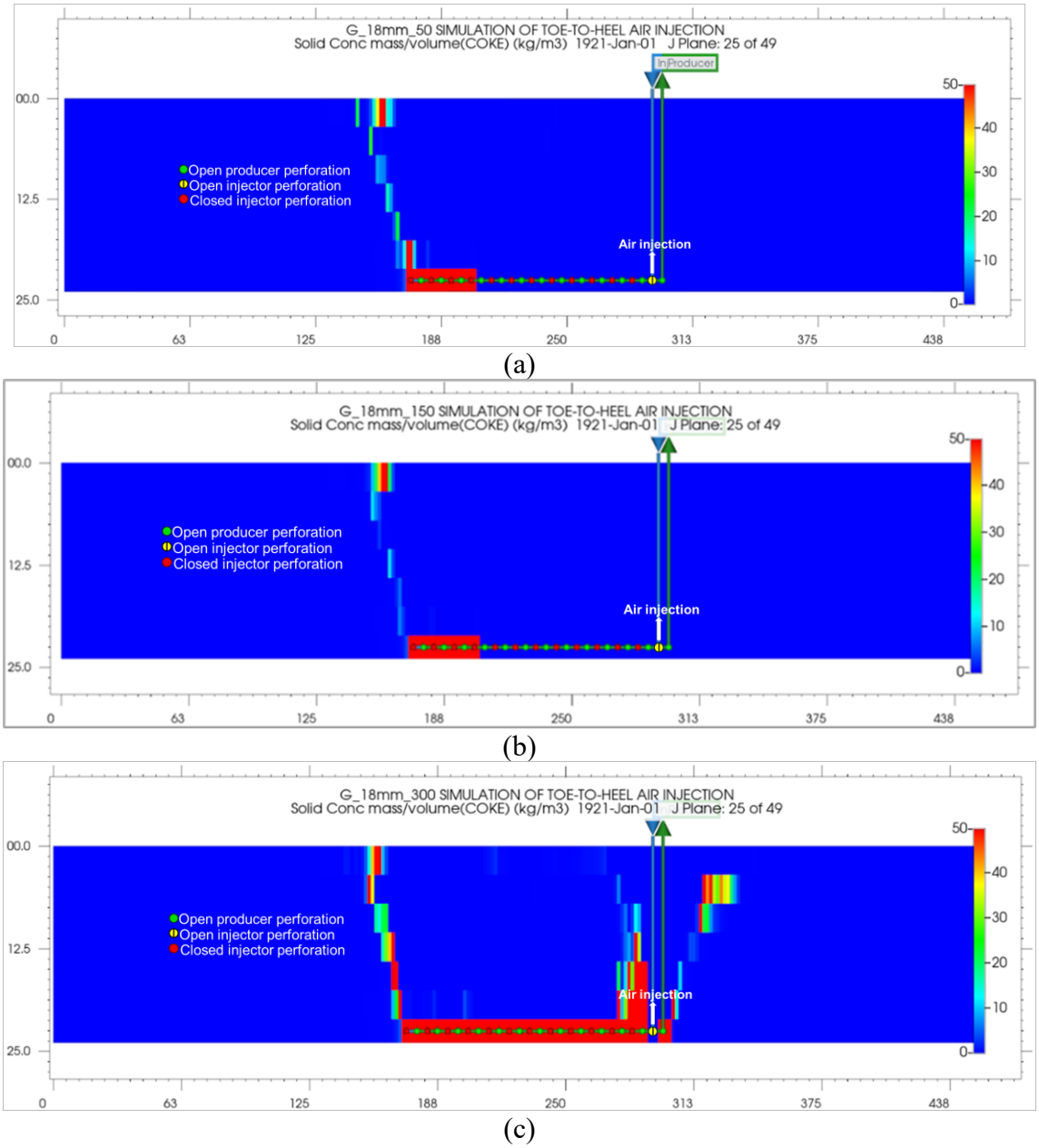

Figure 4.36 Coke availability profiles along the vertical midplane (plane 25 of 49) of Model G at the end of the 20-year simulation for air injection temperatures of (a) 50°C, (b) 150°C, and (c) 300°C

4.3.6.4 Temperature

According to the results shown in Figure 4.34, the temperature at the end of the twenty-year simulation for the case with air injection at 300°C indicates that it exceeds 500°C. This is due to the consumption of deposited coke and the combustion of petroleum pseudo-components, particularly the light component, which releases the most heat of reaction when combusted by oxygen.

However, it is evident that in the models where the injection temperature was 150°C and 50°C, the location of air injection does not lead to coke deposition, nor does it achieve optimal temperatures for in-situ combustion. This is because the injected oxygen is not being consumed in combustion reactions. Consequently, there was a significant increase in oxygen production, particularly noticeable when the fourth perforation was opened in November 1905.

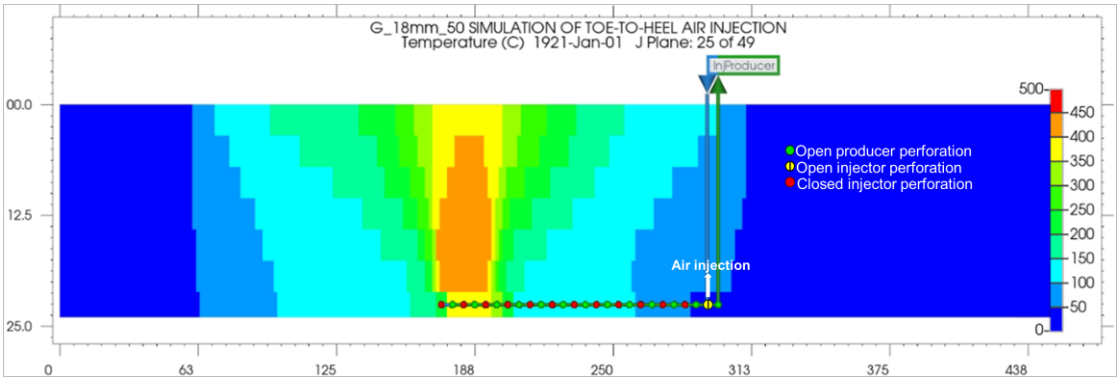

(a)

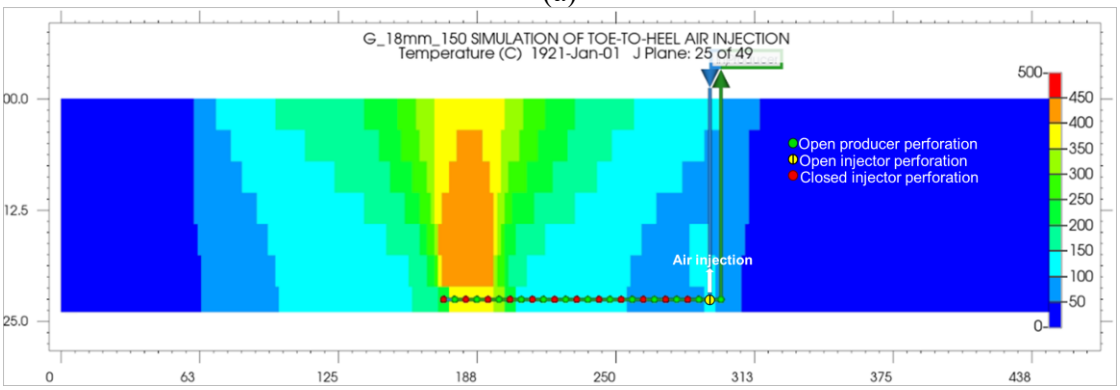

(b)

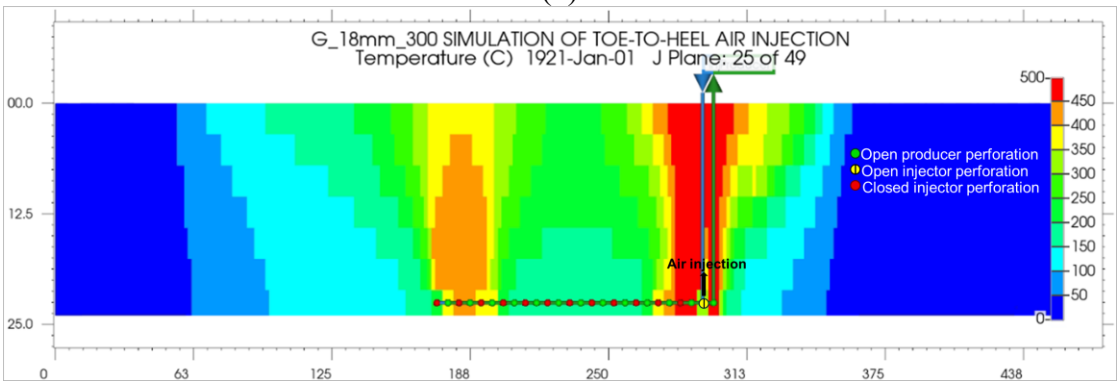

(c)

Figure 4.37 Temperature profile along the vertical midplane for air injection temperatures of (a) 50°C, (b) 150°C, and (c) 300°C

4.3.7 Model H: Single Injector-Producer Wellbore with Advancing Injection interval every 24 months (Dimensions: 450 m x 257 m x 24 m)

4.3.7.1 Model Description

Based on the results from the twenty-year simulation of Model G, where the air injection interval was moved every 18 months at injection temperatures of 300°C, 150°C, and 50°C, a comparative analysis was decided upon. This time, the interval for moving the injection point was increased from 18 to 24 months. The objective was to allow for more coke generation to optimize the combustion process. The simulation was again conducted over 20 years, with the analysis focusing on oil production, temperature, oil saturation, and residual coke concentration. All other parameters and configurations were kept identical to Model G's to isolate the effects of extending the injection interval between perforations.

4.3.7.2 Oil Production

As seen in Figure 4.35, the oil production behaviour for cases with air injection temperatures of 50°C, 150°C, and 300°C appears similar to the trends observed in Figure 4.31, which shows oil production and cumulative oil production results for Model G. For all three cases with varying injection temperatures, oil production remained between 10 and 17 m^3/day for approximately the first 1700 days. After this period, the model with an air injection temperature of 300°C showed a deviation in production, resulting in higher rates compared to the lower temperatures.

This model proved to be the most effective in terms of oil production, achieving values ranging between 20 and 28 m^3/day throughout the simulated period. The production peaks observed in the figure correspond to the moments when the air injection perforation point was changed. By the end of the twenty-year simulation period, the cumulative oil production in the model with a 24-month injection interval at 300°C was the highest, with a total of 162,704 m^3. The models with 150°C and 50°C injection temperatures produced 130,508 m^3 and 122,061 m^3, respectively.

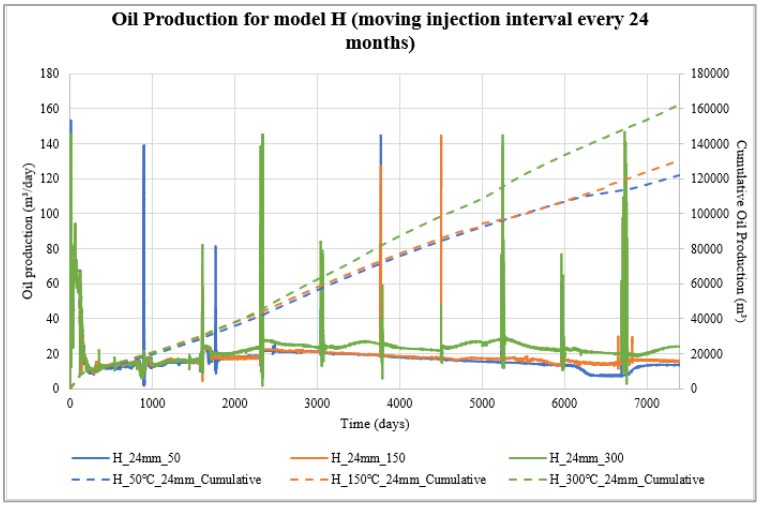

Figure 4.38 Graph of oil production rate and cumulative oil production for numerical Model H at air injection temperatures of 50°C, 150°C, and 300°C.

4.3.7.3 Oil Saturation

According to the oil saturation results shown in Figure 4.36, the sweeping behaviour of the oil is very similar to what was previously observed in Model G. Despite the increased delay in the opening and closing of perforations, now set at 24 months, the oil production behaviour remains almost identical. In the oil saturation profile for the model with an air injection temperature of 300°C, it is evident that when a perforation opens to inject hot air, the viscosity of the surrounding oil decreases significantly, allowing it to flow more easily to the producer well.

However, this effect is not observed when the air injection temperatures are 150°C and 50°C. The grid blocks adjacent to the perforation maintain oil saturation levels between 0.7 and 0.8, indicating suboptimal sweeping efficiency. The model with 300°C air injection significantly influences oil mobilization towards the producer well. By the end of the 20-year simulation, the area behind the well's vertical section—meaning the area behind the well—has been more effectively affected in the model with 300°C air injection compared to the lower temperature models.

This result is not surprising, as the cumulative oil production for the 300°C injection model is 24% and 32% higher than the models with 150°C and 50°C air injection, respectively. Analyzing the oil flux vectors reveals that, in all three cases, oil production is influenced by the oil flow vectors coming from both flanks offset from the horizontal well. In other words, in the vertical planes adjacent to both sides of the vertical midplane, the surrounding oil is more significantly affected by the 300°C hot air injection than the 150°C and 50°C models.

The air flux vectors indicate that the oil flows towards the horizontal well from the upper parts of the reservoir. In the 300°C injection model, the viscosities of the oil descending the reservoir flanks range from 50 to 100 cp at temperatures between 80 and 120°C. In contrast, the 150°C air injection model shows oil viscosities descending the flanks ranging from 440 to 740 cp at temperatures around 84°C. The 50°C air injection model has oil descending from the top of the reservoir with viscosities between 500 and 700 cp and temperatures between 75 and 82°C.

Additionally, the 300°C injection model presents a flue gas concentration 35% higher than the 150°C and 50°C air injection models. This higher flue gas concentration improves the displacement of oil in the upper parts of the reservoir. In-situ combustion leverages the generation of flue gases to displace a more significant amount of oil, demonstrating the advantage of higher-temperature air injection.

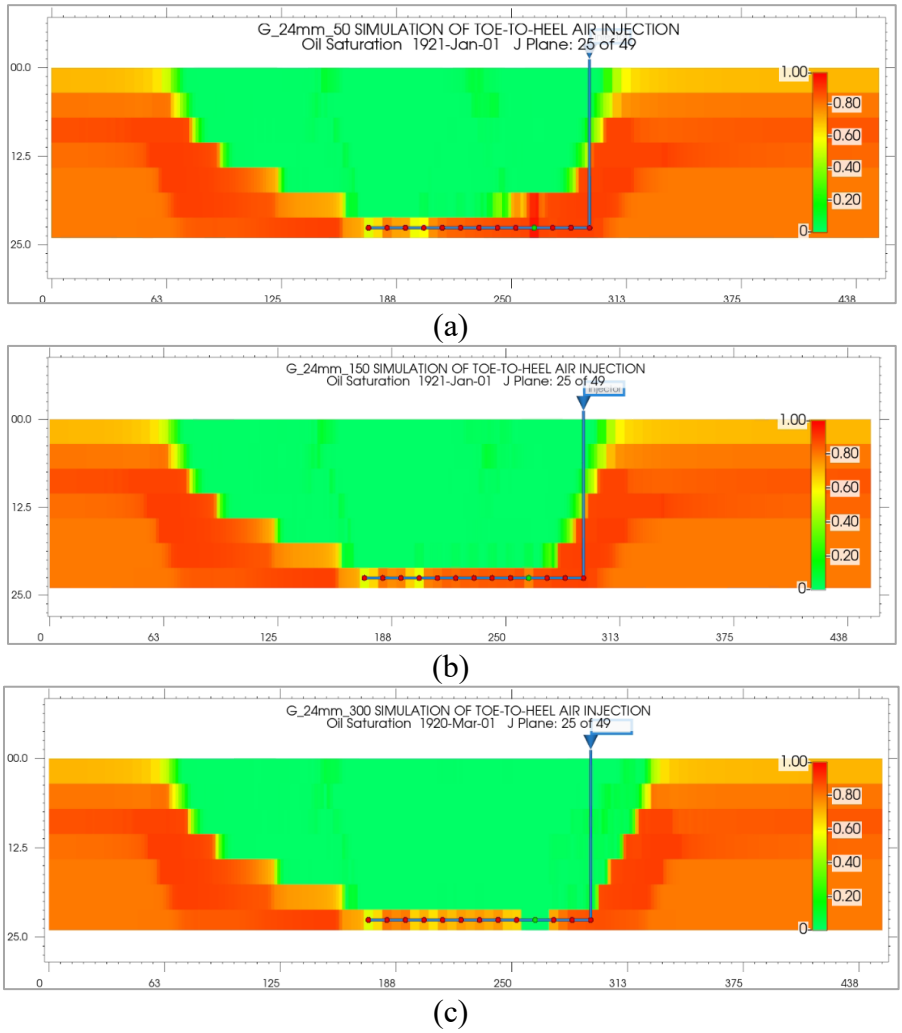

Figure 4.39 Oil saturation profiles for model H at the vertical midplane at the end of the 20-year simulation with air injection temperatures of (a) 50°C, (b) 150°C, and (c) 300°C.

4.3.7.4 Fuel Availability

The average coke availability concentration for the models with air injection at 50°C and 150°C was 233 kg/m³, with a higher concentration near the toe of the horizontal well, as indicated in Figures 4.37a and 4.37b. For the model with air injection at 300°C, the fuel availability results demonstrate that the fuel availability profile is conducive to the progression of in-situ combustion, with values ranging from 28 to 55 kg/m³ until April 1908. Around mid-1908, there is a notable disruption of the coke front, leading to an increased accumulation of oxygen in the reservoir without the expected deposition or consumption of coke necessary for a successful in-situ combustion project.

In terms of coke deposition and consumption, it is evident that as air is injected at different points every two years, it creates a disturbance that results in coke generation in the upper zone adjacent to the injection perforation. This phenomenon generates an expansive coke wave primarily in the first and second layers since the oxygen profile is most active and concentrated in these upper layers of the reservoir. Consequently, coke zones are predominantly formed at the reservoir's top.

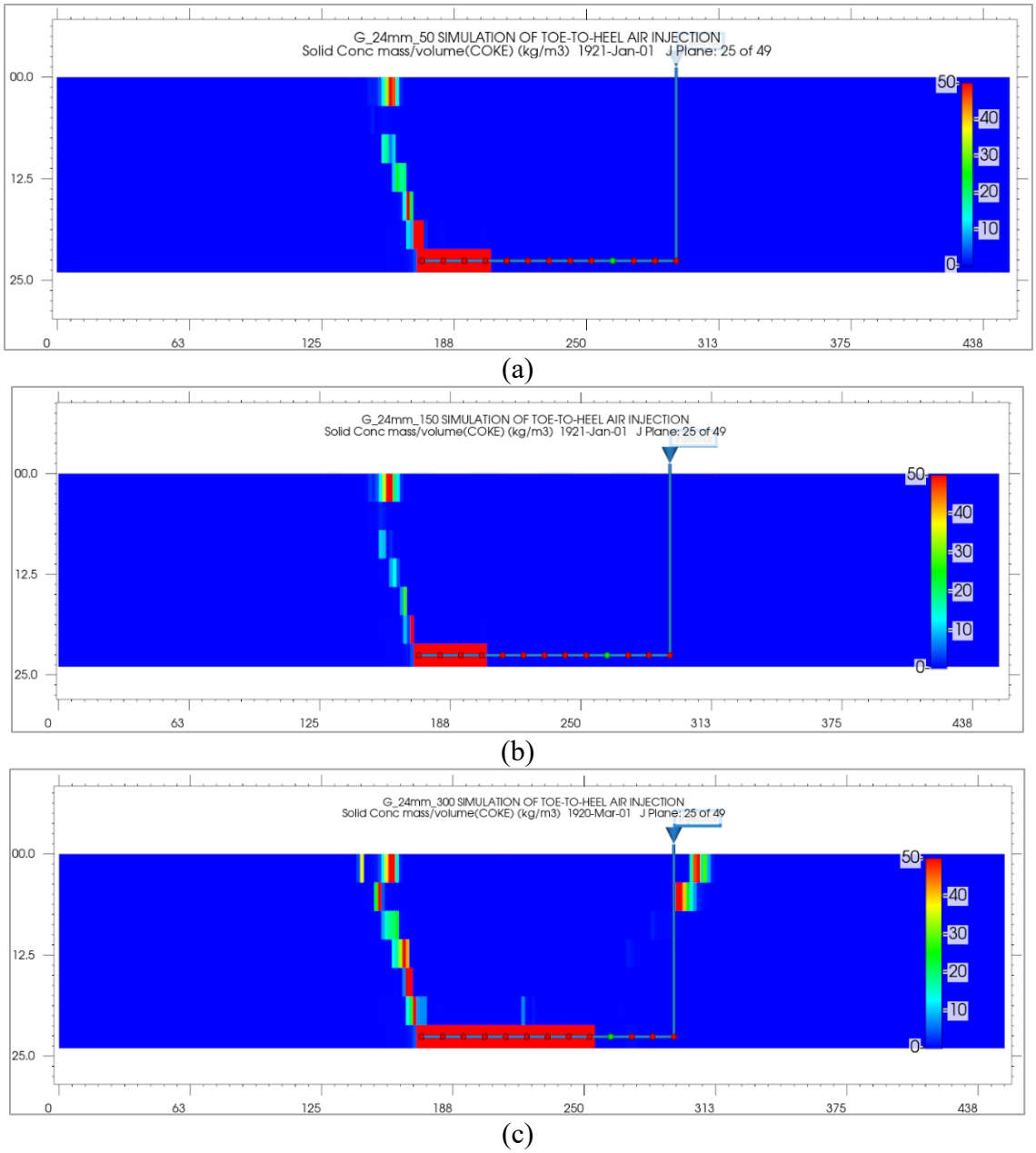

Figure 4.40 Coke availability profiles for Model H at the Vertical Midplane at the End of the 20-Year Simulation with Air Injection Temperatures of (a) 50°C, (b) 150°C, and (c) 300°C

4.3.7.5 Temperature

The results presented in Figure 4.38 illustrate the temperature profiles resulting from the 20-year simulation. In the scenarios where air injection temperatures of 50°C and 150°C were utilized, it is evident that the temperature did not significantly increase, indicating that coke combustion was not occurring in these cases. Conversely, the model with an air injection temperature of 300°C demonstrates a positive response regarding temperature increase. The advancement of the injection

interval every 24 months facilitates effective coke combustion. This exothermic reaction releases heat, which subsequently mobilizes the surrounding oil in the areas near the air injection points.

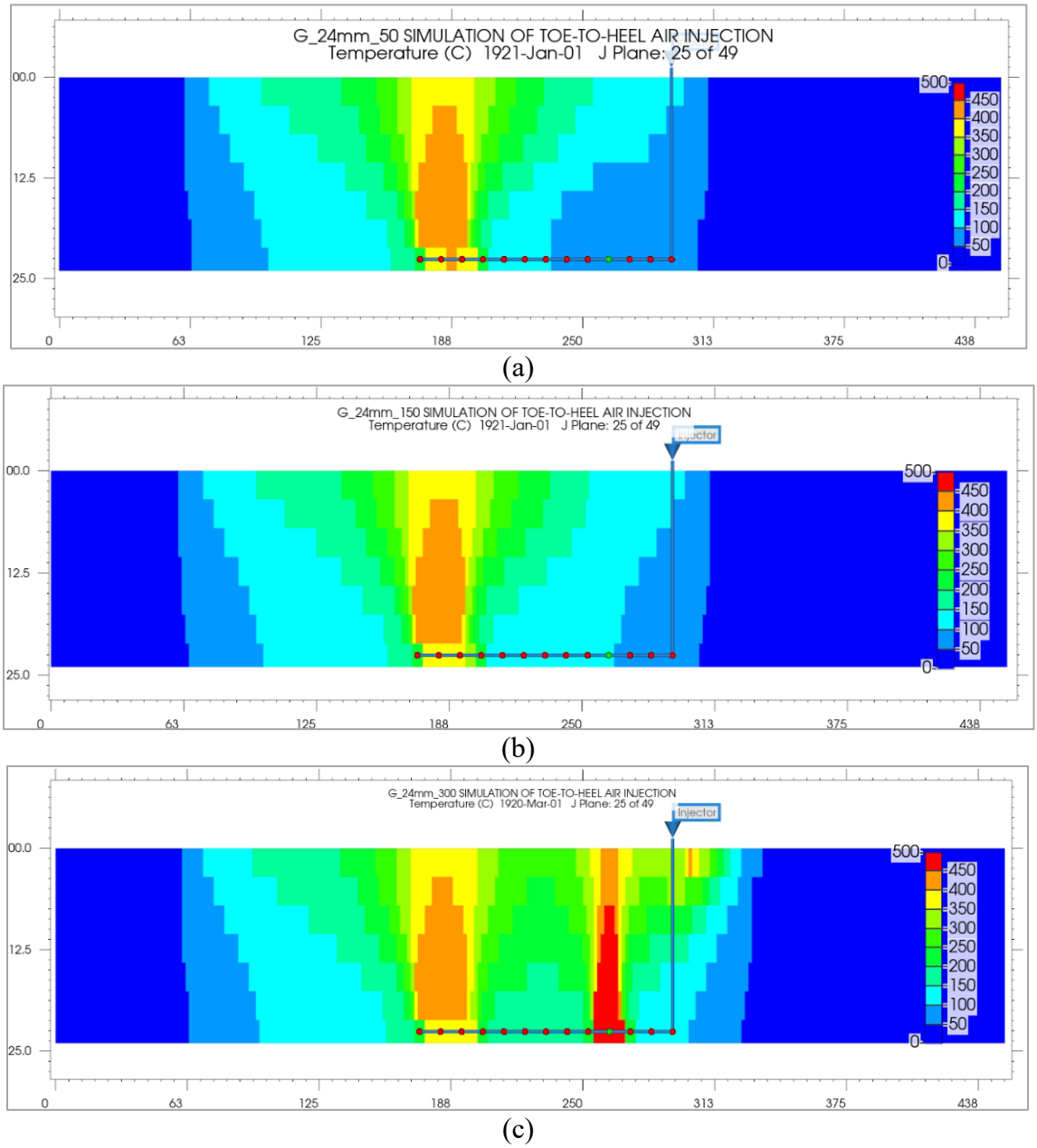

Figure 4.41 Temperature profiles for Model H at the Vertical Midplane at the End of the 20-Year Simulation with Air Injection Temperatures of (a) 50°C, (b) 150°C, and (c) 300°C

4.4 Discussion

4.4.1 Comparison of Model A1 and Model B: impact of elongation of the injector wells

Model A1 and Model B shared the same wellbore configuration, with the primary difference being the depth of the injector wells. In Model B, the injector wells extended to the bottom of the reservoir. This design change led to notable differences in performance.

4.4.1.1 Early Oil Production

In Model B, oil production began earlier, on day 98, compared to day 473 in Model A1. This earlier production is attributed to the more significant accumulation of steam at the toe of Model B, which resulted in a significant pressure increase and, consequently, earlier oil mobilization.

4.4.1.2 Impact of Heavier Oil Fractions and Coke Formation

The presence of heavier oil fractions and coke in Model B facilitated more effective displacement of oil towards the producer well. In contrast, Model A1, with less coke deposited during the pre-ignition heating cycle (PIHC), showed less efficient oil displacement.

4.4.1.3 Temperature Influence

Model B exhibited higher overall temperatures compared to Model A1, which played a crucial role in enhancing oil displacement to the producer well.

4.4.1.4 Coke Deposition

More coke was deposited at the base of Model B, particularly at the end of the combustion front, further contributing to oil displacement efficiency.

4.4.1.5 Oil Production Increase

At the end of the simulation, Model B demonstrated a 48% increase in oil displacement compared to Model A1, highlighting the benefits of elongating the injector wells to cover the entire reservoir depth.

4.4.2 Impact of Increased Injection Rates and Boundary Expansion: Model C

The expansion of the model boundaries, using the same configuration as Model A1, was tested in simulated model C with air injection rates of 10,000 m^3/day and 20,000 m^3/day per injector.

4.4.2.1 Air Injection and Combustion Dynamics:

- *Model C (20,000 m³/day)*

This model showed the initial combustion of coke at the end of the PIHC, with stationary air injection at the top reservoir layer. As pressure increased due to steam injection, oil production trends began to rise irregularly with the advancing combustion front.

- *Model C (40,000 m³/day)*

Doubling the air injection rate resulted in significantly higher coke formation, with an 11-fold increase in coke compared to the 10,000 m³/day model. By the end of the simulation, the maximum coke concentration reached 81 kg/m³, within an acceptable range. However, the model with a 40,000 m³/day injection rate predicted unrealistic coke concentrations of up to 1366 kg/m³.

4.4.2.2 Combustion Front Behavior:

- *Model C, 20,000 m³/day Air Injection*

Multiple combustion fronts were observed in the first reservoir horizontal layer, with fronts progressing towards and away from the producer well's toe.

- *Model C, 40,000 m³/day Air Injection*

This model showed less intense combustion fronts near the back and more towards the producer well. The oil rate began to rise around day 600 due to a pressure drawdown, followed by a surge in oxygen production, which reduced coke combustion and overall reservoir temperature.

4.4.2.3 Comparison

The 20,000 m³/day model showed a delayed decrease in average temperature and an oil production surge around day 1157, indicating a more gradual response than the 40,000 m³/day model.

The increase in model boundaries significantly influences fluid behaviour and chemical interactions, ultimately affecting oil production. Cumulative oil production compared to Model A1

indicated a 63% reduction during the first 1248 simulation days, suggesting further research is needed to understand these dynamics fully.

4.4.3 Implications of Single Acting Producer/Injector Wellbore with Moving and Stationary Injection Intervals: Models D and F

Model D provided a case study featuring a single wellbore functioning as both an injector and a producer, with air injection occurring exclusively through the last perforator located at the toe of the well. This novel approach to THAI presents a new challenge in achieving optimal in-situ combustion processes.

Conversely, Model F is based on the premise that a moving combustion front can be better supported by a mobile air injection inlet. In this model, the air injection point was moved by sequentially opening one perforator at a time every 18 months.

The results showed that Model F exhibited 23% higher oil production than Model D, indicating the effectiveness of the moving injection interval. Over the simulated period of 8.2 years, Model F demonstrated better oxygen consumption and higher combustion efficiency, leading to a 21% reduction in residual coke in the reservoir by the end of the simulation.

In Model D, coke deposition formed more uniform and pronounced combustion zones, moving in an arrow-shaped pattern toward the heel of the well. However, Model F displayed a disrupted combustion zone in the uppermost layer of the reservoir because the air was directed below the coke-deposited area, causing it to combust the previously deposited coke zones.

The fact that the air injection interval in Model F moved one perforator at a time every 18 months allowed the tip of the coke-deposited ring to advance 28% faster than in Model D. The combustion

and temperature profiles suggest that an optimized time interval for air injection along the horizontal well can significantly improve the performance of this technology.

4.4.4 Effects of Extending Model Boundaries in I and J Directions with a Single Producer/Injector Wellbore: Comparing Stationary and Moving Injection Intervals: Models E, G and H

4.4.4.1 Air injection temperature of 50 °C

In Model E, with an air injection temperature of 50°C, where the injection interval remained stationary with only one injector perforator open at the toe of the well throughout the 20-year simulation, the cumulative oil production reached 91,131 m^3. In contrast, the model with a moving air injection interval every 18 months (Model G) showed an improved oil recovery, with a cumulative production of 124,505 m^3, reflecting a 36% increase compared to Model E. Similarly, Model H, which extended the interval between sequential air injection movements from 18 to 24 months, predicted a cumulative oil production of 120,822 m^3, demonstrating a slightly lower improvement of 33% compared to Model E.

The temperature results indicated that Model E maintained consistent combustion temperatures throughout the entire 20-year simulation period. However, Models G and H experienced temperature drops at 4,302 and 6,269 days, respectively. This inconsistency in temperature maintenance could impact the overall efficiency of the combustion process.

Model H predicted higher coke deposition when the injection interval moved along the horizontal well every 24 months. This was evidenced by a 13% increase in net coke reacted compared to Model G. Despite the sequential movement of the injection interval, neither Model G nor Model H exhibited a progressive movement of the coke zone typical of a standard air combustion pattern. The timing of 18 months for Model G and 24 months for Model H proved insufficient for optimal

air injection, indicating a need for further research to understand the dynamics better and improve this novel approach.

The study demonstrates that extending the model boundaries and adjusting the air injection intervals can significantly impact oil recovery and combustion efficiency. However, the optimal timing for moving the air injection interval requires further investigation to achieve the best results.

4.4.4.2 Air injection temperature of 150 °C

In terms of oil production, Models G and H predict almost identical oil recovery after the 20-year simulation, with a minimal difference of only 1%. Both models show significantly less coke deposition in the reservoir than Model E, which uses a stationary injection approach.

- *Coke Deposition Characteristics in Model E (Stationary Injection):*

Coke-rich areas are primarily located at the top of the reservoir, with the coke zone extending longitudinally along the same axis as the horizontal wellbore. This coke zone reaches a distance of 76 meters from the toe of the well.

- *Coke Deposition Characteristics in Models G and H (Moving Injection)*

Coke zones are less pronounced and almost stationary, located around the toe of the well. The coke zone extends only 33 meters from the toe, significantly shorter than in Model E. The moving air injection approach in Models G and H results in the burning of previously deposited coke, leading to reduced coke buildup over time.

Interestingly, despite Models G and H's moving injection intervals, Model E demonstrates better in-situ combustion performance due to its more extensive coke zone. This result suggests that the dynamic air injection strategy in Models G and H, while innovative, may require further refinement regarding the timing and placement of air injections to optimize coke deposition and combustion.

- *Oxygen Production and Combustion Efficiency:*

Model E exhibits higher oxygen consumption, with the produced oxygen mole fraction ranging from 8-9%, indicating efficient combustion. In contrast, Models G and H show higher oxygen production, accounting for 21% of the gas volume, which indicates less efficient combustion as it results in more unconsumed oxygen. This suggests that Model E's stationary injection approach is

more effective in achieving complete combustion compared to the moving injection intervals in Models G and H. The higher efficiency in oxygen utilization in Model E likely contributes to its better overall performance in in-situ combustion. The higher air injection temperature of 150°C in Models G and H did not lead to a well-progressing in-situ combustion mechanism. Further research is necessary to understand better and optimize the air injection strategy to achieve successful in-situ combustion.

The comparison highlights that while Models G and H offer innovative approaches with moving injection intervals, they still fall short in some aspects compared to the stationary injection model (Model E). A better understanding of the optimal air injection parameters, including temperature, timing, and placement, is essential for improving in-situ combustion efficiency and achieving higher oil recovery rates.

4.4.4.3 Air injection temperature of 300 °C

To achieve better combustion efficiency, a temperature of 300°C was selected to assess the impact of higher air injection temperatures. The results demonstrated a significant increase in cumulative oil production, with an augmentation of 35% in Model G and 24% in Model H compared to Model E.

At the end of the 20-year simulation, the temperature patterns in Models E, H, and G revealed distinct behaviours. Model E exhibited a forward-leaning combustion front with temperatures exceeding 400°C, reaching up to 70 meters from the toe of the wellbore, and high temperatures also extended 36 meters behind the toe of the well. In contrast, Models G and H showed improved oil displacement due to newly created combustion fronts every 18 months and 24 months, respectively. This dynamic behaviour was not observed in previous models with lower air injection temperatures.

The higher air injection temperature of 300°C facilitated the advancement of the coke zone in Models G and H. The formation and movement of coke and high-temperature zones along the combustion front created a bulldozing effect, as described by Ado (2017). This phenomenon was absent in models with lower air injection temperatures.

In terms of oil production, Model G, which adjusts the air injection interval along the horizontal well by opening new perforators every 18 months, proved to be the most effective option for

implementing in-situ combustion. This model demonstrated superior coke combustion and enhanced oil seepage, largely due to its higher efficiency in oxygen utilization. Notably, the cumulative oxygen production in Model H was 45% higher than in Model G, indicating that Model G had a more efficient oxygen consumption process, directly contributing to its improved oil recovery performance.

In conclusion, higher air injection temperatures and optimized injection intervals significantly enhance oil recovery and combustion efficiency. Model G, with its moving air injection interval every 18 months, demonstrated superior performance compared to Models H and E. Further research is recommended to fine-tune these parameters for even better performance.

4.4.5 Comparative Analysis of a Single Horizontal Injector/Producer Well with Moving Injection Intervals (Model G) vs. the State-of-the-Art Toe-to-Heel Air Injection with Vertical Injectors and Horizontal Producer (Model C)

Comparing the proposed well configuration of moving the air injection interval every 18 months using a single wellbore (Model G) with the current state-of-the-art THAI method (model C with an air injection rate of 20,000 m^3/day), the proposed method improved oil recovery by 8% over the first 1520 days. Additionally, the new technology began economically viable oil production 420 days earlier than the conventional THAI method. The proposed model also showed a 34% decrease in cumulative oxygen production after 1520 days, indicating more successful oxygen combustion in Model G compared to Model C.

In terms of temperature, Model G achieved much higher temperatures that were favourable for high-temperature oxidation (HTO) reactions, exceeding 500°C in the vertical midplane. In contrast, Model C only reached 150-200°C by the end of the 1520-day simulation. This is corroborated by the amount of coke reacted in Model G, indicating successful in situ combustion. Over the first 1520 days, model G had 31 times more coke net reacted than Model C. Thus, it is concluded that the proposed air injection method significantly improves the current state of the art.

4.4.6 Geomechanical Analysis of In Situ Combustion in the Proposed Model G.

Temperature-induced stress in in situ combustion (ISC) arises from the extreme temperature changes caused by the combustion process. When air is injected and ignites the oil, the resulting combustion front generates significant thermal gradients between the heated and cooler zones.

This leads to thermal expansion of the heated rock, constrained by cooler areas, creating mechanical stress. Uneven expansion and subsequent cooling can cause differential stresses, potentially leading to fractures, deformation, or compaction, affecting reservoir permeability and fluid flow. Additionally, these stresses can compromise wellbore stability, potentially damaging the casing or cement, and even causing wellbore collapse. Understanding and managing temperature-induced stress is crucial for maintaining reservoir integrity and optimizing ISC operations.

Geomechanical risks in ISC stem from temperature, pressure, and fluid dynamics changes within the reservoir. Thermal expansion and contraction can cause fracturing, compaction, or pore collapse, impacting permeability and flow patterns. These stresses also risk wellbore stability, leading to casing damage or collapse. ISC may reactivate faults, causing unintended fluid migration, shear failure, or even micro-seismic events. Reservoir subsidence and surface uplift from compaction and thermal contraction are additional concerns, potentially weakening the caprock and compromising containment. Proper geomechanical modeling and monitoring are vital to mitigate these risks.

Monitoring surface deformations has shown promise in detecting subsurface combustion fronts, as demonstrated in cyclic steam stimulation by (Maharramov & Zoback, 2018). Thermal expansion during ISC can cause land uplift, driven by both thermal stress and pore pressure changes.

In the current study, geomechanical parameters were not included, which represents an area for future improvement. However, pressure maps (Figure 63a–63c) show relatively similar pressure values in models with air injection temperatures of 50°C, 150°C, and 300°C. As expected, Model G with air injection at 300°C predicted higher combustion temperatures, contributing to slightly elevated pressure values.

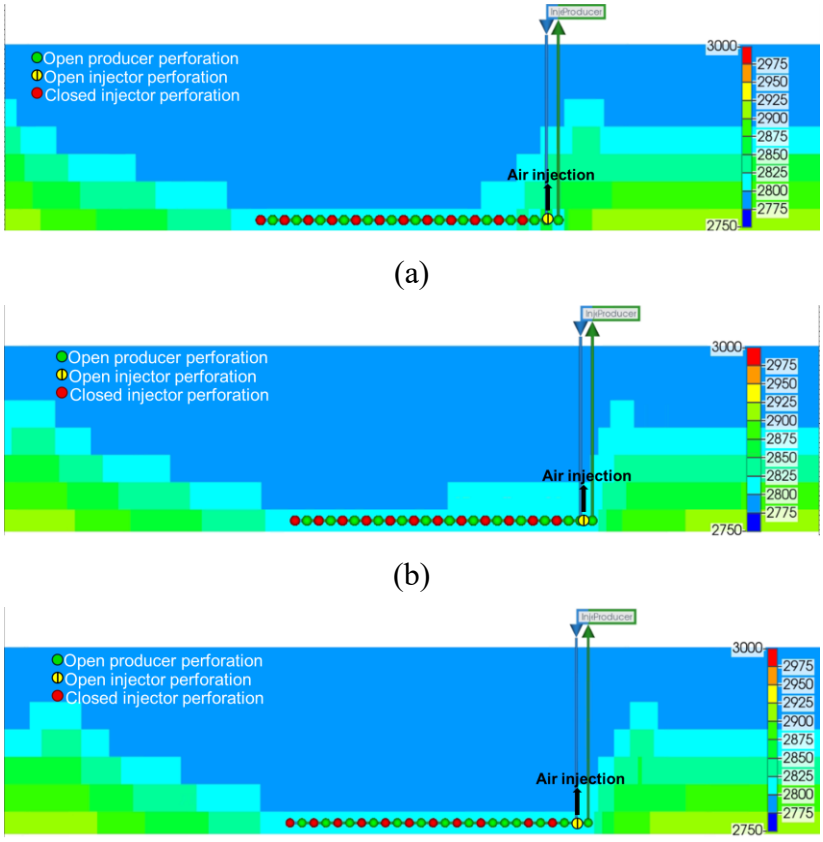

Figure 4.42. Pressure maps (kPa) at the vertical midplane for model G at the end of the 20-year simulation period with air injection temperatures of (a) 50°C, (b) 150°C, and (c) 300°C.

Chapter 5: Conclusions and recommendations for future work

5.1 Conclusions

This thesis investigates a novel approach to in-situ combustion numerical modelling, specifically focusing on a modified variant of toe-to-heel air injection. This modification incorporates a dual-functioning injection/producer single well to optimize the in-situ combustion process.

The research began with a successful verification of a previously defined lab-scale in situ combustion model, validating the results obtained by Ado (2017). Following this verification, a numerical kinetic upscaling methodology, as employed by Ado (2017), was implemented. The upscaled model was then simulated, and its results were presented, demonstrating the potential of this innovative approach for improving in situ combustion efficiency.

Eight different numerical models were carried out in order to determine insights into the elongation of the injector wells, and the expansion of the boundaries in I and J to understand the implications this has in the combustion process. The novel approach of this research is the inclusion of a single wellbore acting dually as producer/injector that has the option of injecting air at the toe and producing along the heel or performing a sequential injection by moving an air injection interval along the well every 18 or 24 months.

In current in situ combustion approaches, particularly in THAI, the airflow is directed toward the toe of the horizontal producer wellbore. However, these injection wells cannot selectively inject air into the most critical areas of the reservoir. The innovative approach presented in this research addresses this limitation by enabling sequential air injection specifically targeted at areas requiring air the most. This method reduces the distance between the injection point and the combustion zone, enhancing the efficiency and effectiveness of the combustion process.

The elongation of injection wellbores to the bottom of the reservoir model in Model B resulted in a 23% increase in cumulative oil production compared to Model A1. Additionally, Model B showed that the coke in the vertical midplane advanced nearly 10 meters further than in Model A1. This deeper injection well strategy significantly enhanced the process's efficiency, generating 4.8 times more coke than Model A1. This increase in coke quantity positively impacted the oil sweep, as the combustion of more coke released additional heat, facilitating the continuation of

the in-situ combustion mechanism. Furthermore, flue gas emissions during the process increased by 25%, indicating that the gas drive mechanism also benefited from the extension of the injector wellbores.

Unlike the original reservoir dimensions in Models A1 and B, Model C provided valuable insights into how expanding the horizontal dimensions can influence behaviour and oil production in an in-situ combustion simulation. In Model C, multiple coke zones were observed to expand laterally within the first layer of the reservoir, even extending in the opposite direction to the horizontal producer wellbore.

However, in model C, with an air injection rate of 20,000 m^3/day, no high-temperature zones were detected, indicating that coke combustion was not occurring. Conversely, the case with an air injection rate of 40,000 m^3/day did witness coke combustion, with temperatures exceeding the coke burning threshold of 400°C. This higher air injection rate led to coke accumulation in the upper sections of the reservoir, reaching up to 184 meters from the injection point by the end of the simulation. Despite the presence of oxygen in both models, the simulation with a total air injection of 20,000 m^3/day did not achieve the desired coke combustion. In contrast, the model with an air injection rate of 40,000 m^3/day demonstrated better oxygen utilization and combustion efficiency.

Models D and F were constructed to introduce a novel approach in this research. Model D utilized similar dimensions to Models A1 and B but featured a single wellbore acting as both injector and producer, with air injection occurring through the last perforator located at the toe of the well. Similarly, Model F replicated this behaviour but incorporated a moving air injection interval every 18 months.

The results indicated that Model F exhibited superior in situ combustion performance, with oxygen production being 6% lower than that of Model D. The reduced oxygen production in Model F was due to a higher rate of coke combustion, validating this method's effectiveness in enhancing oil production. Despite the high-temperature zone not moving along the well as expected, the increased rate of coke deposition and combustion in Model F resulted in a 22% increase in oil production compared to Model D.

Model E was developed to analyze the implications of expanding the dimensions of Model D and to understand how in situ combustion behaves in a larger model. Expanding the model boundaries

in Model E resulted in a 53% increase in oil production compared to Model D, which had smaller dimensions. Additionally, Model E included three subcases with different air injection temperatures: 50°C, 150°C, and 300°C. The results demonstrated that injecting air at 300°C provided the best outcomes for advancing the combustion front and the rate of coke deposition and combustion.

Lastly, an analysis was conducted on the expansion of the dimensions in Model F, leading to the development of Models G and H. This analysis aimed to compare the benefits and disadvantages of moving an air injection interval along the well every 18 and 24 months, respectively.

It was observed that air temperature plays a crucial role in enhancing oil recovery. The highest air injection temperature of 300°C resulted in oil recovery rates that were 32% and 39% higher than those in Models G with air injection temperatures of 150°C and 50°C, respectively. Opening and closing the air injection interval every 24 months for Model H yielded similar oil production values. However, this 24-month interval resulted in an overall average oil production that was 5% lower compared to Model G.

Overall, both Models G and H, which employed sequentially moving air injection intervals, demonstrated an average oil production enhancement of 36% compared to the stationary approach of injecting air solely through the last perforator, as seen in Model E.

Finally, in conclusion, the innovative solution of a single wellbore with a movable air injection interval has proven to be a superior alternative to the current state-of-the-art THAI method, which uses vertical injector wells and a horizontal producer. An 8% increase in oil production was observed in Model G compared to Model C. Additionally, net coke reaction increased by a factor of 31 in model G, and the higher temperatures observed along Model G confirmed enhanced HTO reactions. These findings suggest that this novel approach holds significant potential as an

improvement to the current in situ combustion techniques, although further refinements are needed.

5.2 Recommendations and Future Research

To further enhance the modelling procedure and increase the accuracy of the results, several recommendations are proposed for future research:

Contributions to the models can be enhanced by fine-tuning the kinetic parameters. These parameters were initially derived from the work of Ado (2017), who modified the original kinetic model of Athabasca bitumen proposed by Phillips et al. (1978). Adjusting these parameters could help the model predict more accurate results and optimize the in-situ combustion technology.

Performing a sensitivity analysis on air injection temperature and air injection rates can provide valuable insights. This analysis would help understand the implications of different air fluxes and air-to-oil ratios, which are essential for the success of toe-to-heel air injection projects.

Improving the model by integrating realistic permeability data and heterogeneity patterns in permeability can yield more accurate predictions. Additionally, incorporating the presence of seals or rock layers that impede or deviate fluid flow will enhance the model's accuracy and reliability.

References

Abu-Khamsin, S. A., Brigham, W. E., & Ramey, H. J. (1988). Reaction Kinetics of Fuel Formation for In-Situ Combustion. *SPE Reservoir Engineering*, *3*(04), 1308–1316. https://doi.org/10.2118/15736-PA

Adagülü, G. D., & Akkutlu, I. Y. (2007). Influence of in situ fuel deposition on air injection and combustion processes. *Journal of Canadian Petroleum Technology*, *46*(4), 54–61. https://doi.org/10.2118/07-04-06/2164788/PETSOC-07-04-06.PDF/1

Adegbesan, K. O. (1982). *Kinetic study of low temperature oxidation of Athabasca bitumen*. https://doi.org/http://dx.doi.org/10.11575/PRISM/14687

Ado, M. R. (2017a). *Numerical simulation of heavy oil and bitumen recovery and upgrading techniques*. http://eprints.nottingham.ac.uk/41502/

Ado, M. R. (2017b). *Numerical simulation of heavy oil and bitumen recovery and upgrading techniques*. http://eprints.nottingham.ac.uk/41502/

Ado, M. R. (2020). A detailed approach to up-scaling of the Toe-to-Heel Air Injection (THAI) In-Situ Combustion enhanced heavy oil recovery process. *Journal of Petroleum Science and Engineering*, *187*, 106740. https://doi.org/10.1016/J.PETROL.2019.106740

Ado, M. R. (2021a). Improving heavy oil production rates in THAI process using wells configured in a staggered line drive (SLD) instead of in a direct line drive (DLD) configuration: detailed simulation investigations. *Journal of Petroleum Exploration and Production Technology*, *11*(11), 4117–4130. https://doi.org/10.1007/s13202-021-01269-0

Ado, M. R. (2021b). Improving oil recovery rates in THAI in situ combustion process using pure oxygen. *Upstream Oil and Gas Technology*, *6*, 100032. https://doi.org/10.1016/j.upstre.2021.100032

Ado, M. R. (2022). Electrically-enhanced THAI in situ combustion technology for upgrading and production of heavy oil. *Journal of Petroleum Exploration and Production Technology*, *12*(12), 3373–3386. https://doi.org/10.1007/s13202-022-01530-0

Ado, M. R., Greaves, M., & Rigby, S. P. (2017). Dynamic Simulation of the Toe-to-Heel Air Injection Heavy Oil Recovery Process. *Energy and Fuels*, *31*(2), 1276–1284. https://doi.org/10.1021/acs.energyfuels.6b02559

Ado, M. R., Greaves, M., & Rigby, S. P. (2022). Simulation of catalytic upgrading in CAPRI, an add-on process to novel in-situ combustion, THAI. *Petroleum Research*, *7*(3), 297–307. https://doi.org/10.1016/j.ptlrs.2021.10.002

Afanasev, P., Smirnov, A., Ulyanova, A., Popov, E., & Cheremisin, A. (2023). Experimental Study of Catalytically Enhanced Cyclic Steam-Air Stimulation for In Situ Hydrogen Generation and Heavy Oil Upgrading. *Catalysts*, *13*(8), 1172. https://doi.org/10.3390/catal13081172

Ahmadi, M. (2023). Hybrid of in-situ combustion and steam-based heavy oil recovery. In *Sustainable In-Situ Heavy Oil and Bitumen Recovery* (pp. 327–357). Elsevier. https://doi.org/10.1016/B978-0-323-90848-1.00011-X

Alamatsaz, A. (2014). *Experimental Investigation of In Situ Combustion for Heavy Oils at Low Air Flux*. https://doi.org/10.11575/PRISM/26063

Alberta Energy Regulator. (2023). *Alberta Energy Outlook* .

Aleksandrov, D., Kudryavtsev, P., & Hascakir, B. (2017). Variations in in-situ combustion performance due to fracture orientation. *Journal of Petroleum Science and Engineering*, *154*, 488–494. https://doi.org/10.1016/J.PETROL.2017.02.002

Alexander, J. D., Martin, W. L., & Dew, J. N. (1962). Factors Affecting Fuel Availability and Composition During In Situ Combustion. *Journal of Petroleum Technology*, *14*(10), 1154–1164. https://doi.org/10.2118/296-PA

Alizadeh, A. (2020). *A Robust Kinetic Model for Computer Modelling of In Situ Combustion Processes in Athabasca Oil Sands*. http://hdl.handle.net/1880/112274

Al-Saadoon, F. T. (1970). *Experimental and statistical study of residual oil saturation after gas, water, and steam drive, and fuel availability for the in-situ combustion process*. https://www.osti.gov/biblio/5964660

Anbari, H., Robinson, J. P., Greaves, M., & Rigby, S. P. (2023). Field performance and numerical simulation study on the toe to heel air injection (THAI) process in a heavy oil reservoir with bottom water. *Journal of Petroleum Science and Engineering*, *220*, 111202. https://doi.org/10.1016/j.petrol.2022.111202

Ayasse, C., Bloomer, C., Lyngberg, E., Boddy, W., Donnelly, J., & Greaves, M. (2005, April 5). First Field Pilot of the THAI Process. *Canadian International Petroleum Conference*. https://doi.org/10.2118/2005-142

Belgrave, J. D. M. (1987). *An experimental and numerical investigation of in-situ combustion tube tests*. https://doi.org/http://dx.doi.org/10.11575/PRISM/11278

Belgrave, J. D. M., Moore, R. G., & Bennion, D. W. (1990). The thermal behavior of vertically-operated near-adiabatic in-situ combustion tubes. *Journal of Petroleum Science and Engineering*, *5*(1), 51–65. https://doi.org/10.1016/0920-4105(90)90005-N

Belgrave, J. D. M., Moore, R. G., Ursenbach, M. G., & Bennion, D. W. (1993). A Comprehensive Approach to In-Situ Combustion Modeling. *SPE Advanced Technology Series*, *1*(01), 98–107. https://doi.org/10.2118/20250-PA

Branoiu, G., Dinu, F., Stoicescu, M., Ghetiu, I., & Stoianovici, D. (2021). Half a century of continuous oil production by in-situ combustion in Romania – case study Suplacu de Barcau field. *MATEC Web of Conferences*, *343*, 09009. https://doi.org/10.1051/matecconf/202134309009

Brigham, W., & Castanier, L. M. (2007). Chapter 16 In-situ Combustion. In E. D. Holstein (Ed.), *Petroleum Engineering Handbook, Volume V: Reservoir Engineering and Petrophysics: Vol. V* (pp. 1367–1398). Society of Petroleum Engineers.

Butler, R. M. (1991). *Thermal recovery of oil and bitumen*. Old Tappan, NJ (United States); Prentice Hall Inc. https://www.osti.gov/biblio/5797813

Castanier, L. M., & Brigham, W. E. (2003). Upgrading of crude oil via in situ combustion. *Journal of Petroleum Science and Engineering*, *39*(1–2), 125–136. https://doi.org/10.1016/S0920-4105(03)00044-5

Cheih, C. (1982). State-of-the-Art Review of Fireflood Field Projects (includes associated papers 10901 and 10918). *Journal of Petroleum Technology*, *34*(01), 19–36. https://doi.org/10.2118/9772-PA

Cheng, W. L., Li, T. T., Nian, Y. Le, & Xie, K. (2014). Evaluation of working fluids for geothermal power generation from abandoned oil wells. *Applied Energy*, *118*, 238–245. https://doi.org/10.1016/J.APENERGY.2013.12.039

Chu, C. (1977). A Study of Fireflood Field Projects (includes associated paper 6504). *Journal of Petroleum Technology*, *29*(02), 111–120. https://doi.org/10.2118/5821-PA

Çınar, M. (2013). CREATING ENHANCED GEOTHERMAL SYSTEMS IN DEPLETED OIL RESERVOIRS VIA IN SITU COMBUSTION. *PROCEEDINGS, Thirty-Eighth Workshop on Geothermal Reservoir Engineering*. https://pangea.stanford.edu/ERE/pdf/IGAstandard/SGW/2013/Cinar.pdf

Çınar, M., Hasçakir, B., Castanier, L. M., & Kovscek, A. R. (2011). Predictability of Crude Oil In-Situ Combustion by the Isoconversional Kinetic Approach. *SPE Journal*, *16*(03), 537–547. https://doi.org/10.2118/148088-PA

Coates, R., Lorimer, S., & Ivory, J. (1995). Experimental and Numerical Simulations of a Novel Top Down In-Situ Combustion Process. *Proceedings - SPE International Heavy Oil Symposium*, 487–498. https://doi.org/10.2118/30295-MS

Coates, R., & Zhao, L. L. (2001). Numerical Evaluation of THAI Process. *Canadian International Petroleum Conference 2001, CIPC 2001*. https://doi.org/10.2118/2001-021

Computer Modelling Group Ltd. (2021). *CMG Technologies (STARS User manual)* (2021.10.391.54266). CMG.

Dabbous, M. K., & Fulton, P. F. (1974). Low-Temperature-Oxidation Reaction Kinetics and Effects on the In-Situ Combustion Process. *Society of Petroleum Engineers Journal*, *14*(03), 253–262. https://doi.org/10.2118/4143-PA

Davis, A. P., & Michaelides, E. E. (2009). Geothermal power production from abandoned oil wells. *Energy*, *34*(7), 866–872. https://doi.org/10.1016/J.ENERGY.2009.03.017

Dayal, H. S., Bhushan, B. V., Mitra, S., Sinha, S. K., & Sur, S. (2010). *In-Situ Combustion Opportunities and Anxieties*. https://doi.org/10.2118/126241-MS

Dechaux, J. C., & Delfosse, L. (1979). The negative temperature coefficient in the C2 to C13 hydrocarbon oxidation. I. Morphological results. *Combustion and Flame*, *34*(C), 161–168. https://doi.org/10.1016/0010-2180(79)90089-0

Fassihi, M. R., Yannimaras, D. V., & Kumar, V. K. (1997). Estimation of Recovery Factor in Light-Oil Air-Injection Projects. *SPE Reservoir Engineering*, *12*(03), 173–178. https://doi.org/10.2118/28733-PA

Fazlyeva, R., Rezvani, H., Askarova, A., Khalilnezhad, A., Cheremisin, A., & Riazi, M. (2023). Chapter 5 - In situ combustion. *Thermal Methods*, 155–215. https://doi.org/10.1016/B978-0-12-821933-1.00007-0

Freitag, N. P., & Exelby, D. R. (2006). A SARA- Based model for simulating the pyrolysis reactions that occur in high-temperature EOR processes. *Journal of Canadian Petroleum Technology*, *45*(3), 38–44. https://doi.org/10.2118/06-03-02/2164718/PETSOC-06-03-02.PDF/1

Gadelle, C. P., Burger, J. G., Bardon, C. P., Machedon, V., Carcoana, A., & Petcovici, V. (1981). Heavy-Oil Recovery by In-Situ Combustion - Two Field Cases in Rumania. *Journal of Petroleum Technology*, *33*(11), 2057–2066. https://doi.org/10.2118/8905-PA

Gargar, N. K., Mailybaev, A. A., Marchesin, D., & Bruining, H. (2014). Compositional effects in light/medium oil recovery by air injection: Vaporization vs. combustion. *Journal of Porous Media*, *17*(11), 937–952. https://doi.org/10.1615/JPORMEDIA.V17.I11.10

Gates, I. D., Chakrabarty, N., Moore, R. G., Mehta, S. A., Zalewski, E., & Pereira, P. (2008). In Situ Upgrading of Llancanelo Heavy Oil Using In Situ Combustion and a Downhole Catalyst Bed. *Journal of Canadian Petroleum Technology*, *47*(09). https://doi.org/10.2118/08-09-23

Government of Canada. (2020). *Canada has the third-largest proven oil reserve in the world, most of which is in the oil sands*.

Grant, B. F., & Szasz, S. E. (1954). Development of an Underground Heat Wave for Oil Recovery. *Journal of Petroleum Technology*, *6*(05), 23–33. https://doi.org/10.2118/348-G

Greaves, M., Dong, L. L., & Rigby, S. P. (2012). Simulation Study of the Toe-to-Heel Air Injection Three-Dimensional Combustion Cell Experiment and Effects in the Mobile Oil Zone. *Energy & Fuels*, *26*(3), 1656–1669. https://doi.org/10.1021/ef201925c

Greaves, M., Saghr, A. M., Xia, T. X., Turta, A. T., & Ayasse, C. (2001). THAI - New air injection technology for heavy oil recovery and in situ upgrading. *Journal of Canadian Petroleum Technology*, *40*(3), 38–47. https://doi.org/10.2118/01-03-03/2165754/PETSOC-01-03-03.PDF/1

Greaves, M., & Turta, A. T. (1997). *Oilfield in-situ combustion process* (Patent US5626191A). United States Patent.

Greaves, M., Xia, T. X., & Turta, A. T. (2008). Stability of THAI TM Process-Theoretical And Experimental Observations. *Journal of Canadian Petroleum Technology*, *47*(09). https://doi.org/10.2118/08-09-65

Guo, K., Li, H., & Yu, Z. (2016). In-Situ heavy and extra-heavy oil recovery: A review. In *Fuel* (Vol. 185, pp. 886–902). Elsevier Ltd. https://doi.org/10.1016/j.fuel.2016.08.047

Gutierrez, D., & Mallory, D. G. (2022). *New Insights into the Understanding of In-Situ Combustion: Important Considerations When Modeling the Process*. https://doi.org/10.2118/212268-PA/2821946/spe-212268-pa.pdf/1

Gutiérrez, D., Mallory, D., Moore, G., Mehta, R., Ursenbach, M., & Bernal, A. (2022, April 18). New Paradigm in the Understanding of In Situ Combustion: The Nature of the Fuel and the Important Role of Vapor Phase Combustion. *Day 2 Tue, April 26, 2022*. https://doi.org/10.2118/209411-MS

Gutierrez, D., Moore, R. G., Ursenbach, M. G., & Mehta, S. A. (2012). *The ABCs of In-Situ-Combustion Simulations: From Laboratory Experiments to Field Scale*.

Gutierrez, D., Skoreyko, F., Moore, R. G., Mehta, S. A., & Ursenbach, M. G. (2009). The Challenge of Predicting Field Performance of Air Injection Projects Based on Laboratory and Numerical Modelling. *Journal of Canadian Petroleum Technology*, *48*(04), 23–33. https://doi.org/10.2118/09-04-23-DA

Hajdo, L. E., Hallam, R. J., & Vorndran, L. D. L. (1985). Hydrogen Generation During In-Situ Combustion. *Society of Petroleum Engineers - SPE California Regional Meeting, CRM 1985*, 675–689. https://doi.org/10.2118/13661-MS

Harding, T. (2023). Methods to Enhance Success of Field Application of In-Situ Combustion for Heavy Oil Recovery. *SPE Reservoir Evaluation & Engineering*, *26*(01), 190–197. https://doi.org/10.2118/210600-PA

Hart, A., Wood, J., & Greaves, M. (2017). Laboratory investigation of CAPRI catalytic THAI-add-on process for heavy oil production and in situ upgrading. *Journal of Analytical and Applied Pyrolysis*, *128*, 18–26. https://doi.org/10.1016/J.JAAP.2017.11.004

Hascakir, B., Ross, C. M., Castanier, L. M., & Kovscek, A. R. (2013). Fuel Formation and Conversion During In-Situ Combustion of Crude Oil. *SPE Journal*, *18*(06), 1217–1228. https://doi.org/10.2118/146867-PA

Hayashitani, M., Bennion, D. W., Donnelly, J. K., & Moore, R. G. (1978). Thermal Cracking Models For Athabasca Oil Sands. *All Days*. https://doi.org/10.2118/7549-MS

Howard, F. A. (1923). *Method of Operating Oil Wells* (Patent US1473348A).

Hyne, N. J. (2012). *Nontechnical Guide to Petroleum Geology, Exploration, Drilling & Production* (3rd Edition, Vol. 2). PennWell Books, LLC.

Ismail, N. B., & Hascakir, B. (2020). Impact of asphaltenes and clay interaction on in-situ combustion performance. *Fuel*, *268*, 117358. https://doi.org/10.1016/J.FUEL.2020.117358

Jia, N., Moore, R. G., Mehta, S. A., & Ursenbach, M. G. (2006). Kinetic modelling of thermal cracking and low temperature oxidation reactions. *Journal of Canadian Petroleum Technology*, *45*(9), 21–28. https://doi.org/10.2118/06-09-01/2165178/PETSOC-06-09-01.PDF/1

Kapadia, P. R., Kallos, M. S., & Gates, I. D. (2011). Potential for hydrogen generation from in situ combustion of Athabasca bitumen. *Fuel*, *90*(6), 2254–2265. https://doi.org/10.1016/J.FUEL.2011.02.038

Kapadia, P. R., Kallos, M. S., & Gates, I. D. (2015). A review of pyrolysis, aquathermolysis, and oxidation of Athabasca bitumen. *Fuel Processing Technology*, *131*, 270–289. https://doi.org/10.1016/J.FUPROC.2014.11.027

Kapadia, P. R., Wang, J. (Jacky), Kallos, M. S., & Gates, I. D. (2013). Practical process design for in situ gasification of bitumen. *Applied Energy*, *107*, 281–296. https://doi.org/10.1016/J.APENERGY.2013.02.035

Kisman, K. E., & Lau, E. C. (1994). A New Combustion Process Utilizing Horizontal Wells And Gravity Drainage. *Journal of Canadian Petroleum Technology*, *33*(03). https://doi.org/10.2118/94-03-05

Kovscek, A. R., Castanier, L. M., & Gerritsen, M. G. (2013). Improved Predictability of In-Situ-Combustion Enhanced Oil Recovery. *SPE Reservoir Evaluation & Engineering*, *16*(02), 172–182. https://doi.org/10.2118/165577-PA

Kuhn, C. S., & Koch, R. L. (1953). In-Situ Combustion newest method of increasing oil recovery. *Oil Gas J*, *52*(14).

Kumar, M. (1987, February 1). Simulation of Laboratory In-Situ Combustion Data and Effect of Process Variations. *All Days*. https://doi.org/10.2118/16027-MS

Lake, L. W., & Clegg, J. D. (2007). *Production Operations Engineering*. Society of Petroleum Engineers222 Palisades Creek Drive, Richardson, TX 75080-2040 USA. https://doi.org/10.2118/9781555631185

Li, G., & Wu, J. (2018). Application of In-situ combustion for heavy oil production in China: A Review. *Journal of Oil, Gas and Petrochemical Sciences*, *1*(2), 69–72. https://doi.org/10.30881/jogps.00014

Liu, Y., Huang, H., Xu, X., Liu, Q., Han, D., Cheng, H., Wu, D., & Yan, H. (2020). Novel geochemical proxies derived from 1D simulation of Liaohe oil sand bitumen to monitor in-situ combustion process. *Journal of Analytical and Applied Pyrolysis*, *148*, 104811. https://doi.org/10.1016/J.JAAP.2020.104811

Lopeman, T., Anbari, H., Leeke, G., & Wood, J. (2023). Numerical Modeling of Toe-to-Heel Air Injection and Its Catalytic Variant (CAPRI) under Varying Steam Conditions. *Energy and Fuels*, *37*(1), 237–250. https://doi.org/10.1021/ACS.ENERGYFUELS.2C03069/ASSET/IMAGES/LARGE/EF2C03069_0013.JPEG

Maharramov, M., & Zoback, M. D. (2018). Monitoring of cyclic steam stimulation by inversion of surface tilt measurements. *The Leading Edge*, *37*(5), 350–355. https://doi.org/10.1190/tle37050350.1

Marjerrison, D. M., & Fassihi, M. R. (1992, April 22). A Procedure for Scaling Heavy-Oil Combustion Tube Results to a Field Model. *All Days*. https://doi.org/10.2118/24175-MS

Mills, R. V. A. (1923). The Paraffin Problems in Oil Wells. *U.S. Bureau of Mines Report of Investigation, Government Printing Office*, *RI 2550*, 10–11.

Minakov, A. V., Meshkova, V. D., Guzey, D. V., & Pryazhnikov, M. I. (2023). Recent Advances in the Study of In Situ Combustion for Enhanced Oil Recovery. *Energies*, *16*(11), 4266. https://doi.org/10.3390/en16114266

Mojarab, M., Harding, T. G., & Maini, B. B. (2011). Improving the SAGD Performance by Introducing a New Well Configuration. *Journal of Canadian Petroleum Technology*, *50*(04), 9–18. https://doi.org/10.2118/146626-PA

Montes, A. R., Gutierrez, D., Moore, R. G., Mehta, S. A., & Ursenbach, M. G. (2010). Is High-Pressure Air Injection (HPAI) Simply a Flue-Gas Flood? *Journal of Canadian Petroleum Technology*, *49*(02), 56–63. https://doi.org/10.2118/133206-PA

Moore, R. G. (1993). New Strategies For In Situ Combustion. *Journal of Canadian Petroleum Technology*, *32*(10). https://doi.org/10.2118/93-10-01

Moore, R. G., Belgrave, J. D. M., Mehta, S. A., Ursenbach, M. G., Laureshen, C. J., & Xi, K. (1992, April 4). Some Insights Into the Low-Temperature and High-Temperature In-Situ Combustion Kinetics. *SPE/DOE Enhanced Oil Recovery Symposium*. https://doi.org/10.2118/24174-MS

Moore, R. G., Laureshen, C. J., Belgrave, J. D. M., Ursenbach, M. G., & Mehta, S. A. (1995). In-Situ Combustion in Canadian heavy oil reservoirs. *Fuel*, *74*(8), 1169–1175. https://doi.org/10.1016/0016-2361(95)00063-B

Moore, R. G., Laureshen, C. J., Ursenbach, M. G., Mehta, S. A., & Belgrave, J. D. M. (1999a). A Canadian Perspective On In Situ Combustion. *Journal of Canadian Petroleum Technology*, *38*(13). https://doi.org/10.2118/99-13-35

Moore, R. G., Laureshen, C. J., Ursenbach, M. G., Mehta, S. A., & Belgrave, J. D. M. (1999b). *Combustion/Oxidation Behavior of Athabasca Oil Sands Bitumen*. http://onepetro.org/REE/article-pdf/2/06/565/2593394/spe-59483-pa.pdf/1

Moore, R. G., Ursenbach, M. G., Laureshen, C. J., Belgrave, J. D. M., & Mehta, S. A. (1999). Ramped Temperature Oxidation Analysis of Athabasca Oil Sands Bitumen. *Journal of Canadian Petroleum Technology*, *38*(13). https://doi.org/10.2118/99-13-40

Moschopedis, S. E., & Speight, J. G. (1973). Oxidation of petroleum fractions. *Fuel*, *52*(1), 83. https://doi.org/10.1016/0016-2361(73)90019-7

Moschopedis, S. E., & Speight, J. G. (1975). Oxidation of a bitumen. *Fuel*, *54*(3), 210–212. https://doi.org/10.1016/0016-2361(75)90014-9

Mossop, G. D. (1980). Geology of the Athabasca Oil Sands. *Science*, *207*(4427), 145–152. https://doi.org/10.1126/science.207.4427.145

Nissen, A., Zhu, Z., Kovscek, A., Castanier, L., & Gerritsen, M. (2015). Upscaling Kinetics for Field-Scale In-Situ-Combustion Simulation. *SPE Reservoir Evaluation & Engineering*, *18*(02), 158–170. https://doi.org/10.2118/174093-PA

Panait-Patica, A., Serban, D., & Ilie, N. (2006, June 12). Suplacu de Barcau Field—A Case History of a Successfull In-Situ Combustion Exploitation. *All Days*. https://doi.org/10.2118/100346-MS

Patchett, M., & Lozowy, A. (2012). Reframing Canadian Oil Sands. *Imaginations Journal of Cross-Cultural Image Studies/Revue d Études Interculturelle de l Image*, *3*(2). https://doi.org/10.17742/IMAGE.sightoil.3-2.9

Perkins, G. (2018). Mathematical modelling of in situ combustion and gasification. In *Proceedings of the Institution of Mechanical Engineers, Part A: Journal of Power and Energy* (Vol. 232, Issue 1, pp. 56–73). SAGE Publications Ltd. https://doi.org/10.1177/0957650917721595

Phillips, C. R., Haidar, N. I., & Poon, Y. C. (1985a). Kinetic models for the thermal cracking of Athabasca bitumen: The effect of the sand matrix. *Fuel*, *64*(5), 678–691. https://doi.org/10.1016/0016-2361(85)90055-9

Phillips, C. R., Haidar, N. I., & Poon, Y. C. (1985b). Kinetic models for the thermal cracking of Athabasca bitumen: The effect of the sand matrix. *Fuel*, *64*(5), 678–691. https://doi.org/10.1016/0016-2361(85)90055-9

Pope, C., Ismail, N. B., & Hascakir, B. (2020, August 30). Catalytic Impact of Clays During In-Situ Combustion. *Day 2 Tue, September 01, 2020*. https://doi.org/10.2118/200381-MS

Prowse, D. R., Wallace, E. D., Lott, R. K., & Daigneault, L. E. (1983). *Some Physical Properties of Bitumen and Oil Sand*.

Rahnema, H., Barrufet, M. A., & Mamora, D. (2012). Self-Sustained CAGD Combustion Front Development; Experimental and Numerical Observations. *Proceedings - SPE Symposium on Improved Oil Recovery*, *2*, 1612–1623. https://doi.org/10.2118/154333-MS

Ramey, H. J. (1971). In-Situ Combustion. *Paper Presented at the 8th World Petroleum Conference. Moscow, USSR*. https://onepetro.org/WPCONGRESS/proceedings-abstract/WPC08/All-WPC08/WPC-14229/199040

Ranjbar, M. (1995). Improvement of medium and light oil recovery with thermocatalytic in situ combustion. *Journal of Canadian Petroleum Technology*, *34*(8), 25–30. https://doi.org/10.2118/95-08-02/2169850/PETSOC-95-08-02.PDF/1

Roychaudhury, S., Sur, S., & Sinha, S. K. (1995). *Experience with in situ combustion pilot in presence of edge water*. https://www.osti.gov/biblio/269566

Sarathi, P. S. (1999). *In-Situ Combustion Handbook -- Principles and Practices*. https://doi.org/10.2172/3175

Sequera, B., Moore, R. G., Mehta, S. A., & Ursenbach, M. G. (2010). *Numerical Simulation of In-Situ Combustion Experiments Operated Under Low Temperature Conditions* (Vol. 49, Issue 1). http://onepetro.org/JCPT/article-pdf/49/01/55/2145551/spe-132486-pa.pdf/1

Sharma, J., Dean, J., Aljaberi, F., & Altememee, N. (2021). In-Situ Combustion in Bellevue field in Louisiana – History, current state and future strategies. *Fuel*, *284*, 118992. https://doi.org/10.1016/J.FUEL.2020.118992

Sheinman, A. B., Dubroval, K. K., Charuigin, M. M., Zaks, S. L., & Zinchenka, K. E. (1938). Gasification of Crude Oil in Reservoir Sands. *The Petroleum Engineer, Part 1* .

Song, P., Li, Y., Yin, Z., & Yuan, Q. (2023, May 15). Hydrogen Generation from Heavy Oils via In-situ Combustion Gasification. *Day 3 Wed, May 24, 2023*. https://doi.org/10.2118/212986-MS

Souraki, Y., Ashrafi, M., Karimaie, H., & Torsaeter, O. (2012). Experimental Analyses of Athabasca Bitumen Properties and Field Scale Numerical Simulation Study of Effective Parameters on SAGD Performance. *Energy and Environment Research*, *2*(1). https://doi.org/10.5539/eer.v2n1p140

Speight, J. G. (2013). Thermal Methods of Recovery. In *Heavy Oil Production Processes* (pp. 93–130). Elsevier. https://doi.org/10.1016/B978-0-12-401720-7.00005-8

Storey, B. M., Worden, R. H., & McNamara, D. D. (2022). The Geoscience of In-Situ Combustion and High-Pressure Air Injection. *Geosciences 2022, Vol. 12, Page 340*, *12*(9), 340. https://doi.org/10.3390/GEOSCIENCES12090340

Stosur, J. J. (1977). IN-SITU COMBUSTION METHOD FOR OIL RECOVERY STATE OF THE ART AND POTENTIAL. In *The Future Supply of Nature-Made Petroleum and Gas* (pp. 611–623). Pergamon. https://doi.org/10.1016/B978-0-08-021735-2.50044-6

Sur, S. (2022). *In-Situ Combustion Myths and Facts*. https://doi.org/10.2118/210606-PA/2912346/spe-210606-pa.pdf/1

Taber, J. J., Martin, F. D., & Seright, R. S. (1997). EOR Screening Criteria Revisited— Part 1: Introduction to Screening Criteria and Enhanced Recovery Field Projects. *SPE Reservoir Engineering*, *12*(03), 189–198. https://doi.org/10.2118/35385-PA

Teng, L. ., Song, H. ., Zhang, S. ., Wu, F. ., Xu, D. ., Gong, Y. ., Jiang, Z. ., Gao, H. ., Wang, C. ., & Zhong, L. . (2017, October 17). Investigation on In-Situ Combustion in D66, a Multilayered Heavy Oil Reservoir, Liaohe Oilfield. *Day 2 Wed, October 18, 2017*. https://doi.org/10.2118/186173-MS

Turta, A., Sierra, R., Islam, M., & Singhal, A. (2023). Athabasca Toe-to-Heel Air Injection Pilot: Evaluation of the Spontaneous Ignition Based on Apparent Atomic Hydrogen-Carbon Ratio

Variation. *SPE Reservoir Evaluation & Engineering*, *26*(01), 139–151. https://doi.org/10.2118/212267-PA

Turta, A. T. (2013). *In-Situ Combustion - Ch. 18*.

Turta, A. T. (2022, October 1). *Conventional ISC*. https://insitucombustion.ca/#conventional

Turta, A. T., Chattopadhyay, S. K., Bhattacharya, R. N., Condrachi, A., & Hanson, W. (2007). Current status of commercial in situ combustion projects worldwide. *Journal of Canadian Petroleum Technology*, *46*(11), 8–14. https://doi.org/10.2118/07-11-GE/2165435/PETSOC-07-11-GE.PDF/1

Turta, A. T., Greaves, M., & Grabowski, J. (2018a). *Comprehensive Assessment of Toe-To-Heel Air Injection (THAI) Process. Guidelines for Development of Future Generations of In-Situ Combustion Processes*.

Turta, A. T., Greaves, M., & Grabowski, J. (2018b). *Comprehensive Assessment of Toe-To-Heel Air Injection (THAI) Process. Guidelines for Development of Future Generations of In-Situ Combustion Processes*.

Turta, A. T., Singhal, A., Sierra, R., Greaves, M., & Islam, M. (2023). *Evaluation of the First Field Piloting of the THAI Process: Athabasca Pilot*. https://doi.org/10.2118/212780-MS

Tzanco, E. T., Moore, R. G., Belgrave, J. D. M., & Ursenbach, M. G. (1991). Laboratory Combustion Behaviour Of Countess B Light Oil. *Journal of Canadian Petroleum Technology*, *30*(05), 43–51. https://doi.org/10.2118/91-05-03

Wang, L., Liu, D., Zhang, H., Long, H., Wu, X., Hao, R., Liu, J., & Gao, F. (2016, October 19). The Research and Application of In-Situ Combustion with Gravity Technology in Thermal Developed Heavy Oil Reservoir. *Day 1 Wed, October 19, 2016*. https://doi.org/10.2118/181152-MS

Wei, W. (2020). *In-Situ Combustion for Heavy Oil: Toe-to-Heel Air Injection*. http://hdl.handle.net/1880/112916

Wei, W., Wang, J., Afshordi, S., & Gates, I. D. (2020). Detailed analysis of Toe-to-Heel Air Injection for heavy oil production. *Journal of Petroleum Science and Engineering*, *186*. https://doi.org/10.1016/j.petrol.2019.106704

Weissman, J. G., Kessler, R. V., Sawicki, R. A., Belgrave, J. D. M., Laureshen, C. J., Mehta, S. A., Moore, R. G., & Ursenbach, M. G. (1996). Down-hole catalytic upgrading of heavy crude oil. *Energy and Fuels*, *10*(4), 883–889. https://doi.org/10.1021/EF9501814/ASSET/IMAGES/LARGE/EF9501814F00005.JPEG

Welch, P. A., Verney, M. J., Best, B. P., & Feick, W. P. (2013). *Whitesands In situ Partnership Evaluation of Heavy Oil Reserves Based on Forecast Prices and Costs Kerrobert Property*.

Wolcott, E. R. (1923). *Method of Increasing the Yield of Oil Wells* (Patent US1457479A).

Xia, T. X., & Greaves, M. (2002). Upgrading Athabasca tar sand using Toe-to-Heel air injection. *Journal of Canadian Petroleum Technology*, *41*(8), 51–57. https://doi.org/10.2118/02-08-02/2168764/PETSOC-02-08-02.PDF/1

Xia, T. X., Greaves, M., & Turta, A. (2005). Main Mechanism for Stability of THAI-Toe-to-Heel Air Injection. *Journal of Canadian Petroleum Technology*, *44*(01). https://doi.org/10.2118/05-01-03

Xia, T. X., Greaves, M., Turta, A. T., & Ayasse, C. (2003a). THAI - A "short-distance displacement" in Situ combustion process for the recovery and upgrading of heavy oil. *Chemical Engineering Research and Design*, *81*(3), 295–304. https://doi.org/10.1205/02638760360596847

Xia, T. X., Greaves, M., Turta, A. T., & Ayasse, C. (2003b). THAI - A "short-distance displacement" in Situ combustion process for the recovery and upgrading of heavy oil. *Chemical Engineering Research and Design*, *81*(3), 295–304. https://doi.org/10.1205/02638760360596847

Yang, M., Harding, T. G., & Chen, Z. (2017). An Improved Kinetics Model for in Situ Combustion of Pre-Steamed Oil Sands. *Energy and Fuels*, *31*(4), 3546–3556. https://doi.org/10.1021/acs.energyfuels.6b02582

Yang, M., Harding, T. G., & Chen, Z. (2018, March 13). *Field-Scale Modelling of Hybrid Steam and Combustion In-Situ Recovery Process for Oil Sands using Dynamic Gridding*. https://doi.org/10.2118/189726-MS

Yang, M., & Yang, M. (. (2019). *Numerical Modelling of Hybrid Steam and Combustion Recovery Process for Oil Sands*. http://hdl.handle.net/1880/110691

Yang, S., Han, L., Feng, C., Wang, H., Feng, Y., & Wu, X. (2018). Mechanical performance of casing in in-situ combustion thermal recovery. *Journal of Petroleum Science and Engineering*, *168*, 32–38. https://doi.org/10.1016/j.petrol.2018.04.068

Yannimaras, D. V., & Tiffin, D. L. (1995). Screening of Oils for In-Situ Combustion at Reservoir Conditions by Accelerating-Rate Calorimetry. *SPE Reservoir Engineering*, *10*(01), 36–39. https://doi.org/10.2118/27791-PA

Yuan, C., Sadikov, K., Varfolomeev, M., Khaliullin, R., Pu, W., Al-Muntaser, A., & Saeed Mehrabi-Kalajahi, S. (2020). Low-temperature combustion behavior of crude oils in porous

media under air flow condition for in-situ combustion (ISC) process. *Fuel*, *259*, 116293. https://doi.org/10.1016/J.FUEL.2019.116293

Zamora, V., & Jonathan, A. (2019). *In-Situ Combustion Simulation for A Heavy Oil Naturally Fractured Reservoir*. http://hdl.handle.net/1880/110340

Zhang, X., Wang, J., Wang, L., Li, Z., Hu, W., Dai, Y., Kou, Y., Lei, S., Li, Q., Zhang, W., Li, H., Wang, R., & Feng, Q. (2023). Catalytic capacity evolution of montmorillonite in in-situ combustion of heavy oil. *Fuel*, *333*, 126621. https://doi.org/10.1016/j.fuel.2022.126621

Zhu, Y., Li, K., Liu, C., & Mgijimi, M. B. (2019). Geothermal Power Production from Abandoned Oil Reservoirs Using In Situ Combustion Technology. *Energies 2019, Vol. 12, Page 4476*, *12*(23), 4476. https://doi.org/10.3390/EN12234476

Zhu, Z., Bazargan, M., Lapene, A., Gerritsen, M., Castanier, L., & Kovscek, A. (2011). Upscaling for Field-Scale In-Situ Combustion Simulation. *Society of Petroleum Engineers Western North American Regional Meeting 2011*, 344–357. https://doi.org/10.2118/144554-MS

Zhu, Z., Liu, C., Chen, Y., Gong, Y., Song, Y., & Tang, J. (2021). In-Situ Combustion Simulation from Laboratory to Field Scale. *Geofluids*, *2021*. https://doi.org/10.1155/2021/8153583

Zhu, Z., Liu, Y., Liu, C., & Kovscek, A. R. (2021). In-Situ Combustion Frontal Stability Analysis. *SPE Journal*, *26*(04), 2271–2286. https://doi.org/10.2118/195318-PA